

UNIVERSITY OF OKLAHOMA

GRADUATE COLLEGE

SYNTHESIS OF STRUCTURAL MODELS OF NON-HEME DIOXYGENASES

MIMICS OF THE 3-His-1-CARBOXYLATE TETRAD

A DISSERTATION

SUBMITTED TO THE GRADUATE FACULTY

in partial fulfillment of the requirements for the

Degree of

DOCTOR OF PHILOSOPHY

By

JEROME VOLKMAN

Norman, Oklahoma

2009

SYNTHESIS OF STRUCTURAL MODELS OF NON-HEME DIOXYGENASES
MIMICS OF THE 3-His-1-CARBOXYLATE TETRAD

A DISSERTATION APPROVED FOR THE
DEPARTMENT OF CHEMISTRY AND BIOCHEMISTRY

BY

Dr. Kenneth M. Nicholas, Chair

Dr. Paul F. Cook

Dr. Ronald L. Halterman

Dr. Michael J. McInerney

Dr. Ann H. West

© Copyright by JEROME VOLKMAN 2009
All Rights Reserved.

Acknowledgements

I would like to acknowledge the past and present members of my committee, for their help and advice during my years at the University of Oklahoma. I would also to thank thank particularly my advisor Prof. K. M. Nicholas for is guidance and help throughout my years of research in his laboratory.

My sanity would not have remained intact without past and present members of the Nicholas lab whom I would like to thank for their patience and the long nights spent at the Library. So, thank you Dave, Masa, Angus, Nick and Eric.

Last, but not least, je voudrais remercier ma famille, mes frères et tout particulièrement mes parents, qui m'ont toujours supporté, malgré les épreuves de ces récentes années.

Table of Contents

1	The 3-His-1-Carboxylate Binding Motif in Dioxygenases ...	1
1.1	Introduction.....	1
1.2	Cu-dependent quercetin 2,3-dioxygenases	3
1.2.1	Introduction and background	3
1.2.2	Structure	4
1.2.3	Catalytic mechanism.....	5
1.2.4	Structural and functional models	8
1.3	Acireductone Dioxygenase	9
1.3.1	Introduction and background	9
1.3.2	Structure	11
1.3.3	Catalytic mechanism	12
1.3.4	Structural and functional complexes	14
1.4	Lipoxygenases	16
1.4.1	Introduction and background	16
1.4.2	Structure	18
1.4.3	Catalytic mechanism	19
1.4.4	Structural and functional complexes	21
1.5	Conclusion	24

2	An Efficient Synthesis of <i>Tris</i>[4(5)-imidazolyl]carbinol (4-TIC) a 3-His Model	26
2.1	Introduction and background	26
2.1.1	Introduction	26
2.1.2	Background and retrosynthesis	27
2.1.3	Syntheses of the Tris-Imidazole subunit	29
2.1.3.1	Breslow Synthesis	29
2.1.3.2	Collman Synthesis	31
2.2	Results and Discussion	33
2.2.1	Introduction	33
2.2.2	Synthesis of <i>Tris</i> [4(5)-imidazolyl]carbinol 31 and its derivatives	33
2.2.2.1	Synthesis of 4-TIC 31	33
2.2.2.2	Synthesis of two derivatives 49 and 51	36
2.2.3	Synthesis of a 4-TIC iron (III) complex 52	38
2.2.4	Conclusion	40
2.3	Functionalization of 4-TIC	40
2.3.1	Introduction and background	40
2.3.2	Results and Discussion	44
2.4	Conclusion	46
2.5	Experimental	48

3	Synthesis of the Mixed Carboxylate-Functionalized Carbinol 73 and Study of its Coordination Chemistry	64
3.1	Introduction: retrosynthetic analysis	64
3.2	Synthesis of precursors 80 and 81	66
3.2.1	Synthesis of protected imidazole 85	66
3.2.2	Synthesis of symmetrical bis-imidazolyl ketones 87-89	68
3.2.3	Addition attempts of 85 to 87-89	69
3.2.4	Conclusion	70
3.3	Modification and optimization of precursor syntheses	71
3.3.1	Introduction: oxidation attempts of alcohol 83	71
3.3.2	Modifications and synthesis of precursor 54	71
3.4	Synthesis of bis-imidazolyl ketone 90	74
3.4.1	First approach.....	74
3.4.2	Second approach	74
3.4.3	Addition attempts with the new precursors 90 and 94	76
3.5	Second and third approach of a build-in carboxylate tether	77
3.5.1	Introduction: retrosynthetic analysis.....	77
3.5.2	Synthesis of precursor 98	78
3.5.2.1	Synthesis of diester 98	78
3.5.2.2	Addition attempts	79
3.5.2.3	Conclusion	79

3.5.3	Third approach of a build-in carboxylate tether	80
3.5.3.1	Synthesis of MOM-protected imidazole 100	80
3.5.3.2	Addition attempts to 100 and synthesis of 73	82
3.6	Computational Studies	84
3.6.1	The influence of the protecting groups in terms of electron affinity	84
3.6.2	Ionization of the nucleophiles 36 , 46 , 47 , 101-103	86
3.6.3	Conclusion	87
3.7	Coordination chemistry and metal ion complexation by 73	88
3.7.1	Addition of base and its effect	88
3.7.2	Synthesis of cobalt (III) complex under neutral conditions	88
3.8	Conclusion	90
3.9	Experimental	91
4	Synthesis of the Carboxylate-Functionalized <i>Tris</i>[4-(<i>N</i>- Methyl-2-Isopropyl-Imidazolyl]Methane 105 and its Copper (II) Complex	116
4.1	Introduction: Ligand design and retrosynthesis	116
4.2	Synthesis of the tripod 81 with an extended side-chain	119
4.2.1	Synthesis of 108 by analogy	119
4.2.2	Modified and improved synthesis of 108	122
4.2.3	Addition of 47 to 108 and synthesis of the desired target 106 ...	124

4.2.4	Conclusion	125
4.3	Complexation studies and lessons learned	125
4.4	Synthesis of the carboxylate-functionalized tris[4-(N-methyl-2-isopropyl- imidazolyl)methane	126
4.4.1	Design and retrosynthesis of an optimal ligand for a structural model of the 3-His-1-carboxylate motif.....	126
4.4.2	Synthesis of the optimal ligand 105	128
4.4.2.1	Synthesis of 4-iodo-N-methylimidazole 121	128
4.4.2.2	Synthesis of the imidazole diester 122	129
4.4.2.3	Addition of 121 to 122	130
4.4.2.4	Reduction of carbinols 118 and synthesis of 105	133
4.5	Synthesis of a structural model complex of Cu-dependent 2,3-querctin dioxygenase	135
4.6	Final conclusions and future directions	139
4.7	Experimental	144
	References	161

List of Tables

Table 2.1: pKa of 4-TIC and 2-TIC	28
Table 2.2: Product distribution and yields from scheme 2.19.....	43
Table 2.3: Crystal data and structure refinement for 31 ·3 HCl	55
Table 2.4: Crystal data and structure refinement for 52	58
Table 2.5: Crystal data and structure refinement for 71	62
Table 3.1: Reactions of scheme 3.11	71
Table 3.2: (-)Vertical EA (eV)	85
Table 3.3: HOMO energies of selected nucleophiles	86
Table 3.4: Crystal data and structure refinement for 104	112
Table 4.1: Selected distances of 2,3-QD·QUE and 129	137
Table 4.2: Selected angles of 2,3-QD·QUE and 129	137
Table 4.3: Crystal data and structure refinement for 129	159

List of Figures

Figure 1.1:	Views of Cu-dependent 2,3-quercetin dioxygenase active site from <i>Aspergillus japonicus</i> (PDB entry: 1JUH).....	5
Figure 1.2:	Modeled views of ARD' and ARD active sites	13
Figure 1.3:	SLO-1 active site (waters not shown, PDB entry: 1YGE).....	19
Figure 2.1:	X-ray ORTEP diagram of 31 ·3HCl	35
Figure 2.2:	X-ray ORTEP diagram of 52	39
Figure 2.3:	X-ray ORTEP diagram of 71	46
Figure 3.1:	NOESY experiment on 100	81
Figure 3.2:	LUMOs of 98 and 100 , isocontour at 0.08 au	85
Figure 3.3:	X-ray ORTEP diagram for the dication of 104	89
Figure 3.4:	Binding modes of 73	90
Figure 4.1:	Side and top views of the PM3-minimized structure of 73 ·FeCl ₂	118
Figure 4.2:	Side and top views of the PM3-minimized structure of 106 ·FeCl ₂	118
Figure 4.3:	New design of the N ₃ O-donor ligand	127
Figure 4.4:	NOESY experiment on 122	130
Figure 4.5:	X-ray ORTEP diagram of 127 (unrefined)	132
Figure 4.6:	X-ray ORTEP diagram of 129	136
Figure 4.7:	Views 2,3-QD·QUE (left) and 129 (right)	138

Abstract

Metalloenzymes catalyze various reactions and in particular dioxygenases insert dioxygen into organic substrates. Since these enzymes usually utilize histidines as ligands for the metal cofactor, we focused our attention on the 3-His-1-carboxylate binding motif as it has been shown recently to be a common feature of the cupin superfamily. Most structural and functional models studied substitute the imidazole rings by pyrazoles, pyridines and alkyl amines to simplify the synthetic challenge. However, the different donor/acceptor properties and basicity of imidazole render these models inaccurate. We therefore developed the synthesis of imidazole-containing ligand mimics of the 3-His-1-carboxylate motif. The synthesis of the known tris[(4)-imidazolyl]carbinol, 4-TIC **31**, a mimic of the 3-His binding motif, was improved and optimized making this ligand now easily accessible on gram scale. This access allowed us to characterize its 2:1 complex with iron (III) **52** by X-ray crystallography, the first crystal structure of a metal complex incorporating 4-TIC.

Moreover, we also report the synthesis of a functionalized mixed tripodal unit bearing a short side-chain **73**. Its coordination chemistry has been explored and a 2:1 cobalt complex was prepared and characterized by X-ray crystallography **104**. The coordination properties of the ligand can be described as an N₂O-donor. We also expanded the synthetic route to incorporate an extended side-chain onto a mixed tripodal unit **106**. However, the coordination chemistry was difficult due to the low solubility of the ligands in polar aprotic organic solvents and its propensity to form intractable solids when mixed with metal ions. We thus optimized the ligand design and synthesized **105** with a N₃O

binding mode with Cu (II) and characterized complex **129** by X-ray crystallography. Complex **129** is the first structural model complex of the 2,3-quercetin dioxygenase incorporating all three imidzoles and a carboxylate functional group and is compared to the active site of the enzyme.

Chapter 1

The 3-His-1-Carboxylate Binding Motif in Dioxygenases

1.1 Introduction

The selective oxidation of hydrocarbons, a thermodynamically favored but kinetically disfavored process, is catalyzed by many enzymes *via* dioxygen activation. Most enzymes utilize a metal cofactor in order to circumvent the spin forbidden process of reacting molecular oxygen in a triplet state with organic substrates. The metal cofactor, with an open-shell electronic structure, can directly activate/reduce dioxygen by its coordination or activate the substrate leading to the formation of some radical character on the reactant, which can then react with O₂. The binding of the metal cofactor is often achieved by poly-histidiny motifs, and the 2-His-1-carboxylate triad is generally considered to be the canonical motif of mononuclear nonheme iron oxygenases.^{1,2} However, rather than a general motif, it has recently been revised as a subset of a much larger binding mode observed in the cupin superfamily.³ Based on primary structure homology and tertiary structure, one can regroup enzymes into a superfamily displaying a given number of commonalities. These structurally related proteins found in plants, microbes and higher organisms seem to exhibit two highly conserved motifs: G(X)₅HXH(X)_{3,4}E(X)₆G and G(X)₅PXG(X)₂H(X)₃N. The first β-strand contains two histidines and a glutamic acid residue which are complemented by a third histidine from the second β-strand, thus providing as a whole a recurring metal

binding site throughout the cupin superfamily.⁴ The 2-His-1-carboxylate triad can then be derived by replacing one the histidines of the first strand by Gln or Asp/Glu.⁵ The existence of the cupin superfamily was hypothesized and confirmed by the study of germin and germin-like proteins (GLP). The cupin functions are multiple and display a wide array of activities such as isomerization and epimerization. Germin, an archetypal representative of the cupin superfamily,⁶ possesses a Mn^{II} center with oxalate oxidase^{7,8} and superoxide dismutase (SOD) activities. Germin's active site Mn is octahedral with the His₂GluHis tetrad coordinating bi-facially, as determined by X-ray crystallography. This mode of coordination is very different from the classical Mn-SODs, which do not have a trans carboxylate ligand to histidine.⁹ This coordination specificity was further corroborated by structures of Barley oxalate oxidase,¹⁰ and a manganese dioxygen-dependent oxalate decarboxylase from *Bacillus subtilis*.^{11,12}

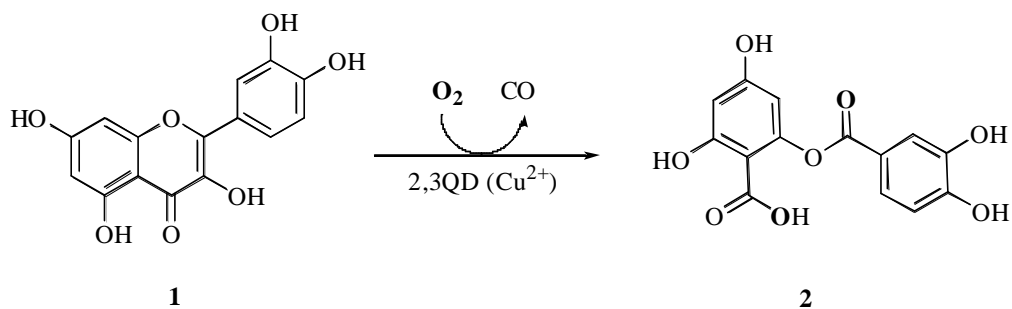
Since we were interested in emulating the unusual reactivity of metalloenzymes by developing biomimetic catalysts and exploring accurate mimics of the important recurring 3-His-1-carboxylate binding mode, we focused our attention on dioxygenases known to activate and insert dioxygen into organic substrates. In the next sections we will detail structures, mechanisms and model studies of three enzymes: 1) quercetin 2,3-dioxygenases, 2) acireductone dioxygenases, both from the cupin superfamily, and 3) the important lipoxygenases which also display the 3-His-1-carboxylate tetrad and have recently attracted the attention of bioinorganic chemists. Spectroscopic and functional models of these poly-histidinyl metalloenzymes have been developed, though very few incorporate poly-imidazole ligand sets. Our work will expand the known models by utilizing imidazole ligands as accurate mimics of histidines. We will develop in the second

chapter our efforts in integrating them into the synthesis of a 3-His-1-carboxylate mimic. We initially improved the synthesis of the known tris[4(5)-imidazolyl] carbinol (4-TIC) ligand and investigated its coordination properties with iron (III) as a 3-His mimic. We further investigated the functionalization of 4-TIC and discovered that the carbinol carbon was prone to substitution reactions under acidic conditions. We will also detail our efforts to incorporate the carboxylate moiety into the tripodal unit and report on the coordination properties of two different 3-imidazole-1-carboxylate ligands. The results obtained allowed us to propose a new ligand design and to synthesize a copper (II) complex with a tetradentate N₃O-donor ligand. This complex is the first structural model of copper-dependent quercetin 2,3-dioxygenase utilizing only imidazoles as nitrogen-donors and a carboxylate side-chain.

1.2 Cu-dependent quercetin 2,3-dioxygenases

1.2.1 Introduction and background

Quercetin 2,3-dioxygenases catalyze the oxygenolysis of two carbon-carbon bonds in quercetin **1** (scheme 1.1) by a metal-promoted insertion of dioxygen. This reaction, calculated to be 88.9 kcal/mol exothermic,¹³ is only reproducible in the laboratory under harsh conditions,¹⁴ illustrating the kinetic inertness of triplet oxygen with organic substrates. Fungi, known to survive on these types of substrates as a sole source of carbon and energy, utilize quercetinases to catalyze the reaction of dioxygen and quercetin **1** yielding 2-(3,4-dihydroxy-benzoyloxy)-4,6-dihydroxy-benzoic acid **2** and carbon monoxide (scheme 1.1).



Scheme 1.1

Quercetin 2,3-dioxygenases have been isolated with different metals, for example:

- i) Quercetin 2,3-dioxygenase from *Bacillus subtilis* was initially isolated as an Fe^{2+} containing enzyme^{15,16} but is active with a wide variety of metals: Mn^{2+} , Co^{2+} , Ni^{2+} , Cu^{2+} . As iron (II) fails to fully restore the apo-protein¹⁷ manganese (II) is considered to be the native metal cofactor.¹⁸
- ii) Quercetinase QueD of *Streptomyces* sp. FLA exhibits a preference for cobalt (II) and nickel (II).¹⁹
- iii) Quercetin 2,3-dioxygenase from *Aspergillus japonicus* is a copper (II)-containing quercetinase. The copper (II)-dependent quercetinases' active site structure and mechanism is well studied and model complexes in biomimetic reactions are reviewed in details within the next section.

1.2.2 Structure

The presence of copper (II) in quercetin 2,3-dioxygenases has been definitively demonstrated^{20,21} and extensively characterized in quercetinase from *Aspergillus niger*, for example.²² The crystal structure of quercetin 2,3-dioxygenase from *Aspergillus japonicus* was solved at 1.6 Å resolution and reported as a dimer displaying two type 2 mononuclear copper centers (figure 1.1). The first center has

a distorted tetrahedral coordination environment with three histidines and a water around copper (II), representing approximately 70% of the conformations. A minor conformation shows a glutamic acid coordinated to the copper center, forming a trigonal bipyramidal structure, with three histidines and the glutamate coordinated (the first carboxylate ligand observed in natural copper-containing proteins). This heterogeneous environment is also found in solution.²³

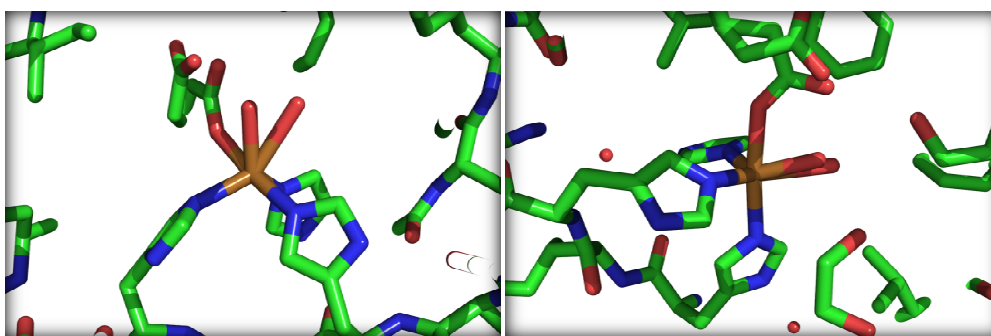
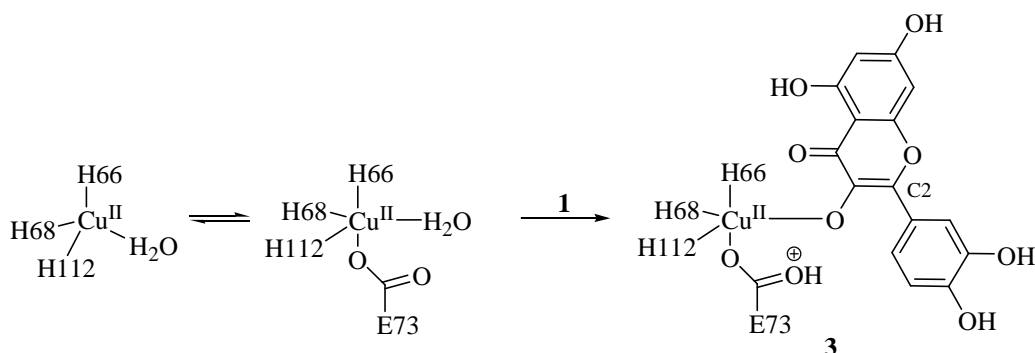


Figure 1.1: Views of Cu-dependent 2,3-quercetin dioxygenase active site from *Aspergillus japonicus* (PDB entry: 1JUH). 3-His-1-Asp copper center with a water molecule bound.

1.2.3 Catalytic mechanism

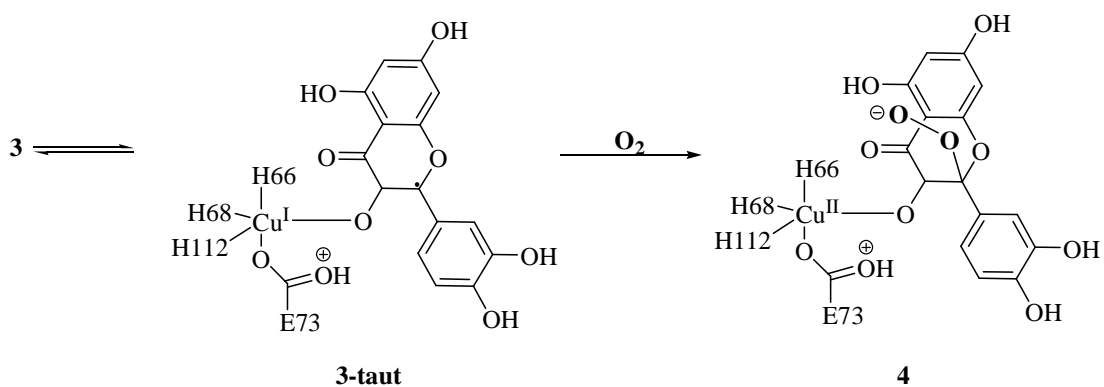
Quercetin 2,3-dioxygenase from *Aspergillus japonicus* was crystallized with quercetin in its active site, allowing the detection of potential interactions between the enzyme and its native substrate. The displacement of a molecule of water by quercetin leads to a single penta-coordinated copper center as demonstrated by EXAFS (Extended X-ray Absorption Fine Structure).²⁴ Quercetin monodentate coordination to copper through its C3 hydroxyl group (C3-OH) is unequivocally confirmed by X-ray structure and the newly formed complex is square pyramidal with some bipyramidal distortion. Constraints of the active site on the substrate is

also noticeable, as carbon C2 is pyramidalized (scheme 1.2), thus increasing its sp^3 character and potentially promoting a carbon-centered radical mechanism. Moreover the coordinated glutamate (Glu-Cu= 2.55 Å) is within hydrogen bond distance to the 3-hydroxy group of quercetin. From these observations the proposed mechanism of the reaction is initiated by a glutamate mediated deprotonation of quercetin, glutamic acid maintaining the proton at proximity until the final step (scheme 1.2). This initial step is supported by: 1) a deflation of the pKa upon copper binding (flavonol is partially deprotonated at pH= 7 in water), and 2) the mutation of Glu73 to Gln results in a 1000-fold loss of activity.



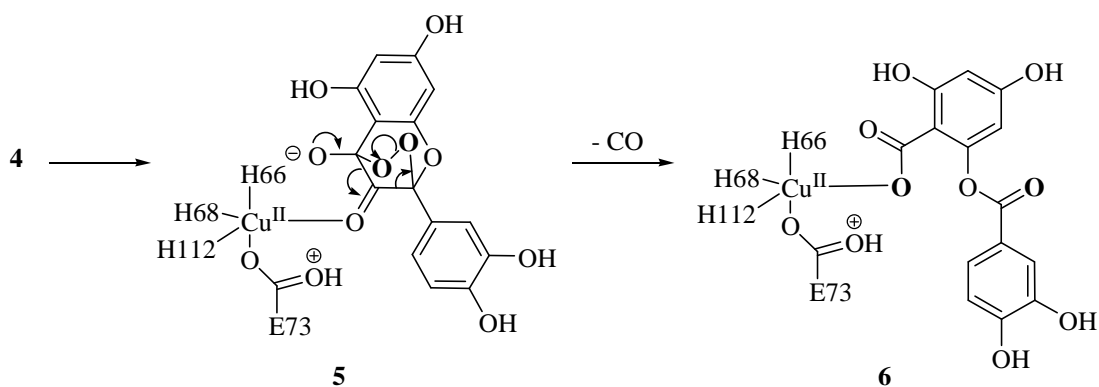
Scheme 1.2

The second step invoked is a valence tautomerism of **3** to **3-taut** (scheme 1.3), in order to circumvent the spin forbidden process.²⁵ It consists of the transfer of a single electron from the substrate to copper, thus producing a Cu^I -flavonoxyl radical, though it was not detected by EXAFS (Extended X-ray Absorption Fine Structure).²⁴ The radical centered on C2 of quercetin **3-taut** is directly attacked by dioxygen, which diffuses to the active site through a putative hydrophobic channel to form **4**.²⁶



Scheme 1.3

An alternative mechanism, wherein dioxygen is initially activated by copper (I) has been proposed based on gas phase calculations,¹³ but analysis of O_2 activation by a copper (I)-substrate radical was not supported by modeling studies in the enzyme's active site, and an intradiol type mechanism is favored.^{27,28} The following step finalizes the formal 1,3 addition (scheme 1.4) to give **5**.

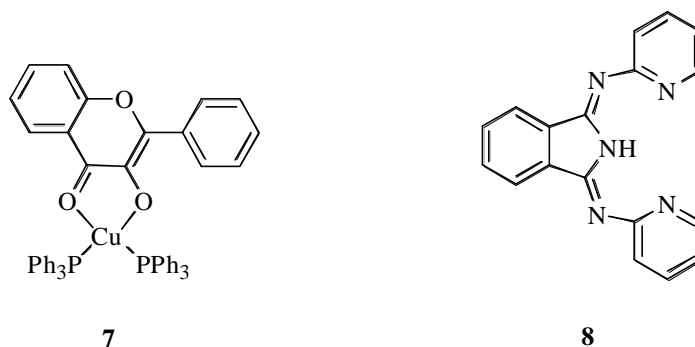


Scheme 1.4

The intermediate **5** decomposes to the desired compound **6** and the proton, removed in the first step, is transferred back to product **6** to give **2**.

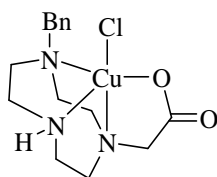
1.2.4 Structural and functional models

Structural and functional model complexes have been synthesized and studied for quite some time, as they could potentially provide insight into enzyme catalysis, but also as potential catalyst for bioremediation of aromatic and heteroaromatic waste products. Copper complexes catalyze the reaction of dioxygen with flavonol or quercetin.²⁹⁻³² The first fully characterized functional model of quercetin 2,3-dioxygenase is $\text{Cu}(\text{PPh}_3)_2\text{fla}$ **7** (fla= flavonolate anion) **7** (scheme 1.5). The tetrahedral copper (I) complex is competent in the oxygenolysis of flavonolate and shown to correctly incorporate labeled dioxygen and release carbon monoxide. This reaction likely proceeds *via* dioxygen activation by a Cu^{I} center.³³ The 1,3-bis(2-pyridylimino)isoindoline (IndH) ligand **8** (scheme 1.5) was also used with Cu^{I} and Cu^{II} to form flavonolate^{34,35} complexes as functional models.



Scheme 1.5

The most relevant copper (II) complex, **9**, incorporating a N_3O -donor set, is a functional model with a moderate turnover rate of 6 per hour at 90 °C in DMF (scheme 1.6).³⁶ Interestingly external carboxylate ligands have been reported elsewhere to enhance catalysis rates.^{37,38}



9

Scheme 1.6

Conclusion

The structural models, including **7-9**, are very approximate, which is reflected in the lack of a good spectroscopic model of the enzyme's active site. The critical steps of the mechanism have not been addressed by the model chemistries and a better understanding of the regioselectivity of the electrophilic attack by dioxygen is necessary. Ultimately any single model might not be able to fully explain the regioselectivity as the mechanism in bulk solvent is likely to differ greatly from the enzymatic one. Also the selectivity of the 1,2 versus the 1,3 addition of dioxygen on the quercetin core is also intriguing as the 1,2 addition, not leading to the desired products, was calculated to be energetically favorable. The functional models are competent but a lot of room remains for improvements, as the reaction was limited to DMF and high temperatures were required (70 to 100 °C).²⁹⁻

36

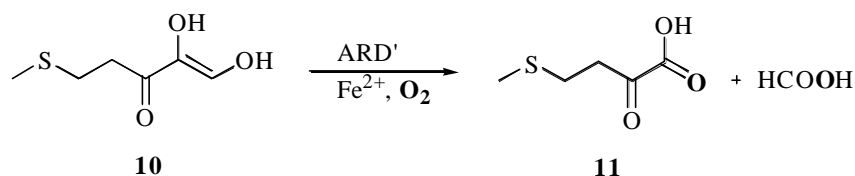
1.3 Acireductone Dioxygenase

1.3.1 Introduction and background

In the methionine salvage pathway, the penultimate step is the dioxygenation of acireductone by AciReductone Dioxygenase (ARD'). Two

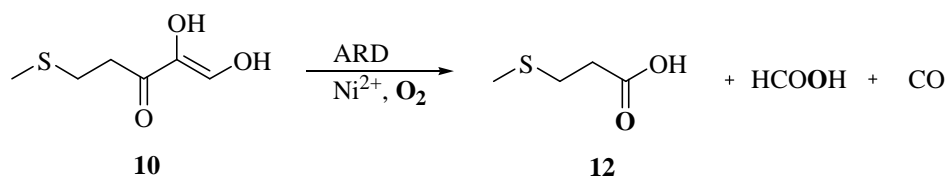
monomeric forms exist and share the same polypeptide chain but differ in their metal content. Iron (II) and nickel (II) impart very different physical and chemical properties to the protein, and either enzymatic activity could be reconstituted from the apo-protein by incubation with the appropriate metal. They were chromatographically separated and have distinct catalytic activity.

ARD', an iron (II) containing enzyme, catalyzes an on-pathway 1,2 oxygenolytic decomposition of acireductone, **10**, to yield the α -keto acid precursor **11** to methionine (scheme 1.7). Dioxygen labeling proved the incorporation of both oxygen atoms into the formate and the keto-acid products.³⁹ The enzyme could still catalyze this reaction when reconstituted with Mg^{2+} ions, albeit with lower activity.^{40,41}



Scheme 1.7

The nickel (II)-containing protein ARD catalyze an off-pathway reaction, *via* a 1,3 oxygenolysis, producing 3-methyl thiopropionate, **12**, formate and carbon monoxide (scheme 1.8).^{40,42,43} The enzyme's activity was conserved when nickel was replaced by Mn^{2+} and Co^{2+} , albeit with a lower activity. Labeling studies with dioxygen showed that ARD incorporates both oxygen atoms into formate and **12**.³⁹



Scheme 1.8

1.3.2 Structure

The nickel and iron containing enzymes seem to possess approximately the same octahedral coordination with exactly the same ligands. Both use the same residues of the polypeptide chain, three histidines and a glutamate in a pseudo octahedral environment, with one or two unknown remaining ligands.

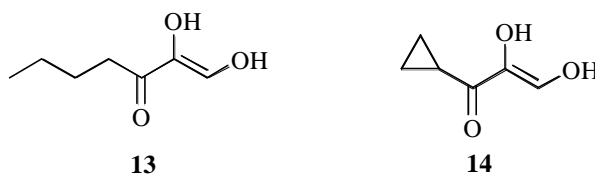
The structure of ARD from *Klebsiella* ATCC 8724 was determined in solution by NMR experiments, and is consistent with a Ni²⁺ center coordinated by the cupin superfamily motif: 2-His-Glu-His.⁴⁴⁻⁴⁶ The structure was further refined and confirmed by XAS (X-ray Absorption Spectroscopy) to obtain a clearer picture of the paramagnetic nickel (II) coordination. EXAFS analysis points to 3 or 4 His and 2 or 3 other O/N ligands.^{47,48}

ARD' coordination environment was determined by XAS including EXAFS and XANES (X-ray Absorption Near Edge Spectroscopy) which also support an octahedral geometry.⁴⁹

A partial structure of a related ARD or ARD' (metal unknown) from *Mus musculus* has been resolved by X-ray crystallography, but two ligands on the metal center remain unknown.⁵⁰

1.3.3 Catalytic mechanism

XAS analysis of substrate binding in both enzymes supports the displacement of two ligands one of which is thought to be a histidine.^{47,48,51} The mechanisms of ARD and ARD' were probed by using a monoanionic desthio analogue, **13** ($\lambda_{\text{max}} = 305 \text{ nm}$, $\epsilon = 20000 \text{ M}^{-1} \text{ cm}^{-1}$, $\text{pK}_{\text{a}1} = 4.0$ and $\text{pK}_{\text{a}2} = 12.2$; scheme 1.9)⁵² binding the metal center as a dianionic ligand causing a similar shift in the λ_{max} for both enzymes ($\lambda_{\text{max}} = 345 \text{ nm}$, $\epsilon = 14000 \text{ M}^{-1} \text{ cm}^{-1}$). Moreover, a cyclopropyl analogue **14** inhibited both enzymes under aerobic conditions. Based on these results a radical mechanism was proposed.⁵²



Scheme 1.9

The apparent metal-guided selectivity is tentatively rationalized by the pocket's size and shape of the active site, which is subtly controlled by the metal coordination. The iron containing enzyme allows for an extended substrate conformation (figure 1.2 and scheme 1.10) and thus a 1,2 coordination of the substrate, **10** (5 membered chelate), is hypothesized prior to an electron transfer to O_2 . In the nickel form, bulk within the pocket enforces a 1,3 coordination of **10** (figure 1.2 and scheme 1.10) prior to an electron transfer to O_2 (scheme 1.10).⁴⁹

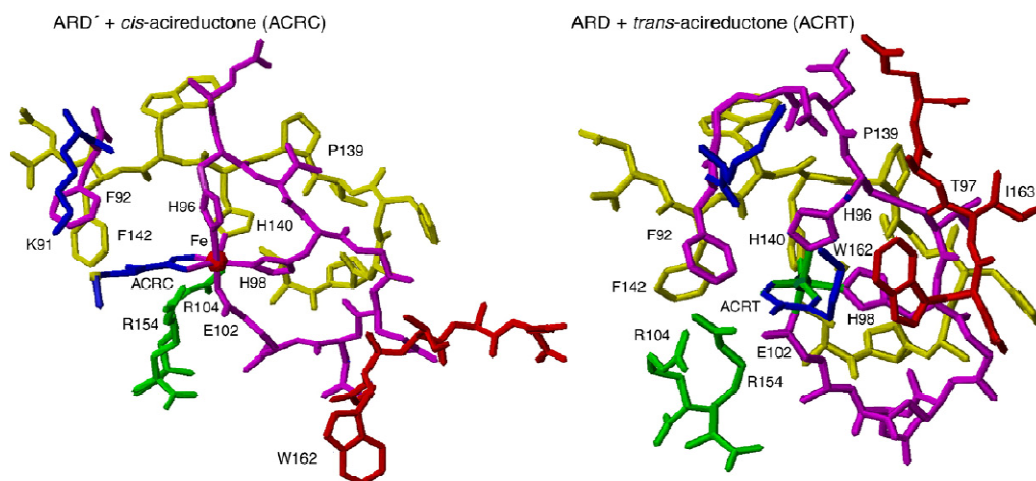
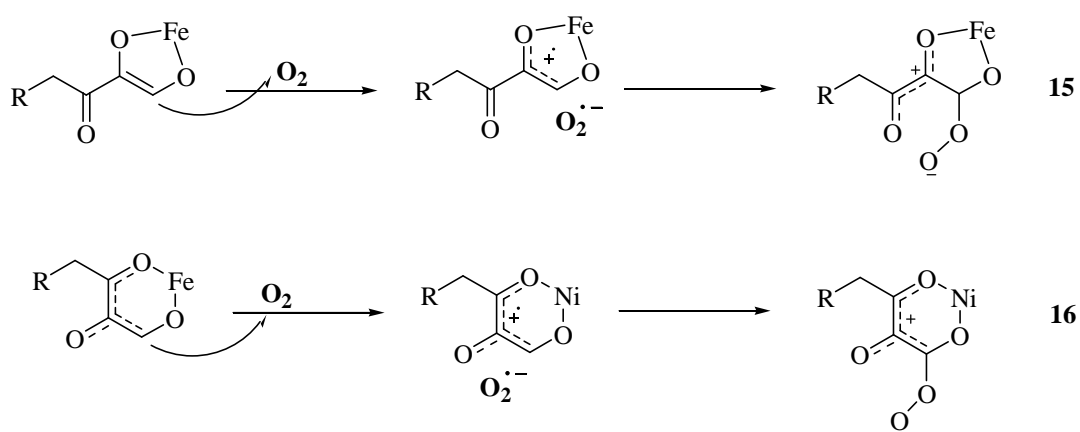
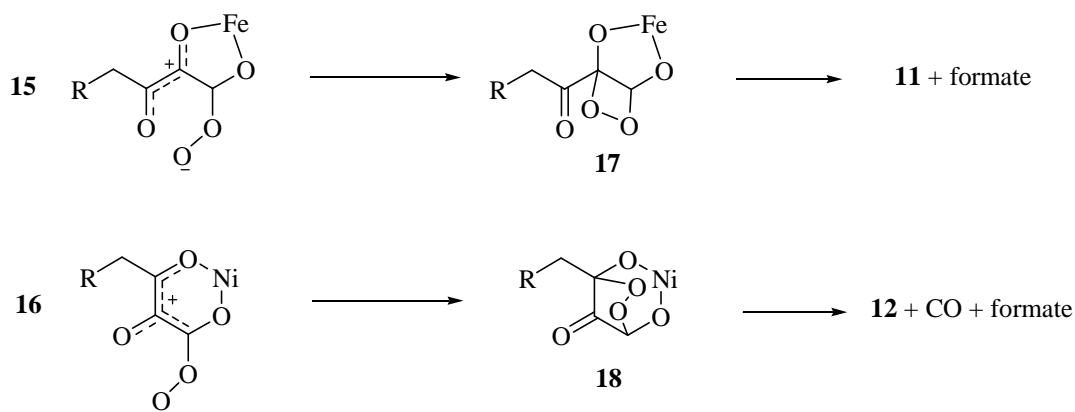


Figure 1.2: AMBER modeled views of ARD' and ARD active sites⁴⁹



Scheme 1.10

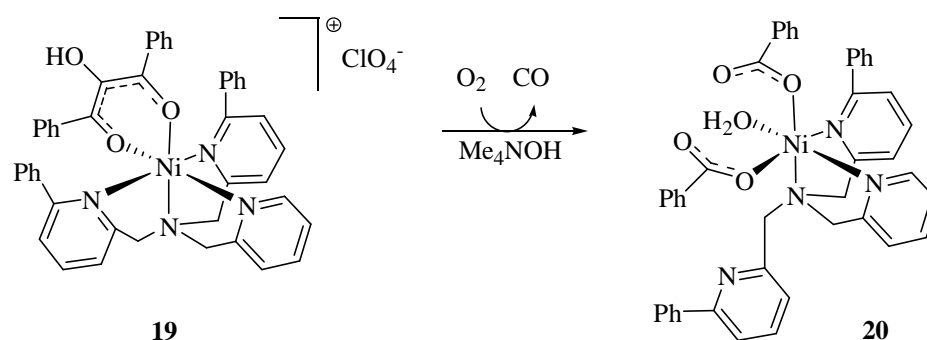
Recombination of the radicals produces peroxide, **15** or **16**, that either attacks in a 1,2 fashion, in the case of a 5 membered ring chelate to form **17**, or in a 1,3 fashion for a six membered ring chelate to form **18** (scheme 1.11). Both intermediates lead after decomposition to their respective products.



Scheme 1.11

1.3.4 Structural and functional complexes

Octahedral Ni(II) complexes containing four nitrogen donors were synthesized and characterized by X-ray crystallography and their solution structure confirmed by NMR spectroscopy and conductance.⁵³ These complexes are primarily based on aryl-appended *tris*((2-pyridyl)methyl)amine ligands which have been very successful in coordination chemistry.⁵⁴ The first and excellent functional model of Ni ARD was produced by L. M. Berreau who characterized a mixed ligand-monoanionic substrate analogue complex **19** (scheme 1.12).



Scheme 1.12

The X-ray structure showed symmetrical bidentate binding of the substrate through O1 and O3, diagnostic of a fully delocalized anion. The absorption spectrum displayed a $\lambda_{\text{max}} = 399 \text{ nm}$ and $\epsilon = 2400 \text{ M}^{-1} \text{ cm}^{-1}$. Upon addition of one equivalent of base a shift in the absorption was observed ($\lambda_{\text{max}} = 420 \text{ nm}$ and $\epsilon = 2500 \text{ M}^{-1} \text{ cm}^{-1}$) and labeling studies showed incorporation of oxygen atoms at C1 and C3 from dioxygen to yield the complexed carboxylic acids **20** and carbon monoxide.^{55,56}

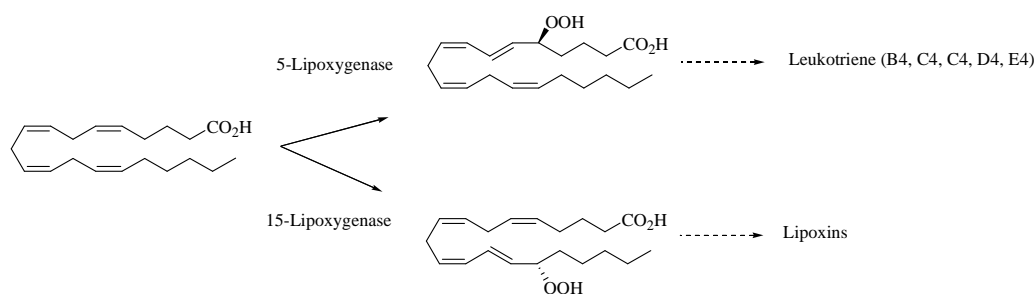
Conclusion

The study of biomimetic Ni-ARD complexes is an emerging new field which should lead to a better understanding of the enzyme's mechanism. The work done by L. M. Berreau is a good example on how a model complex can give important insights into the enzymatic reaction. The coordination mode of the model substrate led to a refined mechanism by biochemists and further studies of these complexes should reveal even more details. Important points remain to be addressed *via* concerted efforts on the biochemical and small molecule modeling fronts. A definitive identification of the displaced ligands would further our understanding of the enzymatic reaction. A comparison of the acid-base reaction in copper-dependent quercetinase is interesting, as the deprotonation of the monoanionic acireductone, much more difficult than neutral quercetin, may require histidine, a stronger base than glutamate. This scenario is consistent with experimental observations. The second step is also dramatically different from copper quercetinase where no valence tautomerism is considered, and a radical superoxide has been implicated. The low oxidation state of iron and the redox inertness of nickel are probably responsible for this type of mechanism.

1.4 Lipoxygenases

1.4.1 Introduction and background

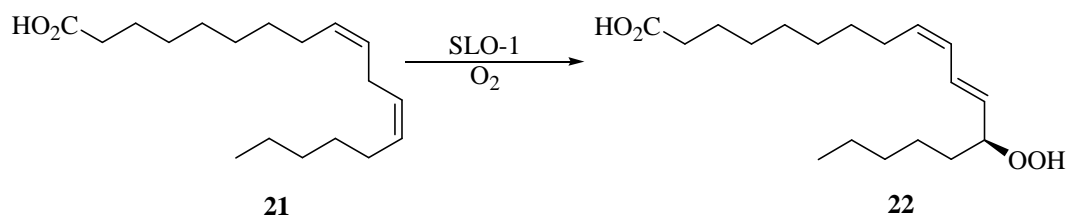
Lipoxygenases are mononuclear non-heme iron enzymes catalyzing the regiospecific and stereospecific insertion of dioxygen into fatty acids. These dioxygenases are found in mammals, higher plants and even fungi. Their isolation and implication in the inflammatory response⁵⁷ and cancer growth regulation in humans led to an increased effort in the elucidation of their structures and their mechanisms of action.⁵⁸ The arachidonic acid cascade is essentially divided into two pathways (scheme 1.13): 1) the cyclooxygenase pathway which leads to the production of prostaglandins (not shown) and 2) the lipoxygenase pathway involved in the synthesis of lipoxins and leukotrienes. These primary metabolites are implicated in vaso and broncho-constriction and granulocyte chemotaxis.⁵⁹ Leukotrienes are synthesized from arachidonic acid by insertion of dioxygen to the C5 position by 5-Human Lipoxygenases (5-HLO) which are denominated by the position activated on the arachidonic acid skeleton; whereas lipoxins are formed by insertion of dioxygen to C15 and C5 by respectively 15-HLO and 5-HLO. 12-HLOs have also been involved in lung cancer growth.⁶⁰



Scheme 1.13

The soybean lipoxygenases (SLO) are isolated and purified from soybean seeds, where they are found in high concentration. To date three different forms have been isolated: SLO-1, SLO-2 and SLO-3. SLOs have been implicated in growth regulation, wound repair, and pest resistance. They also show some antimicrobial and antifungal activity.⁶¹ SLOs are water soluble globular enzymes and possess a single polypeptide.⁶² The stability and ease of purification of soybean lipoxygenase-1 (SLO-1) has made it a representative model of the whole family and by extension a model enzyme for the mammalian lipoxygenases. SLO-1 specifically oxidizes the 1,4-diene motif of linoleic acid but was also competent in the catalysis of monounsaturated fatty acids yielding enones.⁶³

In the particular case of SLO-1, linoleic acid **21** was oxidized to 13(*S*)-hydroperoxy-9,11-octadecadienoic acid (13-HPOD) **22**, with the specific feature of adding dioxygen antarafacially to the hydrogen abstracted by the enzyme (scheme 1.14).⁶⁴



Scheme 1.14

The enzyme was isolated in its ferrous state and exhibited a lag time, during which a non-enzymatic oxidation of the diene by dioxygen produced hydroperoxyacids, which have been shown to activate the enzyme by oxidizing iron (II) to iron (III).⁶⁵ The high spin ferric form, or yellow form, exhibited an axial ($g \sim 6$, $S = 5/2$) EPR

signal and is a yellow chromophore ($\lambda_{\text{max}} = 350 \text{ nm}$, $\epsilon = 2000 \text{ M}^{-1} \text{ cm}^{-1}$). This absorption is attributed to a charge transfer from a hydroxide ligand to iron (III).⁶⁶ Interestingly when an excess of 13-HPOD **22** was used a purple form was produced with a rhombic signal for its EPR spectrum.⁶⁷ The enzyme is considered to be a fast enzyme with a $k_{\text{cat}}/K_{\text{m}} = 3.10^7 \text{ M}^{-1}\text{s}^{-1}$,⁶⁸ and multiple kinetic studies have established the rate limiting step of SLO-1, at temperatures greater than 32 °C, to be the cleavage of the doubly activated C-H bond. An unusual kinetic isotope effect was also reported and measured to be around 80.⁶⁹⁻⁷¹ This unusually large kinetic isotope effect and its little temperature dependence raised the possibility of a quantum mechanical tunneling pathway which was also observed in the human 15-HLO (KIE= 47 ± 7).⁷²

1.4.2 Structure

The structure of SLO-1 has been elucidated by X-ray crystallography (figure 1.3).⁷³⁻⁷⁵ In its ferrous form a distorted octahedral active site was found, with a first coordination sphere composed of: 1) three histidines, His499, His504 and His 690, bound through their N ϵ 2 atom 2) a terminal iso-leucine, Ile839, and 3) a molecule of water. A loosely bound asparagine, Asn694, at 3.0 Å from the ferrous center completes the first coordination sphere and enforces an octahedral geometry (figure 1.3). A similar crystal structure of SLO-3⁷⁶ is also available as well as a rabbit 15-LOX which display four histidines, rather than an asparagine.⁷⁷

Asparagine 694 is partially coordinated to the ferrous center resulting in two coordination modes: five and six coordinates (5C/6C) in a ratio of approximately 60/40. The enzyme achieves this state of loose binding by controlling the orientation of Asn rather than restricting its approach to the metal.⁷⁸ It is involved in

an extended hydrogen bond network, which could be disrupted by single point mutation or addition of a low molecular weight alcohol inducing a change in the populations of 5/6C.^{79,80} The ferric state is only a 5C center and the presence of the hydroxide, a strong donor, with a short Fe-OH bond (1.9 Å) was confirmed by EXAFS.⁸⁰

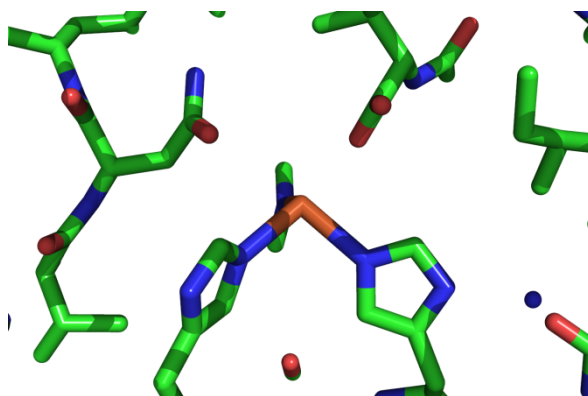


Figure 1.3: SLO-1 active site (waters not shown, PDB entry: 1YGE). H499, H504, H690 and terminal isoleucine coordinating Fe(II), water not shown.

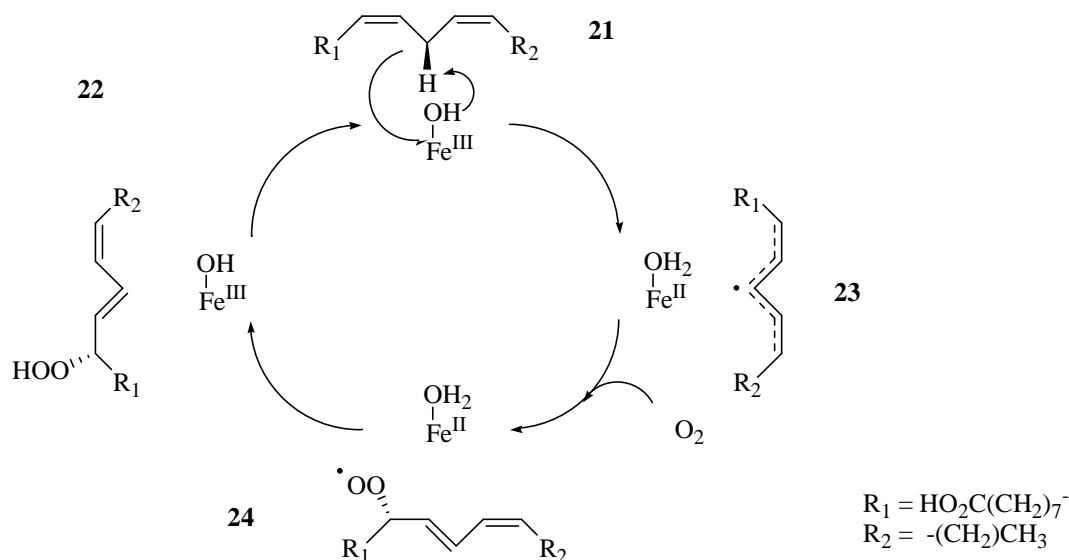
1.4.3 Catalytic mechanism

Three different mechanisms⁸¹ were initially proposed, but a consensus has been reached and is supported by experimental data and computational studies.⁸² The initial step is the abstraction of the doubly activated allylic hydrogen of linoleic acid **21** to form a pentadienyl radical moiety **23** (scheme 1.15).⁸³ This hydrogen abstraction has been calculated to be exothermic by approximately 12.6 kcal/mol. The iron (III) hydroxide motif is significantly different from the high valent oxo-iron center usually invoked in nonheme iron enzymes, and was unambiguously shown to be responsible for hydrogen abstraction by kinetic studies.⁸⁴ SLO-1 has a high Fe^{II/III} reduction potential of 0.6 V (versus hydrogen)⁸⁵ and it is essential for

the catalytic efficiency. Raising the E° of the couple $\text{Fe}^{\text{II}}/\text{Fe}^{\text{III}}$ by diminishing the number of ligands is regarded as one of the main driving forces for the H-abstraction step. Moreover this model was supported by the study of mutants. N694H was produced and displayed an only six coordinate iron (III) center, histidine becoming a ligand for iron. The reduced catalytic activity is rationalized in terms of decreased reduction potential of the metal center.⁸⁶ Another singly mutated lipoxygenase N694C formed an only six coordinate iron center in its oxidized form, further corroborating the rational.⁸⁷

According to DFT calculations, as the hydrogen atom is shifted from carbon to oxygen no spin density develops on any of the three collinear atoms involved.^{78,82} However, the spin density manifests itself in the diene moiety and the iron center lending credence to a proton coupled electron transfer mechanism, the electron being directly transferred from the diene to the iron (III).⁷⁸ This step, suggested to occur *via* tunneling of the proton has elicited a vigorous debate in the literature as the role of the protein's motions and dynamics have been a point of contention.⁸⁸⁻⁹³

The product of the second step **24**, a peroxy radical, experimentally detected is the result of a direct addition of dioxygen to the pentadienyl radical. The calculated transition state (2 kcal/mol) is low lying and the process is exergonic by 8 kcal/mol.⁸² Under thermodynamic control in solution the dioxygenation of C9, C11 and C13 was reversible with a preference for C11⁹⁴ rather than C13, as observed in the enzyme. Single point mutagenesis revealed the importance of steric factors to the step's regioselectivity and a channel guiding the dioxygen's access to the organic substrate has therefore been proposed, thought to control the antarafacial addition to C13 to give **22**.^{95,96}



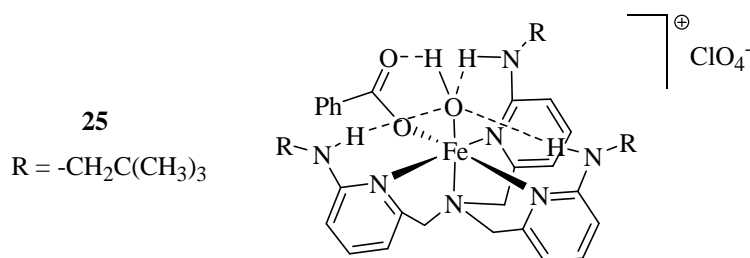
Scheme 1.15

The purple form, usually observed when an excess of hydroperoxide was present, is due to an alkylperoxo moiety coordinated end-on to the iron center, the structure of which has been confirmed by X-ray crystallography.⁹⁷ This metastable form of lipoygenase produced carbon centered and peroxy radicals⁸³ but also decomposed to regenerate the ferric form of lipoygenase and 13-(*S*)-HPOD **22** also obtained directly from **24**.

1.4.4 Structural and functional complexes

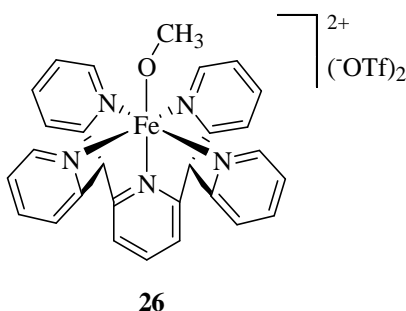
Initial reports of lipoygenase mimics modeled the histidine facial triad with polypyrazolylborate ligands, structurally different and undesirably negatively charged.⁹⁸ The synthetically challenging terminal ferric hydroxide motif presumed to be the catalytically relevant species, was produced by using tris-(6-neopentylamino-2-pyridinylmethyl)amine), tnpa. The distorted octahedral environment of the iron (II) complex **25** (scheme 1.16) provided two factors

important to the stability of the complex. The steric bulk of the neopentyl unit prevented polymerization and the hydroxide was stabilized by hydrogen bonding.^{99,100}



Scheme 1.16

Stack and co-workers^{101,102} have been successful in designing an iron complex **26** (scheme 1.17) displaying the desired iron (III)-methoxide motif, mimicking the hydroxide ligand in lipoxygenases. The ligand, composed of four pyridines, enforced a six coordinate square pyramidal structure with little differences between iron (II) or (III).



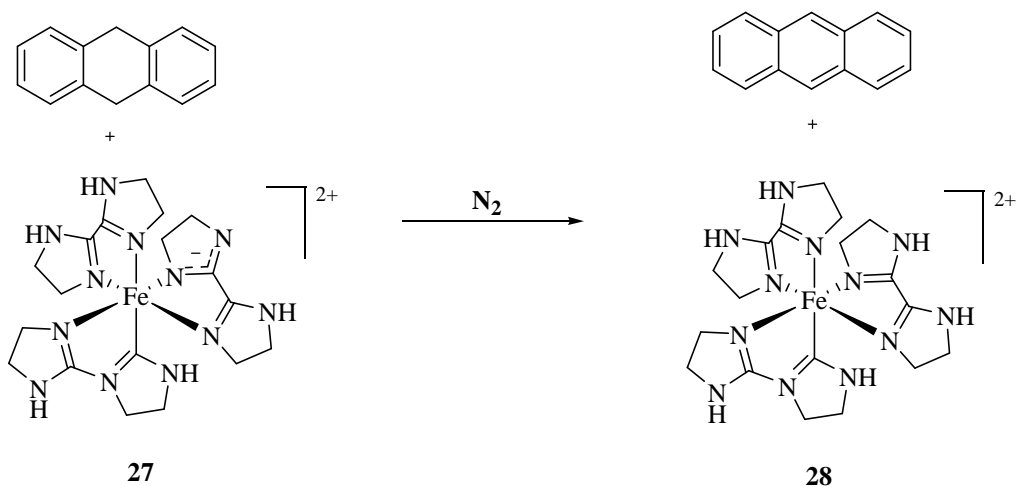
Scheme 1.17

One of the main features of the iron (III) complex **26** was its short Fe-O bond (1.782(3) Å) and its large Fe-O-CH₃ angle (165°) supporting the notion of multiple bond character between iron and oxygen. The redox potential of the high spin iron (III) complex was measured at 0.730 V vs. SHE. The complex abstracted hydrogen

atom from numerous substrate and followed kinetics consistent with a first order in the complex and substrate. The highest KIE measured with this complex is 6.5 with toluene, and a thermodynamic justification of the reaction was provided. Hydrogen atom abstraction reactions by organic compounds, transition metals^{103,104} and metal oxos¹⁰⁵⁻¹⁰⁷ follow the Polanyi relationship correlating the rates and activation parameters with the carbon-hydrogen bond strength. The driving force for hydrogen abstraction is generally reflected in the thermodynamic affinity for hydrogen, i.e. H^+ and e^- . A calculated bond dissociation energy for the Fe^{II} -HOME of 83.5 ± 2 kcal/mol made the iron (III) competent for hydrogen atom abstraction on 1,4 cyclohexadiene and exhibited a linear correlation between the $\log(k_{\text{reac}})$ and the bond dissociation energy (BDE).¹⁰²

A new type of manganese-dependent lipoxygenase was recently discovered and is mechanistically similar to SLO-1.¹⁰⁸⁻¹¹⁰ Using the same ligand, Stack *et al.* synthesized a Mn^{III} -OH complex which displayed the same general behavior as **26**. A redox potential of 0.81 V was measured and a bond dissociation energy of 82 ± 2 kcal/mol. The KIEs were lower and seemed to be less sensitive to BDE.¹¹¹ This complex was also compared to an Fe^{III} -OH complex obtained with a slightly modified ligand.¹¹²

A closely related work done by Mayer and co-workers¹¹³⁻¹¹⁵ investigated the ability of iron(III) (HBim)(H₂Bim)₂(ClO₄)₂ **27** (scheme 1.18) to abstract hydrogen atoms. The metal complex was competent and abstracted hydrogen atom from weak C-H bonds. The formation of an N-H bond estimated at 76 ± 2 kcal/mol was the driving force of the reaction.



Scheme 1.18

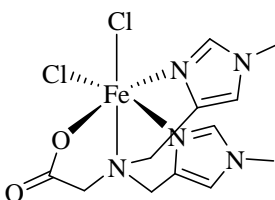
Conclusion

Lipoxygenases are fascinating enzymes and the hydrogen atom abstraction step has elicited an intensive and fruitful research in biochemistry, small molecule mimics and computational chemistry. However, the models studied did not utilize biologically accurate ligand sets and used mainly pyridines as substitutes for histidines. One of the major features of lipoxygenases not reproduced by models are the very large kinetic isotope effects, but structural models have reproduced the spectroscopic signatures of lipoxygenases and functional models have benefitted from a firmer reframed theoretical ground.

1.5 Conclusion

The three specific dioxygenases described here incorporate the 3-His-1-carboxylate binding motif and utilize either copper (II), nickel (II), iron (II/III). These enzymes all proceed by different type of substrate activation mechanisms allowing organic molecules to react with triplet oxygen. All structural and functional model complexes designed and synthesized for these enzymes avoid the utilization of the biomimetic imidazole ligands. The closest structural ligand **29**¹¹⁶

(scheme 1.19) of the 3-His-1-carboxylate motif, though designed to mimic superoxide dismutase active sites,¹¹⁷ only incorporate two imidazole units at the C2 position and a tertiary amine.



29

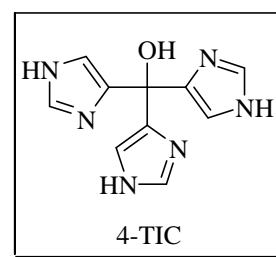
Scheme 1.19

The replacement of the third imidazole by an amino group, to simplify the synthesis, was likely not to reproduce accurately the binding environment and the electronic character of the metal. The scarcity of poly-imidazole ligand set stems from the difficulty of their syntheses and purifications, and the imidazoles are thus often replaced by aliphatic amines, pyridines or pyrazoles. However, such substitutes are structurally and electronically inaccurate and unlikely to reproduce the electronic character of the metal center. Structurally, only pyrazoles are good models as five membered hetero-aromatic rings, but are found to be stronger π and σ donors, as well as stronger π acceptors than histidine.¹¹⁸ All three nitrogen donor substitutes possess very different donor/acceptor properties *vis a vis* histidine and imidazole derivatives.¹¹⁸⁻¹²⁰ These different electronic properties are also reflected in the wide range of aqueous basicities: (pKa imidazolium, 7.0; pyrazolium, 2.5; pyridinium 5.2; tertiary ammonium 9-11) of the nitrogen donors. Therefore both the understanding of enzymatic catalysis and the design of efficient low molecular weight catalysts (functional models) would likely be improved by a faithful coordination environment. We therefore engaged in the synthesis of bio-accurate ligands possessing the N₃O-donor set.

Chapter 2

An Efficient Synthesis of the *Tris*[4(5)-imidazolyl]carbinol

(4-TIC) a 3-His Model



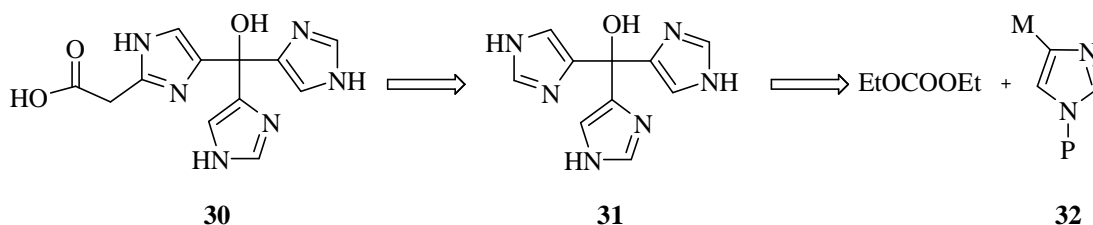
2.1 Introduction and background

2.1.1 Introduction

Hydrolytic and redox non-heme metalloenzymes generally utilize the binding properties of poly-histidinyl ligand sets to coordinate metals. In particular the three histidinyl nitrogen donor set is often found as part of the first coordination sphere in metalloenzymes active sites. Although many structural and spectroscopic models along with some functional models of poly-histidinyl-metalloenzymes have been prepared, very few incorporate the poly-imidazole ligand set. In order to address the lack of a good ligand set for the 3-His-1-carboxylate motif found in dioxygenases and the shortcomings of substitutes for imidazoles, we engaged in the design and synthesis of poly-imidazole ligands; and sought to produce biomimetic metal complexes with facial three histidinyl donor set functionalized by a carboxylate pendant arm.

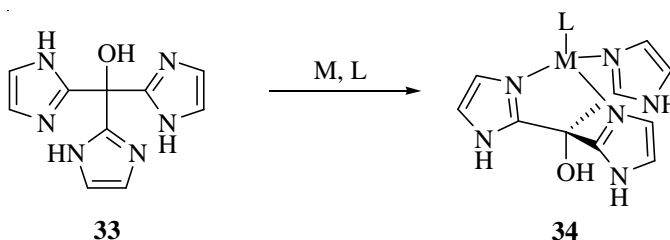
2.1.2 Background and retrosynthesis

The bi-facially coordinating ligand **30** was initially conceived as an extension of the tris[4(5)-imidazolyl]carbinol (4-TIC) (**31**, scheme 2.1) molecule first synthesized and reported by Breslow *et al.*¹²¹ This led us to consider the final target as the combination of two parts: a tripod and a pendent arm. The route to the desired ligand was divided into two stages: 1) a late stage functionalization of 4-TIC by appending the tether and 2) its synthesis utilizing imidazole as a starting material.



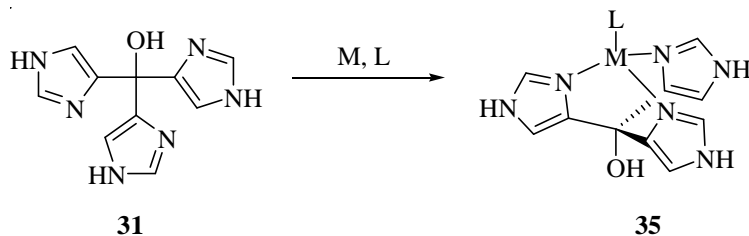
Scheme 2.1

The first synthetic challenge addressed was the synthesis of the tripodal unit as two different isomers could be envisaged (schemes 2.2 and 2.3). The first isomer possessing an all C2 point of attachment (2-TIC) **33** is much simpler to obtain than the all-C-4 carbinol (4-TIC) **31**.



Scheme 2.2

However, the all-C4 tripodal unit, though more difficult to access, was the one favored as it is a stronger binder and a better biomimetic model in its coordination for Zn^{2+} , Co^{2+} and Cu^{2+} .¹²¹



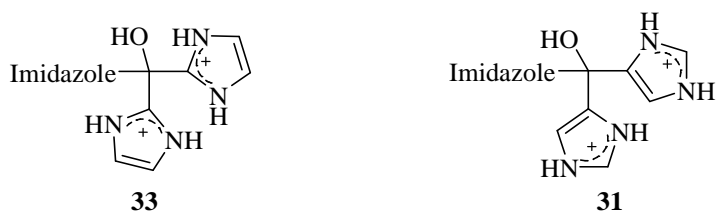
Scheme 2.3

These coordinating properties parallel the basicity of the ligands as 2-TIC, a weaker base than 4-TIC, is also a weaker complexing agent (table 2.1).

Compound	pK ₁	pK ₂	pK ₃
4-TIC	6.95	5.23	3.37
2-TIC	6.12	3.59	<1.5

Table 2.1: pK_a of 4-TIC and 2-TIC¹²¹

This observation was rationalized by electrostatic repulsion.¹²¹ Upon protonation or metal binding, positive charges develop on the nitrogen atoms of all three rings in close proximity, but for geometric reasons the charges on 4-TIC **31** are further apart and thus less destabilizing than on **33**.



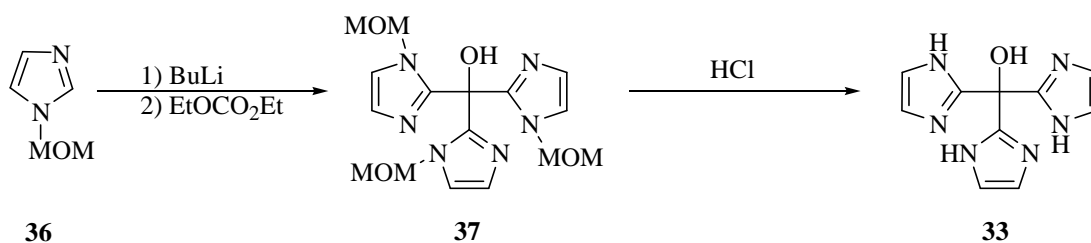
Scheme 2.4

The stronger binding affinity and biological relevance rendered the 4-TIC ligand more interesting and desirable.¹²¹ 4-TIC itself had already been reported and Collman's synthesis¹²² appeared to be especially well suited to our plan as the introduction of the pendent arm was simplified by an unprotected 2-position on the imidazole rings.

2.1.3 Syntheses of the 3-Imidazole subunit

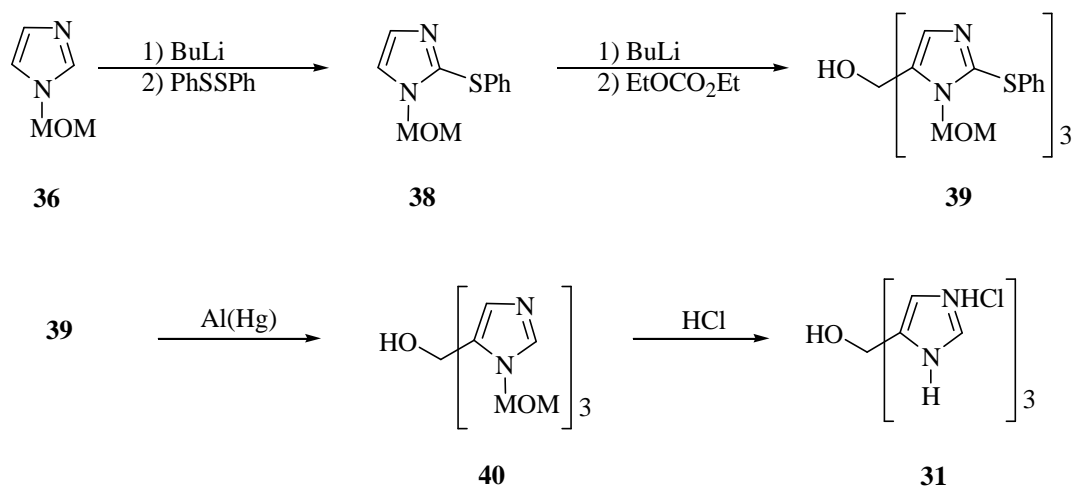
2.1.3.1 Breslow Syntheses

The syntheses of poly-imidazole ligands are few and far between with the initial work on imidazole based tripodal ligands reported by Breslow and coworkers.^{121,123} The 2-substituted tripod (scheme 2.5) was easily prepared in two steps by deprotonation by butyl lithium (BuLi) of the 2-position ortho-directed by the MOM protecting group **36**, followed by addition of diethylcarbonate. The MOM-protected 2-TIC **37** could then be deprotected under strongly acidic conditions to yield 2-TIC **33**.



Scheme 2.5

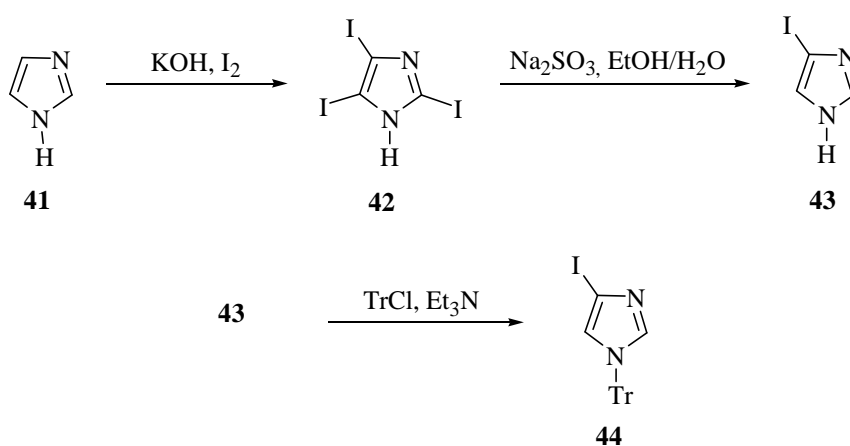
The synthesis of tris(4-imidazolyl)carbinol (4-TIC) (scheme 2.6) was more complicated than the 2-TIC isomer as the regioselectivity of 4-substitution was only achieved by protecting the 2-position of **36** by a thiophenyl group to yield **38**. The synthesis further employs the ortho-directing and protecting group MOM, which was critical in the deprotonation of the 5-position of **38**. Breslow *et al* reported that lithium diisopropylamine (LDA) was a sufficient base to deprotonate the C5 position, although reports elsewhere have advocated the replacement of LDA by BuLi as it appeared that LDA is an insufficiently strong base.¹²⁴ The organolithium thus formed was then trapped with diethylcarbonate to yield the tris(5-imidazolyl)carbonyl derivative **39**. The first deprotection step of the C2 position was effected by an Al(Hg) amalgam in low yield and it is important to realize that compound **40** obtained cannot be used for coordination chemistry as the tripod is linked at the C-5 position. It therefore must be further N-protected under acidic conditions to produce the desired 4-TIC. Synthesis of the target **31** was achieved in 5 steps (including the initial protection of imidazole) in 3-16% yield, but this route was deemed unsuitable for production of large amounts of the compound as reproduction with slight modifications did not substantially improve the yields.¹²⁴



Scheme 2.6

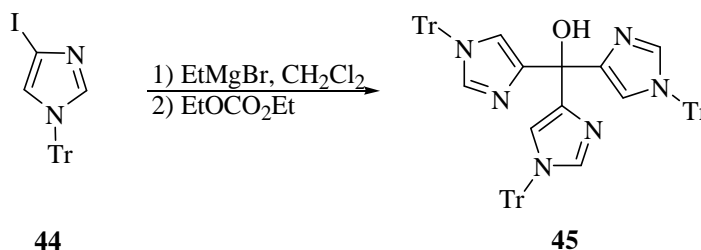
2.1.3.2 Collman Synthesis

A different approach to 4-TIC was developed by Collman *et al.*¹²² and utilized N-trityl-4-iodoimidazole as a key intermediate **44**, which was synthesized in three steps by an established procedure (scheme 2.7). Imidazole **41** was initially per-iodinated (**42**) and then selectively 2,4(5)-de-iodinated with aqueous sodium sulfite (**43**).¹²⁵ The protection of 4(5)-iodo-imidazole **43** with trityl chloride (Tr-Cl), a bulky protecting group, led to the formation of the 5-iodo regioisomer exclusively.¹²⁶



Scheme 2.7

The selective metal halogen exchange (scheme 2.8), only reported to proceed with iodine,¹²⁷⁻¹²⁹ produced the 4-substituted Grignard reagent.¹³⁰ Even with the 2-position unprotected the organomagnesium bromide formed is kinetically trapped in methylene chloride and does not rearrange to more stable isomers (i.e. 2 and 5). It was then reported to add to diethylcarbonate to directly form the 4-imidazolyl tripod **45**.



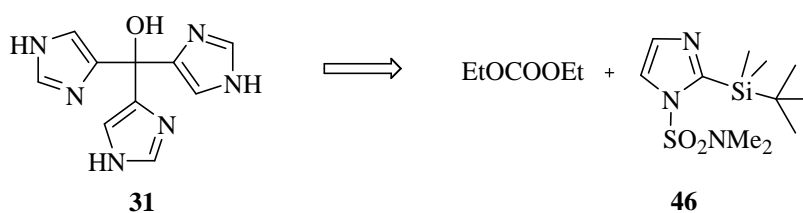
Scheme 2.8

In our hands two problems were encountered with the N-trityl protected 4-TIC synthesis. The use of iodine and the massive trityl protecting group was not conducive to large scale synthesis as they constitute most of the mass and once removed only a small quantity of the final product was obtained. Secondly, as illustrated in greater detail later, the sterically demanding trityl protecting group dramatically changed the reactivity of the substrate, and hindered most electrophilic attacks. These considerations guided the design of a more efficient and practical synthesis.

2.2 Results and Discussion

2.2.1 Introduction

Our approach (scheme 2.9) to 4-TIC was developed with the previous syntheses in mind and the goal to develop a practical and rapid route to 4-TIC. We envisioned obtaining the tripod from the doubly protected imidazole **46**, as the critical choice of the N-protection by *N,N*-dimethylsulfamoyl guaranteed the ease of deprotonation of both C2 and C5 positions. Moreover, as the tripod would require further functionalization at the C2 position the *tert*-butyldimethylsilyl (TBDMS) protecting group was chosen as it is easily and selectively removed by fluoride.



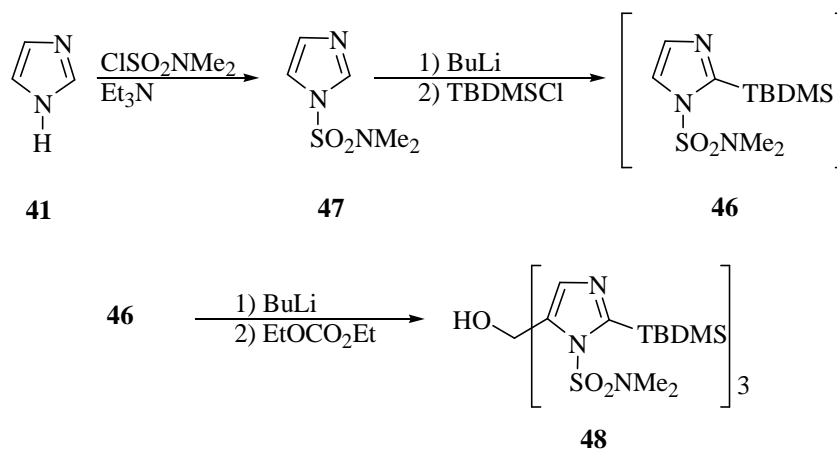
Scheme 2.9

2.2.2 Synthesis of Tris[4(5)-imidazoly]carbinol **31** and its derivatives

2.2.2.1 Synthesis of 4-TIC **31**

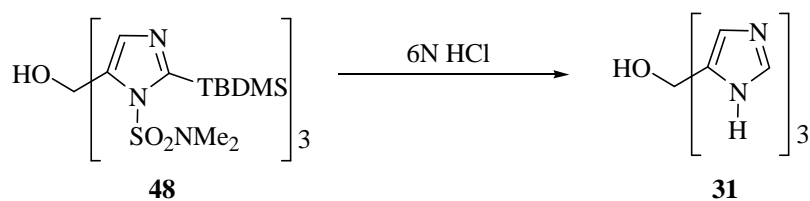
Imidazole **41** (scheme 2.10) reacted readily with *N,N*-dimethylsulfamoyl chloride and triethylamine to yield in excellent yield (90%) the *N*-protected imidazole **47**.¹³¹ Easily prepared on large scale the sulfonamide was a good starting material for the synthesis of 4-TIC. The sulfonamide **47** could then be protected at the 2-position by addition of one equivalent of BuLi and TBDMSCl at -78 °C.¹³² The intermediate **46** thus formed was then deprotonated once more, in the same pot,

by addition of a second equivalent of base. Deprotonation at the 5-position was carried out at $-78\text{ }^{\circ}\text{C}$ and addition of diethyl carbonate results in the formation of the desired product **48** in good yield (70%) without purification.¹³³



Scheme 2.10

The product, a white solid, was fully characterized by nuclear magnetic resonance (NMR) and by mass spectrometry. The ^1H NMR spectroscopy confirmed the substitution of the 2 and 4 positions of the imidazole nucleus **48** as the remaining C4-proton at δ 6.38 ppm was a singlet; the presence of a hydroxy group was supported by infra-red (IR) spectroscopy with a broad absorption band at 3300 cm^{-1} . The doubly protected tripod was finally completely deprotected (scheme 2.11) in one step in 6N HCl at reflux for 90 minutes. The crude product was then purified by cation exchange chromatography which provided either the known neutral form **31** in 88% yield, when ammonium hydroxide was used as an eluent, or to the trihydrochloride salt **31** \cdot 3HCl in 80% yield, when replaced by 6N HCl.



Scheme 2.11

The characteristic resonance of the more deshielded C2-proton as a doublet ($J= 0.9$ Hz) δ 7.64 ppm and the disappearance of the methyl group of the protecting groups by ^1H NMR spectroscopy indicated that the desired product was obtained. This structure was further corroborated by ^{13}C NMR spectroscopy and mass spectrometry which exhibited an $[(\text{M} - \text{OH})^+]$ base peak. A crystal obtained by slow evaporation of a solution of the tri-hydrochloride salt **31** in methanol yielded crystals suitable for X-ray crystallography. The structure of the tri-hydrochloride salt was obtained (figure 2.1) and showed the expected structure involved in an extensive hydrogen bond network with chloride ions and methanol molecules:

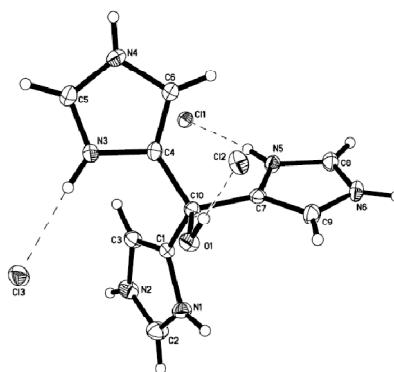
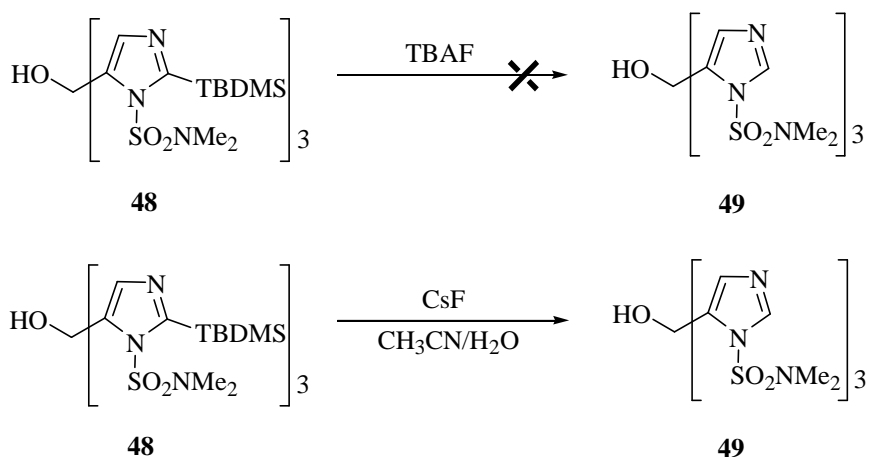


Figure 2.1: X-ray ORTEP diagram of **31**·3HCl

Selected bond distances (Å): O(1)-C(10)= 1.4157(11); N(1)-C(2)= 1.3259(14); N(1)-C(1)= 1.3811(12); N(2)-C(2)= 1.3235(14); N(2)-C(3)= 1.3717(13). Selected bond angles (°): C(2)-N(1)-C(1)= 108.46(8); C(2)-N(2)-C(3)= 109.32(9); C(3)-C(1)-N(1)= 107.11(8); N(2)-C(2)-N(1)= 108.50(9); C(1)-C(3)-N(2)= 106.62(9).

2.2.2.2 Synthesis of two derivatives **49** and **51**

The selective deprotection at the 2-position was initially attempted by the action of TBAF which led to complex mixtures (scheme 2.12). This unexpected difficulty might be attributable to TBAF's basicity in THF promoting an elimination reaction give N-sulfonamide-imidazole **46** and the symmetrical ketone. This pathway, likely to be driven by steric relief, was shut down when CsF in aqueous acetonitrile was used and yielded **49** in 88% yield. The presence of water in the system was assumed to moderate the basicity of fluoride.

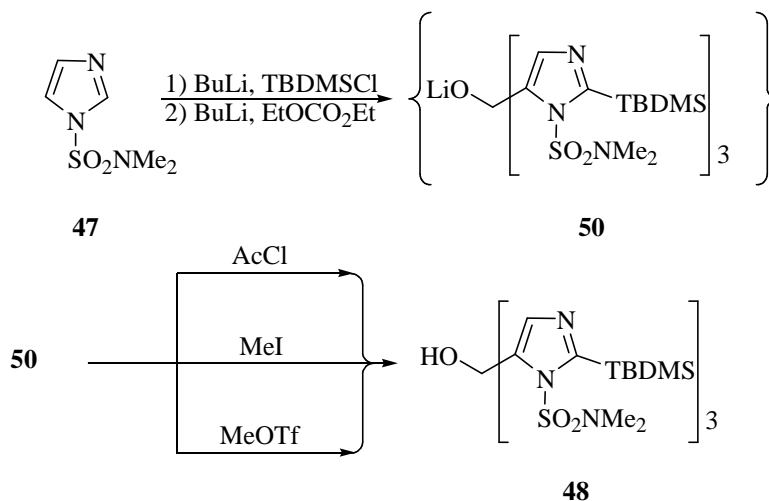


Scheme 2.12

The two doublets of both imidazole protons ($J = 1.2$ Hz) at δ 8.01 ppm and δ 6.35 ppm observed by ^1H NMR spectroscopy and the resonance of the methyl group from the N-protecting group at δ 2.91 ppm indicated of the selective C2-deprotection of the imidazole nucleus in **49**.

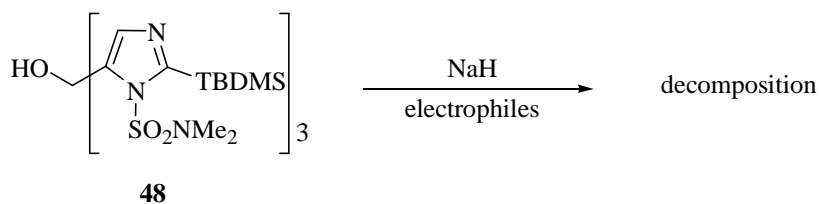
This practical route to 4-TIC **31** and its selective C2-deprotection led us to consider the next stage of the synthetic plan as the functionalization of the ligand and its coordinating properties would be hampered by the presence of a hydroxy

group. We therefore tried to modify its reactivity by investigating several tactics to install protecting groups. Direct attempts (scheme 2.13) to protect the product *in situ* were carried out with various electrophiles. These trapping experiments initially involved acetyl chloride and failed, resulting in the isolation of the carbinol **48**. As the steric hindrance of two quaternary carbons only separated by one oxygen atom in the presumed intermediate may have been responsible for the observed inertness, two other electrophiles were tested: iodomethane (MeI) and methyl triflate (MeOTf). Both of these trapping agents also failed to protect the carbinol *in situ*.



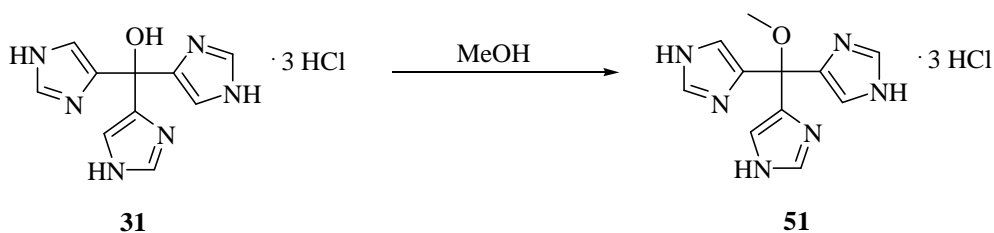
Scheme 2.13

Attempts also carried out on the pure starting carbinol **48** by sodium hydride (NaH) treatment in THF at 0 °C followed by addition of AcCl, MeI or MeOTf led to decomposition of the starting material (scheme 2.14). The decomposition of **48** by NaH was observed by TLC analysis and supports the interpretation of the TBAF experiments with fluoride a base in THF.



Scheme 2.14

Methylation of the alcohol (scheme 2.15) was finally achieved under acidic conditions by methanolysis of the tri-cationic form of **31** in quantitative yield. The reaction is thought to occur *via* protonation of the tertiary alcohol by one of the protonated imidazoles, resulting in the loss of water and the formation of **51**.



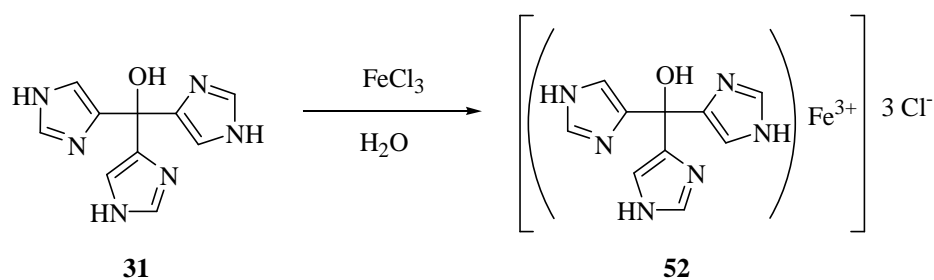
Scheme 2.15

The desired product, a white solid, proved to be extremely hygroscopic and displayed the expected resonance of the added methyl group at δ 3.35 ppm by ^1H NMR spectroscopy and a slight upfield shift in the doublets of the aromatic imidazole from δ 9.12 ppm to δ 9.02 ppm.

2.2.3 Synthesis of a 4-TIC iron (III) complex **52**

With the tripod in our hands confirmation of its coordinating properties was sought as no crystal structure of a 4-TIC metal complex was known. The tripod was found to readily form a 2:1 complex (scheme 2.16), as a brown solid, in water with

iron trichloride. Suitable crystals for X-ray crystallography were obtained from a concentrated solution in methanol (figure 2.2). The structure of the complex was determined and it is the first structure of any metal complexed by 4-TIC. It displayed all three nitrogen donors of the ligand coordinated to the iron center in an octahedral arrangement, constituted by two 4-TIC ligands and its bond lengths and angles were not significantly different from 2-TIC complexes.



Scheme 2.16

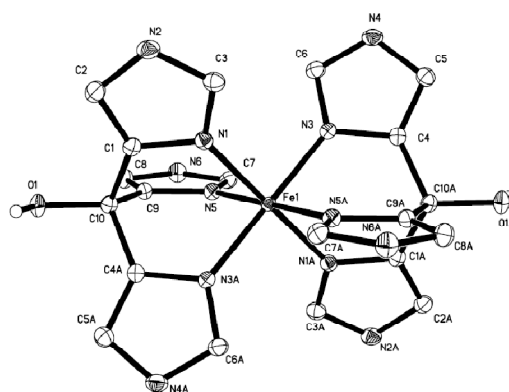


Figure 2.2: X-ray ORTEP diagram of **52**

Selected distances (Å): Fe(1)-N(1)= 1.9535(15); Fe(1)-N(3)= 1.9414(16); Fe(1)-N(5)= 1.9662(15); N(1)-C(3)= 1.329(2); N(1)-C(1)= 1.378(2); C(1)-C(10)= 1.516(2). Selected bond angles (°): N(3)-Fe(1)-N(1)= 92.96(6); N(3)-Fe(1)-N(5)= 92.89(6); N(1)-Fe(1)-N(5)= 86.68(6); C(9)-C(10)-C(1)= 106.13(15); O(1)-C(10)-C(9)= 110.74(14).

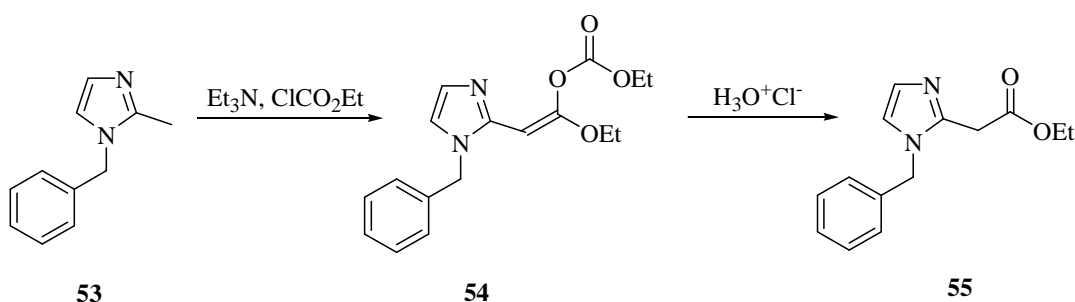
2.2.4 Conclusion

This improved and shortened route, 50-55% overall yield from imidazole, is a three pot procedure with limited and simple purification steps. Indeed the two previous syntheses are longer and technically much more difficult as the imidazole derivatives are purified by column chromatography on silica gel with eluents saturated with ammonia.¹²² This important improvement of the synthesis of 4-imidazolyl carbinols helped us to push forward large quantities of the fully deprotected material. It also facilitated the investigation of the coordination chemistry of 4-TIC. Potential further modifications of the 2-position could now be reasonably envisioned as we turned our attention to discover efficient functionalizations of imidazoles at the 2-position with a model substrate.

2.3 Functionalization of 4-TIC

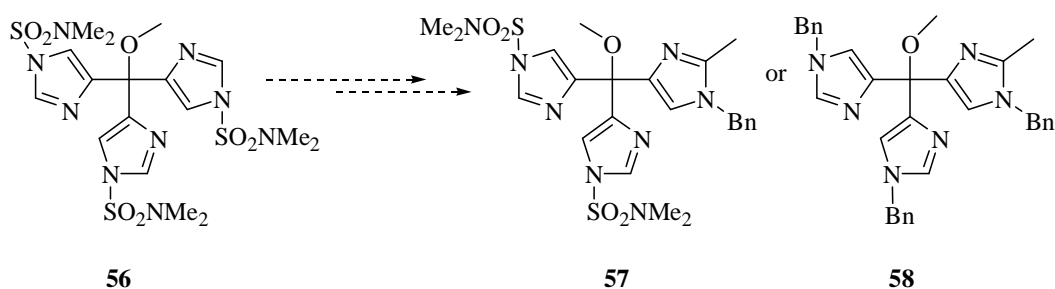
2.3.1 Introduction and background

The functionalization of imidazoles at the 2-position can be carried out in various ways. The preparation of 2-(2-imidazolyl)acetophenones¹³⁴ (scheme 2.17), for example, demonstrates the feasibility of addition of an ester group and though encouraging this strategy would not be easily transposed to our problem.



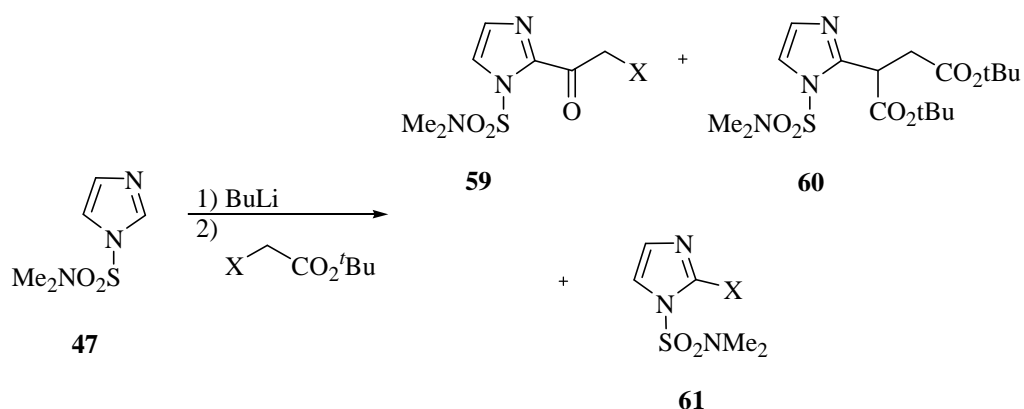
Scheme 2.17

This procedure requires the presence of two specific features: 1) a methyl group at the 2-position of the imidazole **53** and 2) an activating protecting group. The first requirement could conceivably be met by simple addition of the methyl group onto the N-protected 4-TIC **56** (scheme 2.18), but additional modifications of the protecting groups are likely to render the route to **57** or **58** very lengthy. Moreover, the poor solubility properties and the difficulty in purifying poly-imidazole tripods in general would render impractical such a route.



Scheme 2.18

The formation of organolithium species, using strong bases such as BuLi, and their addition to halogenoacetates was also considered. However, the reactivity of 2-lithio-imidazoles with different *t*-butyl halogenoacetates was moderated by the neighboring protecting group, as reported in a study of additions of sulfonamide **47** to *t*-butyl halogenoacetates¹³⁵ (scheme 2.19):

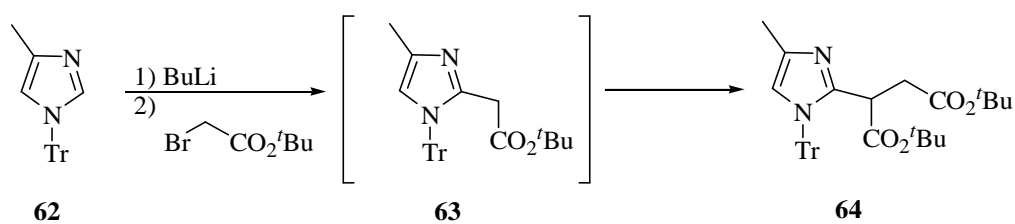


Scheme 2.19

	X= Cl	X= Br	X= I
47 , R ¹ = R ² = H	33 (66 %)	0	35 (26 %)

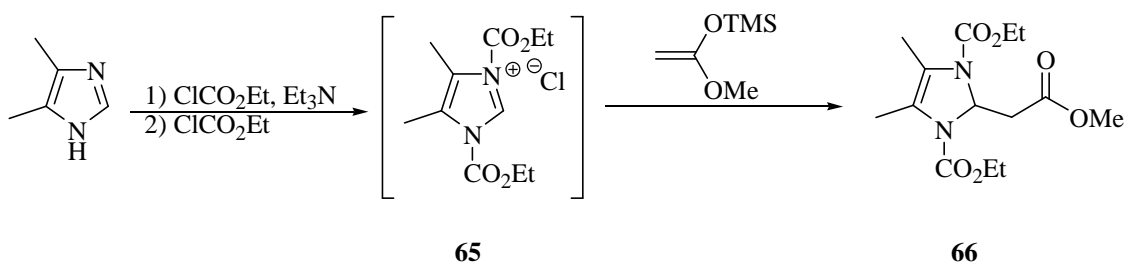
Table 2.2: Product distribution and yields from scheme 2.19¹³⁵

The chloro-derivative underwent attack at the ester to furnish the chloroketone **59**, whereas the *t*-butyl iodoacetate transferred iodine to the imidazole in low yields, product **61**. Substitution at the C2 position under classical conditions is rather capricious and the reactivity seems to be hampered by the electron withdrawing sulfamoyl protecting group. Moreover, when the bromo-acetate did behave in the desired way (scheme 2.20) (e.g. with the trityl protecting group) the product **63** apparently further reacted and produced the *t*-butyl acetate **64**.



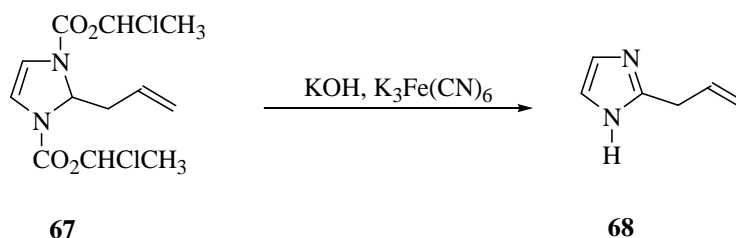
Scheme 2.20

We therefore sought milder and more selective conditions in order to effect the required transformation. Itoh and coworkers' work was deemed more reasonable and further investigated.^{136,137} The reactivity of the imidazole nucleus can be greatly modified by purposefully choosing activating groups. When protected by a strong electron withdrawing group and activated further by a second one (scheme 2.21), the 2-position of the imidazolium salt **65** becomes electrophilic and undergoes the addition of Mukaiyama-type nucleophiles to yield imidazoline **66**.



Scheme 2.21

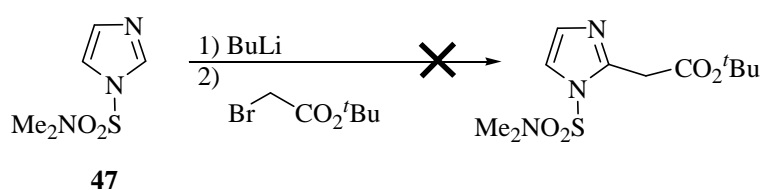
The imidazoline **67** can in a second step be re-aromatized to imidazoles **68** with potassium hydroxide and potassium ferric cyanide in refluxing dioxane-water (scheme 2.22).



Scheme 2.22

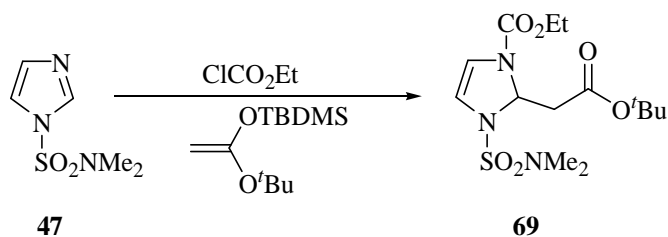
2.3.2 Results and Discussion

We initially sought to confirm Coutts *et al.*¹³⁵ report as a successful addition of *t*-butyl bromoacetate would have provided us with a direct entry to functionalized 4-TIC. However, analysis of the crude products by ¹H NMR spectroscopy showed the starting material and other unidentified compounds (scheme 2.23).



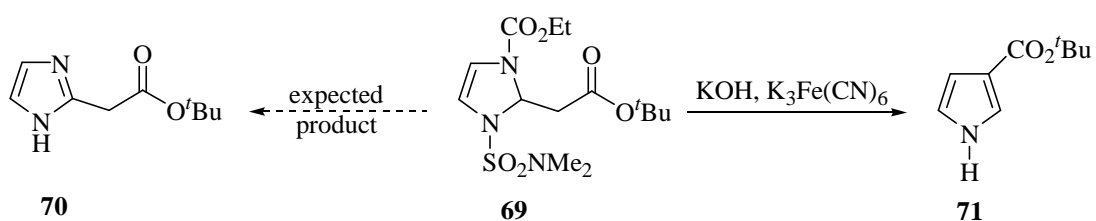
Scheme 2.23

We therefore turned our attention to a preliminary study of the applicability of Itoh's chemistry. The reactions were performed on a model substrate **47** in order to determine its reproducibility and practicality. Moreover, we were also greatly interested in the re-aromatization step as only one imidazole-containing substrate **68** had been reported. This reaction was reproduced with our particular ketene silyl acetal¹³⁸ to give us the desired imidazoline **69** in good yields (55%) as a colorless oil (scheme 2.24). The loss of aromatic resonances in the product was confirmed by ¹H and ¹³C NMR spectroscopy.



Scheme 2.24

We then proceeded to test the functional group tolerance of the deprotection and aromatization steps as the ester was potentially reactive under the conditions of the oxidation (scheme 2.25).



Scheme 2.25

Upon treatment of **69** with potassium hydroxide followed by addition of *o*-chloranil or ferric salts a white solid was isolated in 63% yield and characterized by ¹H and ¹³C NMR spectroscopy. The unusual low field resonances of an aromatic nucleus and the absence of the expected molecular ion by mass spectrometry excluded the formation of **70**. The mass of the isolated compound was missing 14 au, corresponding to a nitrogen atom. Crystals obtained from a solution of **71** in methanol were analyzed by X-ray crystallography which established the structure of the compound to be a pyrrole derivative (figure 2.3).

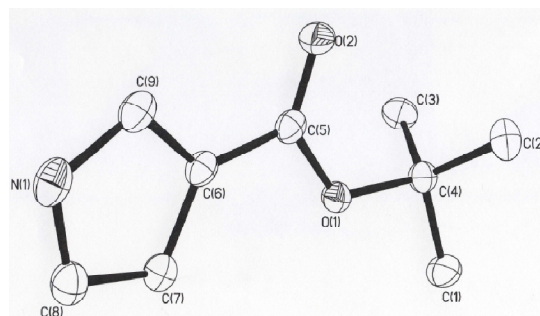


Figure 2.3: X-ray ORTEP diagram of **71**

Selected distances (Å): C(6)-C(7)= 1.4291(14); C(7)-C(8)= 1.3704(15); C(8)-N(1)= 1.3743(15). Selected angles (°): C(9)-C(6)-C(7)= 107.19; C(9)-C(6)-C(5)= 124.01(9); C(7)-C(6)-C(5)= 128.64; C(8)-C(7)-C(6)= 106.77(9)

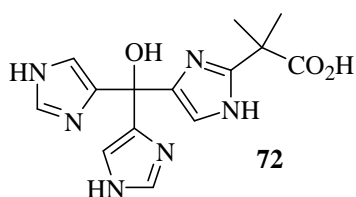
Formation of pyrrole **71** can be rationalized by the presence of an acidic methylene group alpha to the carboxyl group and by the good nucleofugacity of the sulfonamide, both of which could promote an initial elimination-ring opening step. This would then be followed by loss of the sulfonamide group and finally ring closure. This Tiffeneau-Demjanov rearrangement^{139,140} further highlights the potential problem posed by acidic C-Hs flanked by the ester and imidazole nucleus.

2.4 Conclusion

To summarize we developed a practical and efficient route to the 4-TIC ligand in a three pot procedure in excellent yield (50-55%) over three steps.¹⁴¹

We also explored further functionalization of 4-TIC but no satisfactory method was found and we thus re-evaluated our approach. The more conservative option was to push the current line of investigation by slight modifications of the deprotection step. Using acidic conditions to deprotect the carbamate and

sulfonamide might be a more selective. However, a second and more radical approach was finally chosen. The original the organic target was modified since the methylene group appeared to be responsible for most side reactions observed. It was replaced by a geminal dimethyl group which would most likely preempt other potential side reactions during the synthesis of a 3-Imidazole-1-carboxylate ligand. The new target **72** therefore incorporated this new feature (scheme 2.26):



Scheme 2.26: New ligand proposed

2.5 Experimental

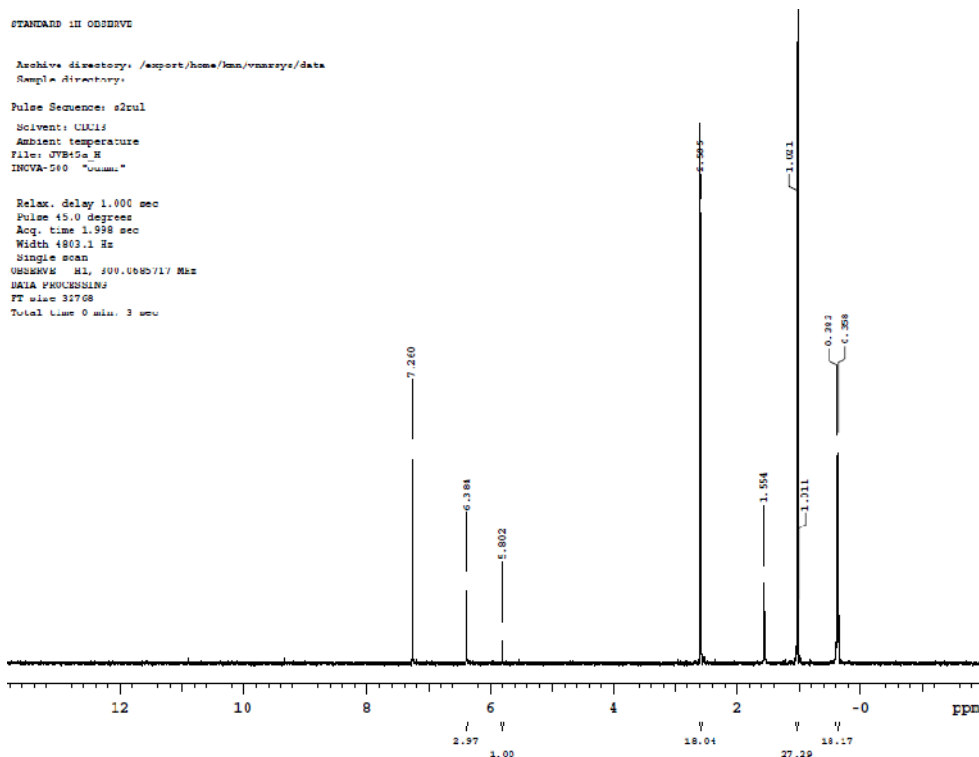
Materials and Methods:

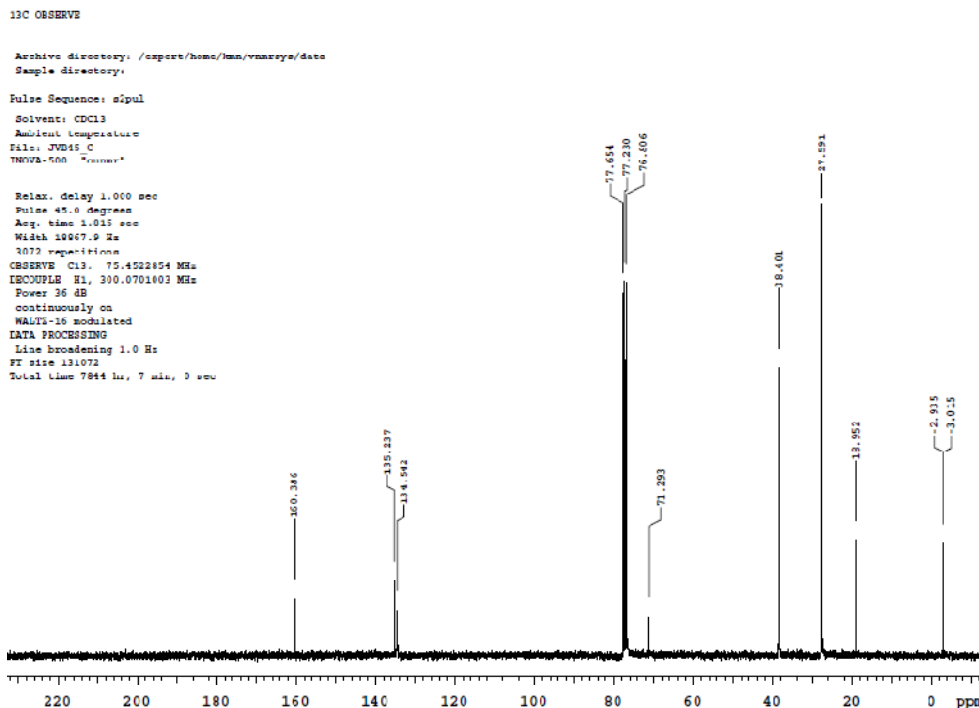
All operations were carried out under argon by means of standard Schlenk and vacuum-line techniques. Organic solvents were dried by standard procedures and distilled under Ar before use. CH₂Cl₂ was dried over CaH₂ and distilled under Ar before use; THF was dried over Na using benzophenone as indicator and distilled under Ar before use; methanol was dried over Mg and I₂ and distilled under argon. Glassware was oven-dried at 110 °C overnight. IR spectra were recorded in KBr pellets with a Perkin-Elmer 283-B infrared spectrophotometer (resolution 4 cm⁻¹). The ¹H (300 MHz), and ¹³C (75.5 MHz) NMR spectra were recorded on a Varian Mercury-300 spectrometer. Mass spectra were acquired on a Finnigan TSQ 700 spectrometer (ESI) in methanol solution. Compound **47**¹³¹ was prepared by a known procedure and matched the spectroscopic data available.

Tris(1-*N,N*-dimethylsulfamoyl-2-*t*-butyldimethylsilyl-5-imidazolyl)carbinol **48**:

1-(*N,N*-Dimethylsulfamoyl)-imidazole (1.85 g, 10.6 mmol) **47** was dissolved in dry THF (90 mL) under a positive pressure of Ar. With vigorous stirring, the temperature was lowered to -78 °C and a solution of *n*-BuLi in pentane (11.1 mmol, 5.9 mL of a 1.88 M solution, 1.05 eq.) was added drop-wise. After stirring for 30 min, a solution of *t*-butyldimethylsilyl chloride (12.7 mmol, 1.91 g, 1.2 eq.) in dry THF (2 mL) was added *via* cannula. The reaction mixture was then left at room temperature overnight. The solution was cooled to -78 °C and a solution of *n*-BuLi (11.7 mmol, 6.2 mL of a 1.88 M solution, 1.1 eq) was added drop-wise. After stirring for 30 min, neat diethyl carbonate (3.0 mmol, 425 μL, 0.33

eq.) was added drop-wise. The reaction was left in the dry ice-acetone bath, slowly warming to room temperature. After stirring 24 h, ethyl acetate (50 mL) was added to the reaction, and the solution was washed with brine (3 × 20 mL). The organic phase was dried with MgSO₄, and the solvent removed under reduced pressure. During solvent removal a white solid precipitated, which was filtered off and washed with ethyl acetate. The filtrate was concentrated and the procedure was repeated to afford of the desired product as a white solid (2.19 g, 70%). No further purification was necessary. Melting point: decomposes above 185 °C; IR (KBr) 3477, 2933, 2995, 2964, 1462, 1372, 1157, 959 cm⁻¹; ¹H NMR (300 MHz, CDCl₃) δ 6.38 (s, 3H), 5.80 (s, 1H), 2.59 (s, 18H), 1.02 (s, 27H), 0.38 (s, 9H), 0.36 (s, 9H); ¹³C (75.5 MHz, CDCl₃) δ 160.4, 135.2, 134.5, 71.3, 38.4, 27.6, 19.0, -2.9, -3.0; HRMS (ESI +): exact mass calculated for C₃₄H₆₇N₉NaO₇S₃Si₃ [M + Na]⁺ 916.3531. Found 916.3550.





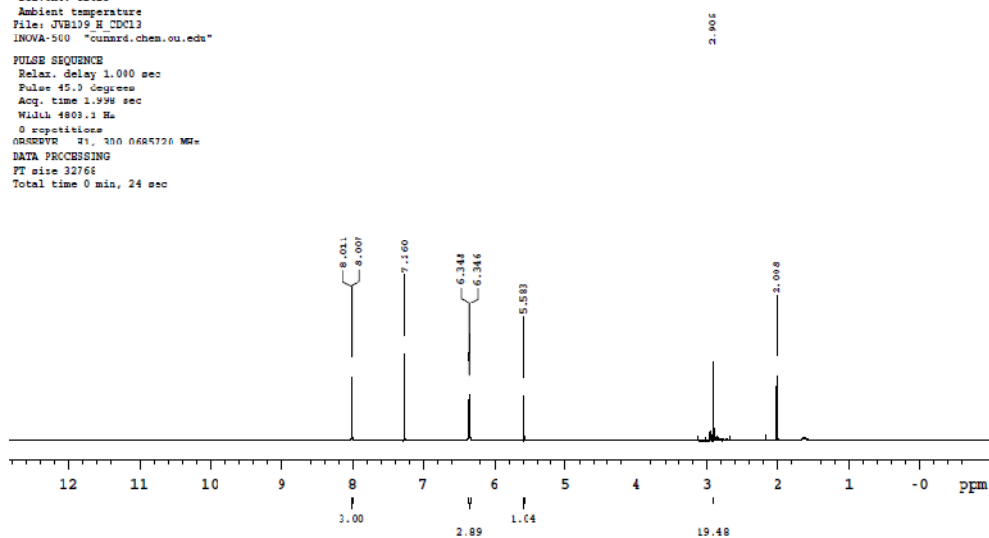
Tris(1-*N,N*-dimethylsulphamoyl-5-imidazolyl)carbinol 49:

Tris(1-*N,N*-dimethylsulphamoyl-2-*t*-butyldimethylsilyl-5-imidazolyl)carbinol **48** (2.04 g, 2.3 mmol) and 2.0 g (13.2 mmol, 5.8 eq.) of CsF and H₂O (10 mL) were added to CH₃CN (90 mL). The stirred suspension was refluxed for 24 h. The organic phase was separated and dried over MgSO₄. Upon concentration of the organic phase a solid precipitated which was filtered off and dried; affording the desired product as a white solid (1.11 g, 88% yield). No further purification was necessary. Melting point: decomposes above 130 °C; IR (KBr) 3489, 3138, 2949, 1555, 1467, 1393, 1165, 1092, 1046, 984, 845, 729, 587; ¹H NMR (300 MHz, CDCl₃) δ 8.01 (d, 3H, *J*= 1.2 Hz), 6.35 (d, 3H, *J*= 1.2 Hz), 5.58 (s, 1H), 2.91 (s, 18H); ¹³C (75.5 MHz, CDCl₃) δ 141.5, 133.4, 132.7, 68.6, 38.5; HRMS (ESI +): exact mass calculated for C₁₆H₂₆N₉O₇S₃ [M + H]⁺ 552.1112. Found 552.1137.

STANDARD 14 (SUSPENS)

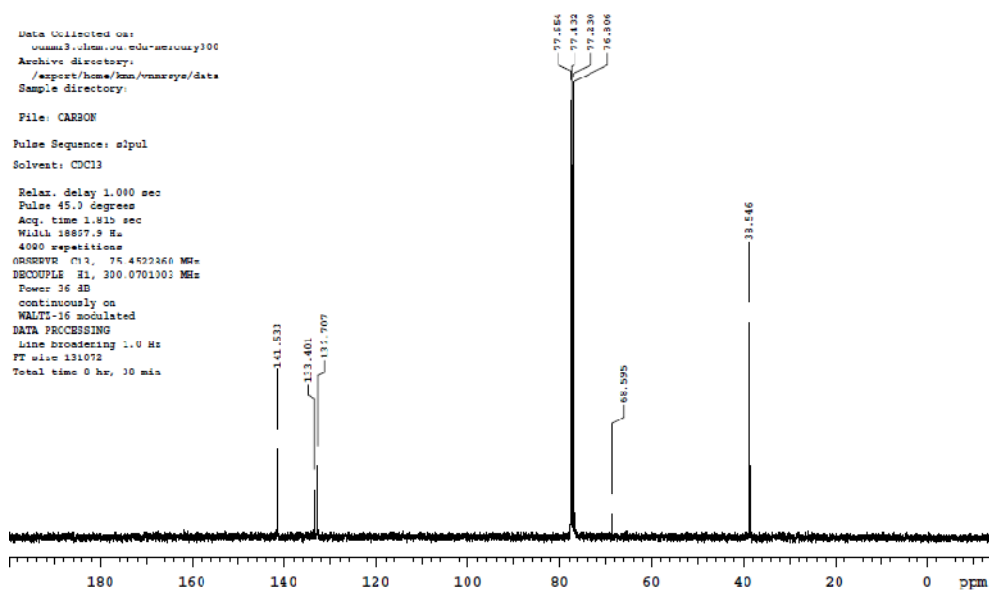
Archive directory: /export/home/knn/vnmrsws/data
Sample directory:

Pulse Sequence: sfpul
Solvent: CDCl3
Ambient temperature
File: JVE119_H_CDCl3
INOVA-500 "cumrad.chem.ou.edu"
PULSE SEQUENCE
Relax. delay 1.000 sec
Pulse 45.0 degrees
Acq. time 1.998 sec
Width 4809.1 Hz
0 repetitions
OBSERVE F1, 300.0685720 MHz
DATA PROCESSING
FT size 32768
Total time 0 min, 24 sec



13C OBSERVE

Data Collected on:
cumrad.chem.ou.edu-uvicopy100
Archive directory:
/export/home/knn/vnmrsws/data
Sample directory:
File: CARBON
Pulse Sequence: sfpul
Solvent: CDCl3
Relax. delay 1.000 sec
Pulse 45.0 degrees
Acq. time 1.915 sec
Width 18807.9 Hz
4000 repetitions
OBSERVE C13, 75.4822260 MHz
DECOUPLE F1, 300.0701100 MHz
Power 16 dB
continuously on
WALTZ-16 modulated
DATA PROCESSING
Line Processing 1.0 Hz
FT size 131072
Total time 0 hr, 10 min

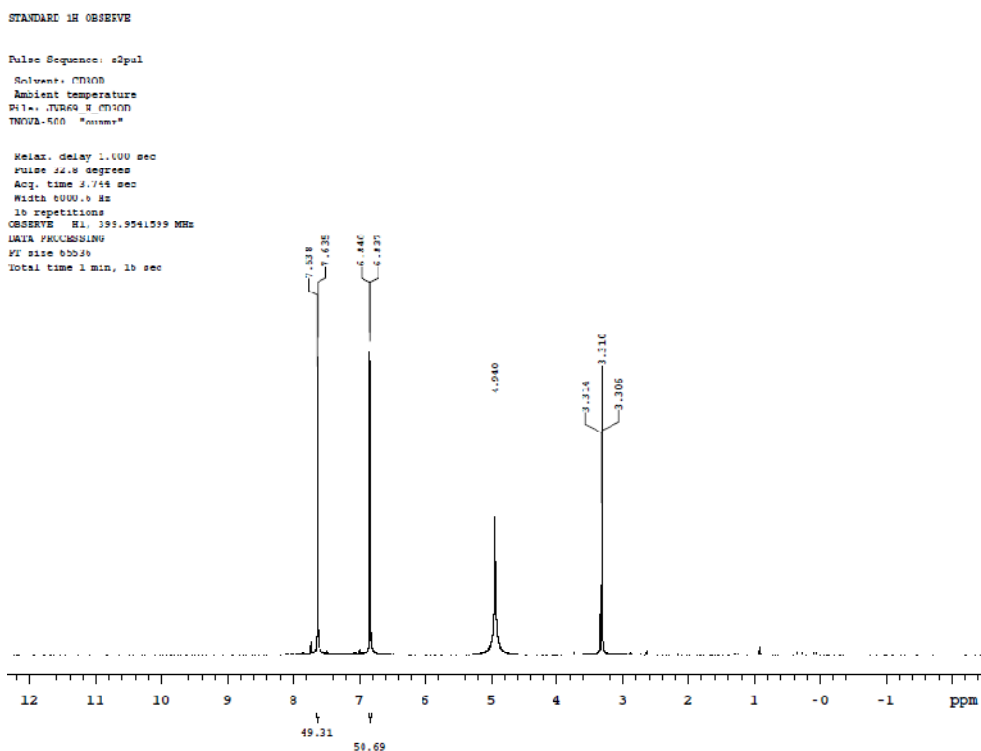


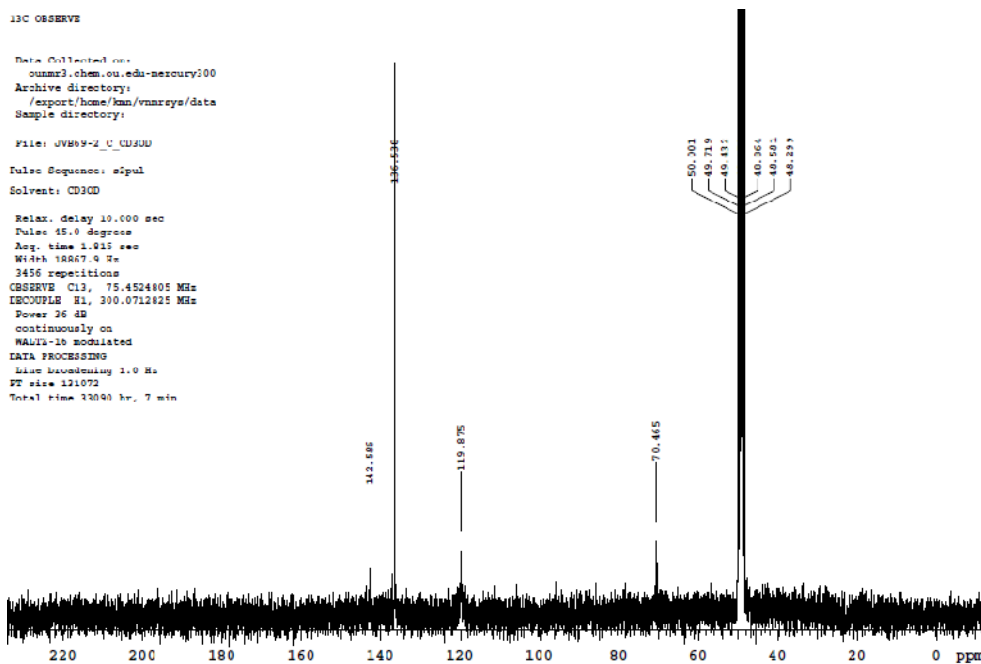
Tris(4(5)-imidazolyl)carbinol hydrochloric salt 31·3 HCl:

Tris(1-*N,N*-dimethylsulfamoyl-2-*t*-butyldimethylsilyl-5-imidazolyl)carbinol **48** (1.60 g, 1.79 mmol) was refluxed in hydrochloric acid (50 mL, 1.5 M) for 90 min. The solvent was evaporated under reduce pressure. Column chromatography on a Dowex 50WX8-100 resin (20 mL) with water followed by 6 M hydrochloric acid yielded the tri-hydrochloride salt as a white solid (487 mg, 80% yield). When

6% NH₄OH was used instead of hydrochloric acid the neutral tripod **31** was obtained (362 mg, 88% yield). Suitable crystals for X-ray crystallography were obtained by slow evaporation of a solution of **31**·3 HCl in methanol.

Tris(4(5)-imidazolyl)carbinol **31**: decomposes at 130 °C; IR (KBr) 3386, 3142, 2844, 2605, 1455, 1111,1088, 945, 826, 618 cm⁻¹; ¹H NMR (300 MHz, CD₃OD) δ 7.64 (d, *J*= 1.2 Hz, 3H), 6.84 (d, *J*= 1.2 Hz, 3H); ¹³C (75.5 MHz, CD₃OD) δ 142.6, 136.5, 119.9, 70.5; HRMS (ESI +): exact mass calculated for C₁₀H₁₀N₆NaO [M + Na]⁺ 253.0814. Found 253.0821.





Tris(4(5)-imidazolyl)carbinol hydrochloride salt (**31·3 HCl**) a white solid decomposes above 175 °C; IR (KBr) 3165, 3111, 2980, 2830, 2594, 1625, 1467, 1420, 1100, 1065, 818 cm^{-1} ; ^1H NMR (300 MHz, CD_3OD) δ 9.12 (s, 3H), 7.75 (s, 3H); ^{13}C (75.5 MHz, CD_3OD) δ 137.8, 135.1, 120.2, 66.6; HRMS (ESI +): exact mass calculated for $\text{C}_{10}\text{H}_{10}\text{N}_6\text{NaO}$ $[\text{M} + \text{Na}]^+$ 253.0814. Found 253.0821.

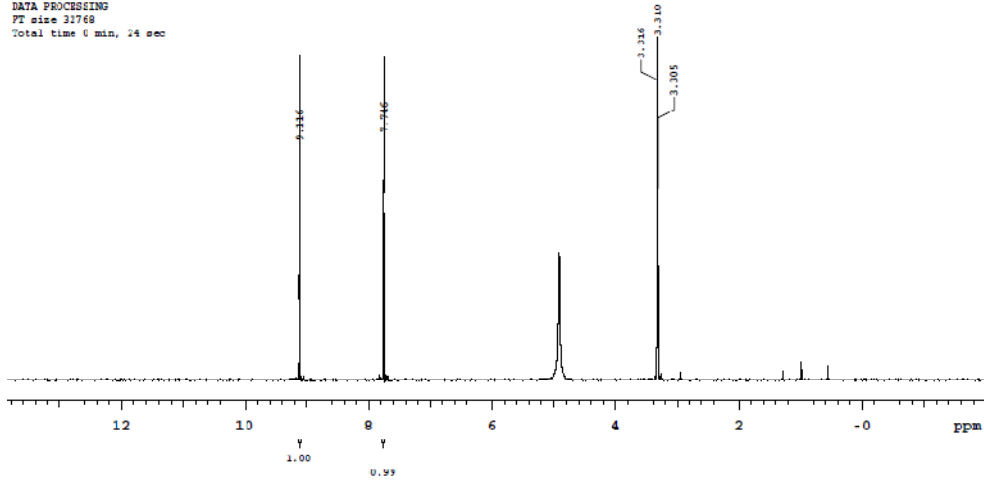
STANDARD IN OBSERVE

Archive directory: /export/home/knn/vnmrsvs/data
Sample directory:

Pulse Sequence: s2pul

Solvent: CD3OD
Ambient temperature
File: JVB51h_colamn_1
INOVA-500 "cinnar"

Relax. delay 1.000 sec
Pulse 45.0 degrees
Acq. time 1.998 sec
Width 4802.1 Hz
0 repetitions
OBSERVE H1, 300.0697524 MHz
DATA PROCESSING
FT size 32768
Total time 0 min, 24 sec



13C OBSERVE

Archive directory: /export/home/knn/vnmrsvs/data
Sample directory:

Pulse Sequence: s2pul

Solvent: CD3OD
Temp. 20.0 C / 299.1 K
File: JVB51 C CD3OD
INOVA-500 "cinnar"

Relax. delay 1.000 sec
Pulse 45.0 degrees
Acq. time 1.815 sec
Width 10067.0 Hz
15640 repetitions
PROBHD 5mm 1H 13C QNP400 MHz-
DCOUPLE E1, 300.0712625 MHz
Power 36 dB
continuously on
WALTZ-16 modulated
DATA PROCESSING
Line broadening 1.0 Hz
FT size 131072
Total time 7014 hr, 7 min, 0 sec

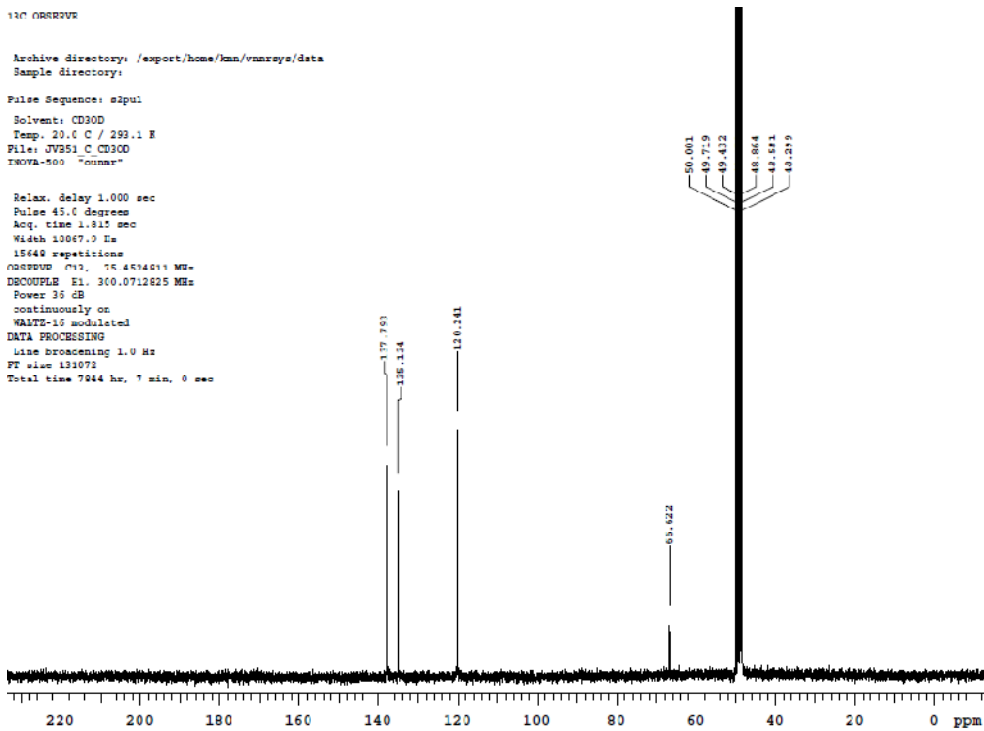
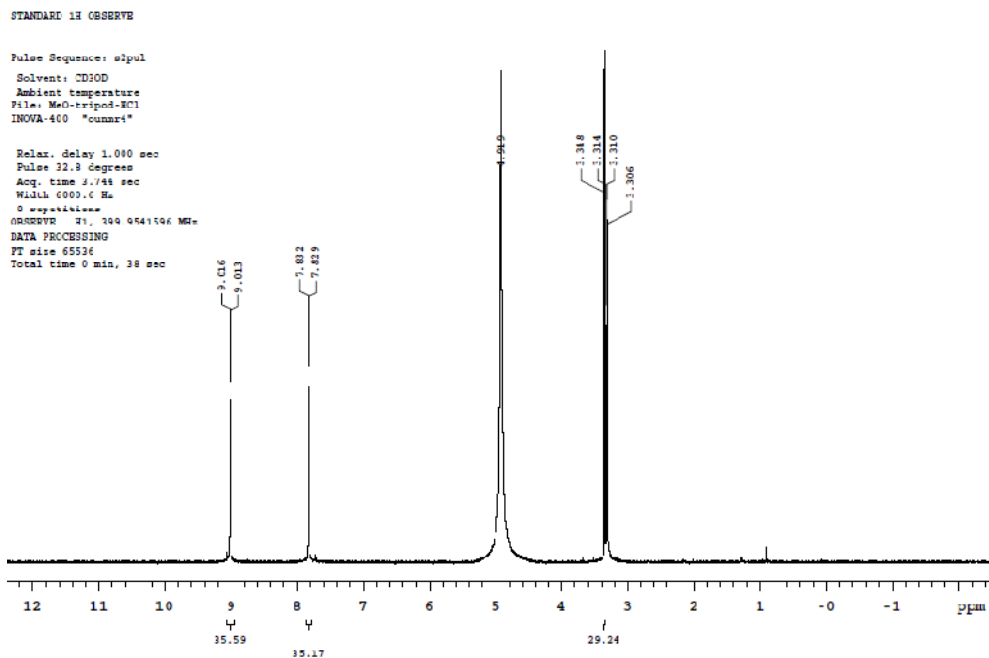


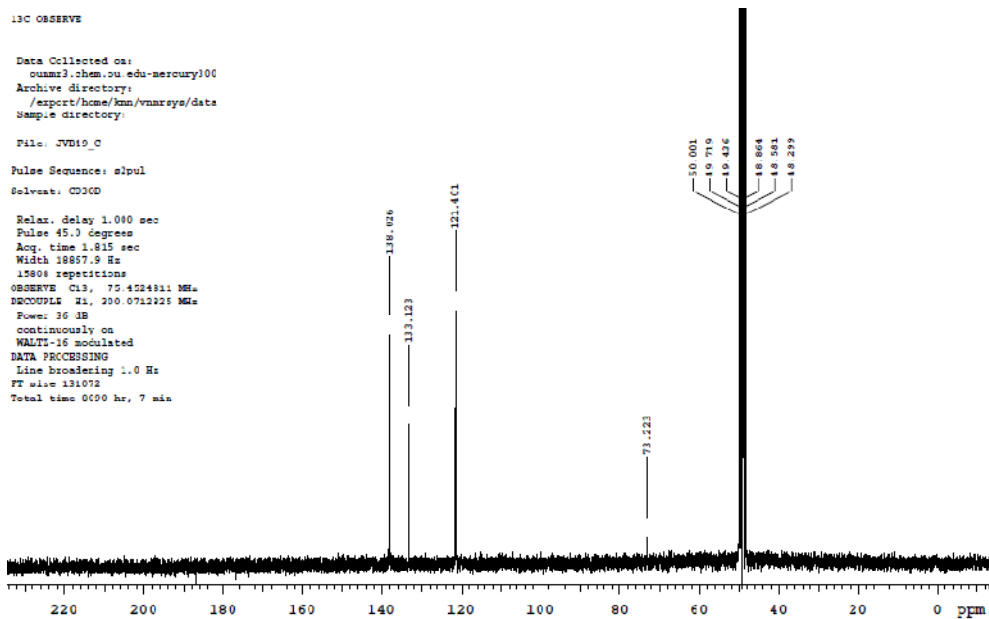
Table 2.3: Crystal data and structure refinement for **31·3 HCl**

Empirical formula	$C_{10}H_{13}Cl_3N_6O$
Formula weight	339.61
Temperature	120(2) K
Wavelength	0.71073 Å
Crystal system	Monoclinic
Space group	P2(1)/n
Unit cell dimensions	a= 7.5651(5) Å, $\alpha= 90^\circ$.
	b= 22.9874(15) Å, $\beta= 94.2420(10)^\circ$.
	c= 8.3708(5) Å, $\gamma= 90^\circ$.
Volume	1451.71(16) Å ³
Z	4
Density (calculated)	1.554 Mg/m ³
Absorption coefficient	0.636 mm ⁻¹
F(000)	696
Crystal size	0.22 x 0.08 x 0.02 mm ³
Theta range for data collection	1.77 to 27.49°.
Index ranges	-9<=h<=9, -29<=k<=28, -10<=l<=10
Reflections collected	17459
Independent reflections	3318 [R(int)= 0.0171]
Completeness to theta= 27.49°	99.8 %
Absorption correction	Semi-empirical from equivalents
Max. and min. transmission	0.9874 and 0.8728
Refinement method	Full-matrix least-squares on F ²
Data / restraints / parameters	3318 / 0 / 182
Goodness-of-fit on F ²	1.045
Final R indices [I>2sigma(I)]	R1= 0.0279, wR2= 0.0705
R indices (all data)	R1= 0.0297, wR2= 0.0719
Largest diff. peak and hole	0.454 and -0.250 e.Å ⁻³

Tris(4(5)-imidazolyl)methoxymethane hydrochloric salt-methanol **51**:

Tris(4(5)-imidazolyl)carbinol hydrochloride **31**·3 HCl (201 mg, 0.59 mmol) dissolved in dry MeOH (20 mL) was refluxed for 19 h under positive pressure of N₂. A soxhlet apparatus was used whose thimble was filled with activated 4Å molecular sieves. The solution was concentrated under reduced pressure and acetone was added to precipitate the desired product, which was filtered off and dried. The product co-crystallized with one molecule of methanol (determined by NMR) in quantitative yield. The methanol-free product (hygroscopic) could be obtained as a white solid by extensive washing with acetone prior drying. IR (KBr) 3103, 2995, 2833, 2609, 1602, 1474, 1104, 841, 618 cm⁻¹; ¹H NMR (300 MHz, CD₃OD) δ 9.02 (d, *J*= 1.2 Hz, 3H), 7.83 (d, *J*= 1.2 Hz, 3H), 3.35 (s, 3H); ¹³C (75.5 MHz, CD₃OD) δ 137.7, 133.6, 121.0, 73.3, 53.3; MS (ESI+): [M – MeO]⁺= 213.09





Bis(tris(4(5)-imidazolyl)carbinol)iron(III) chloride **52**:

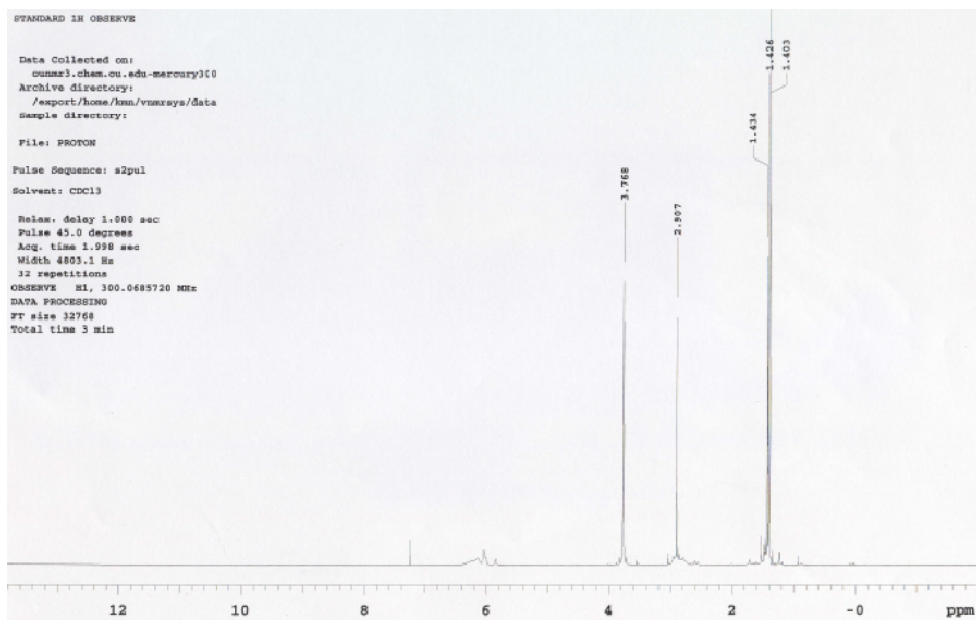
FeCl₃ (46 mg, 0.29 mmol, 1 eq.) and tris(4(5)-imidazolyl)carbinol **31** (132 mg, 0.58 mmol, 2 eq.) were dissolved in H₂O (10 mL) and stirred for 3 h. The solvent was removed under reduced pressure and the crude material dissolved in MeOH. Upon slow evaporation dark brown crystals formed and were filtered off, and washed with acetone, yielding **52** (141 mg, 74% yield).

Table 2.4: Crystal data and structure refinement for **52**

Empirical formula	$C_{24} H_{40} Cl_3 Fe N_{12} O_8$
Formula weight	786.88
Temperature	99(2) K
Wavelength	0.71073 Å
Crystal system	Triclinic
Space group	P-1
Unit cell dimensions	$a = 10.7760(8) \text{ \AA}, \alpha = 83.5450(10)^\circ.$
	$b = 10.9987(8) \text{ \AA}, \beta = 80.8150(10)^\circ.$
	$c = 16.6397(13) \text{ \AA}, \gamma = 63.8040(10)^\circ.$
Volume	$1745.0(2) \text{ \AA}^3$
Z	2
Density (calculated)	1.498 Mg/m^3
Absorption coefficient	0.724 mm^{-1}
F(000)	818
Crystal size	$0.38 \times 0.26 \times 0.24 \text{ mm}^3$
Theta range for data collection	$2.07 \text{ to } 27.50^\circ.$
Index ranges	$-13 \leq h \leq 13, -14 \leq k \leq 14, -21 \leq l \leq 21$
Reflections collected	21063
Independent reflections	7841 [R(int)= 0.0143]
Completeness to $\theta = 27.49^\circ$	99.0 %
Absorption correction	Semi-empirical from equivalents
Max. and min. transmission	0.8453 and 0.7704
Refinement method	Full-matrix least-squares on F^2
Data / restraints / parameters	7841 / 6 / 437
Goodness-of-fit on F^2	1.016
Final R indices [$I > 2\sigma(I)$]	R1= 0.0421, wR2= 0.1156
R indices (all data)	R1= 0.0434, wR2= 0.1166
Largest diff. peak and hole	1.819 and $-0.952 \text{ e. \AA}^{-3}$

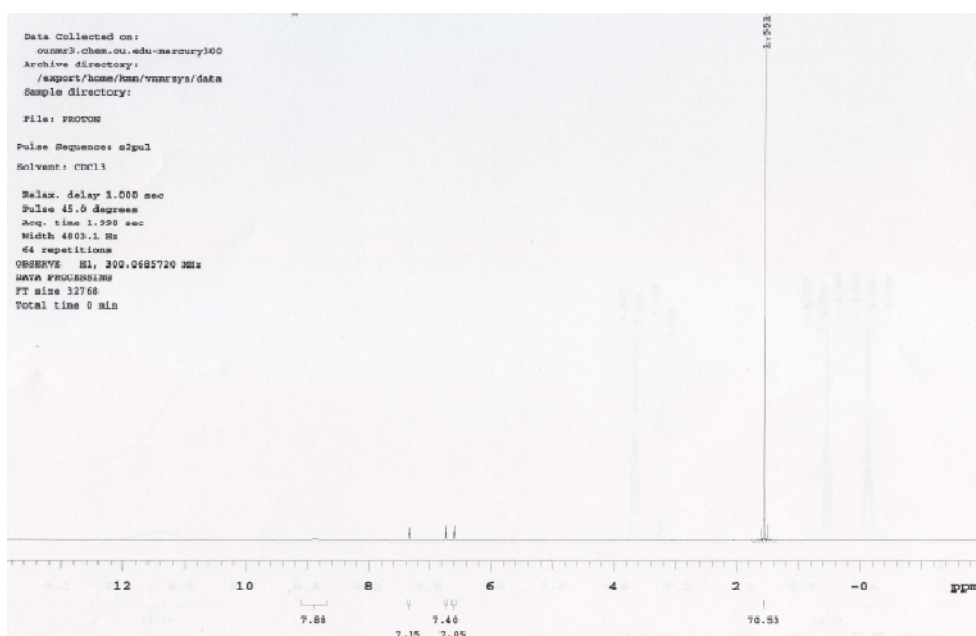
3-Dimethylsulfamoyl-2-ethoxycarbonylmethyl-2,3-dihydro-imidazole-1-carboxylic acid ethyl ester **69**

To a stirred solution of **47** (1.02 g, 5.8 mmol, 1 eq.) in freshly distilled acetonitrile (30 mL) the ketene silyl acetal¹³⁸ (2.98 g, 11.6 mmol, 2 eq.) was added. The reaction mixture was then cooled to 0 °C and methyl chloroformate (0.38 mL, 4.8 mmol, 1.2 eq.) added dropwise. The reaction mixture was left to warm to room temperature for 2 h. The solvents were removed in vacuo and the crude was purified by flash column chromatography on silica gel (6 hexanes: 4 AcOEt) to yield **69** as a colorless oil (1.17 g, 56% yield). The product was characterized by ¹H (300 MHz, CDCl₃) δ 6.00 (broad multiplet, 3H), 3.77 (s, 3H), 2.91 (s, 6H), 2.90 (s, 2H), 1.43 (s, 9H); MS (ESI+) exact mass calculate for C₁₂ H₂₁ N₂ O₆ S [M + H]⁺ 335.12. Found 335.14.



1H-Pyrrole-3-carboxylic acid tert-butyl ester **71**

To a stirred solution of imidazoline **69** (1.17 g, 3.22 mmol) in acetonitrile (70 mL), a 1N NaOH (9 mL) solution was added and then refluxed for 4 h. To the room temperature reaction mixture AcOEt (50 mL) were added and the organic phase was then washed with brine (2 × 20 mL) and dried over anhydrous MgSO₄. The solvent was removed under vacuum and the solid resulting was purified by flash column chromatography (7 hexanes: 3AcOEt) to yield **71** as a white solid (339 mg, 63% yield). IR (KBr) 3344, 2980, 1674, 1550, 1477, 1420, 1369, 1350, 1246, 1136; ¹H NMR (300 MHz, CDCl₃) δ 7.34 (m, 1H), 6.73 (m, 1H), 6.59 (m, 1H), 1.551 (s, 9H); ¹³C NMR (75.5 MHz, CDCl₃) δ 164.8, 123.2, 118.6, 118.2, 79.7, 28.4; MS (ESI +): exact mass calculated for C₉H₁₃NO₂Na [M + Na]⁺ 190.1. Found 190.2.



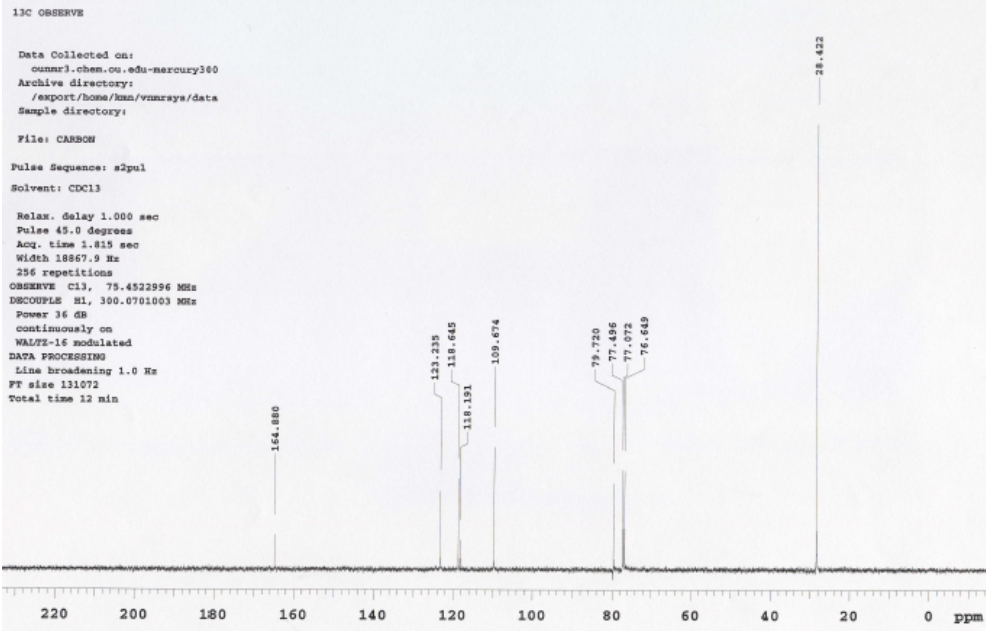


Table 2.5: Crystal data and structure refinement for **71**

Empirical formula	C ₉ H ₁₃ N O ₂
Formula weight	167.20
Temperature	110(2) K
Wavelength	0.71073 Å
Crystal system	Monoclinic
Space group	P2(1)
Unit cell dimensions	a= 5.9895(5) Å, α= 90°.
	b= 8.2125(7) Å, β= 91.5430(10)°.
	c= 9.3453(7) Å, γ= 90°.
Volume	1745.0(2) Å ³
Z	2
Density (calculated)	1.208 Mg/m ³
Absorption coefficient	0.085 mm ⁻¹
F(000)	180
Crystal size	0.32 x 0.24 x 0.14 mm ³
Theta range for data collection	2.18 to 28.30°.
Index ranges	-7<=h<=7, -10<=k<=10, -12<=l<=11
Reflections collected	5249
Independent reflections	2125 [R(int)= 0.0187]
Completeness to theta= 27.49°	96.7 %
Absorption correction	None
Max. and min. transmission	0.9881 and 0.9732
Refinement method	Full-matrix least-squares on F ²
Data / restraints / parameters	2125 / 1 / 112
Goodness-of-fit on F ²	1.078
Final R indices [I>2sigma(I)]	R1= 0.0298, wR2= 0.0762
R indices (all data)	R1= 0.0299, wR2= 0.0763
Absolute structure parameter	0.8(7)
Largest diff. peak and hole	0.154 and -0.271 e.Å ⁻³

Deprotection attempt of **48** using TBAF (scheme 2.12):

To a solution of tris(1-*N,N*-dimethylsulfamoyl-2-*t*-butyldimethylsilyl-5-imidazolyl)carbinol **48** (0.200 g, 0.224 mmol) in THF (10 mL), a 1 M solution of TBAF (3 mL) was added dropwise. The solution turned yellow and was stirred for 2 h at room temperature. The organic phase was separated and dried over MgSO₄. TLC (95 EtOAc: 5 MeOH) and ¹H NMR spectroscopy analysis of the crude mixture revealed a complex mixture which could not be purified.

In situ protection of **48** (scheme 2.13):

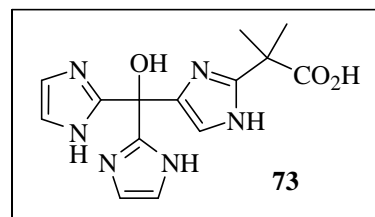
See prior procedure to synthesize **48**. The procedure was only modified in its quenching procedure whereby EtOAc and H₂O were replaced by the desired electrophile and stirred at room temperature for 1 h. Aqueous work-up gave **48** in yields not significantly different from the normal procedure.

Addition of bromo-acetic acid *tert*-butyl ester to **47** (scheme 2.23):

1-(*N,N*-Dimethylsulfamoyl)-imidazole (0.500 g, 2.85 mmol) **47** was dissolved in dry THF (30 mL) under a positive pressure of Ar. With vigorous stirring, the temperature was lowered to -78 °C and a solution of *n*-BuLi in pentane (3.14 mmol, 1.7 mL of a 1.88 M solution, 1.1 eq.) was added drop-wise. After stirring for 30 min, bromo-acetic acid *tert*-butyl ester (3.14 mmol, 0.47 mL) was added neat. The reaction mixture was then left at room temperature overnight and quenched with H₂O. The organic phase was separated and the organic solvent removed under reduced pressure to yield the starting material by ¹H NMR analysis of the crude mixture and unidentified products.

Chapter 3

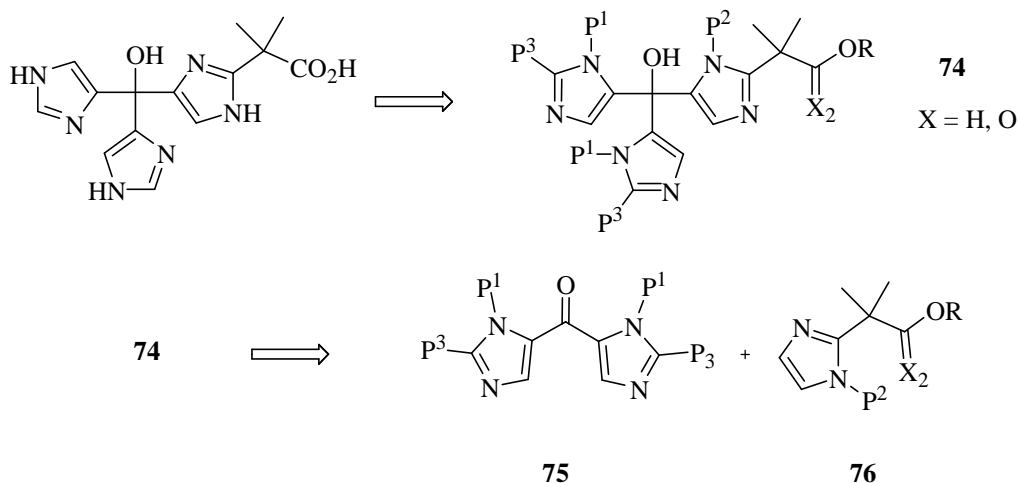
Synthesis of the Mixed Carboxylate-Functionalized Carbinol **73** and Study of its Coordination Chemistry



3.1 Introduction: retrosynthetic analysis

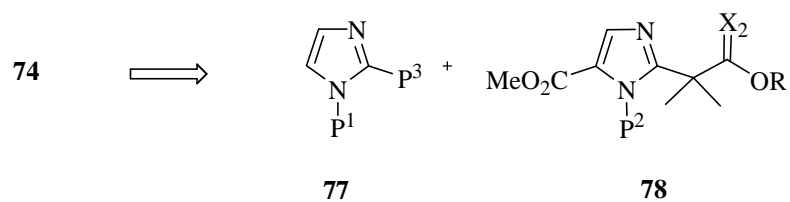
The initial route devised to reach the desired target **73** appeared problematic due to unforeseen difficulties encountered in purifying these poly-imidazole containing molecules, compounded by unfavorable physical properties such as poor solubility. All but methanol and water were found to solubilize 4-TIC and thus with such a limited arsenal of solvents most transformations considered became almost intractable. In order to secure enough material and study the coordination chemistry of the 3-Imidazole-1-carboxylate ligand, it became clear that these properties always be kept in mind when designing a synthetic plan in order to maximize yields and ease of isolation. The direct illustration of this strategy is the incorporation the pendant arm in one of the initial building blocks rather than the initial late functionalization strategy (scheme 3.1 and 3.2). Indeed, the fewer the number of steps involving the tripod itself the greater the chances of success, and therefore the target was envisioned *via* two different routes. The first one investigated (scheme

3.1) was the addition of a functionalized imidazole moiety **76** already bearing the pendant arm to a bis-imidazole ketone **75**.



Scheme 3.1

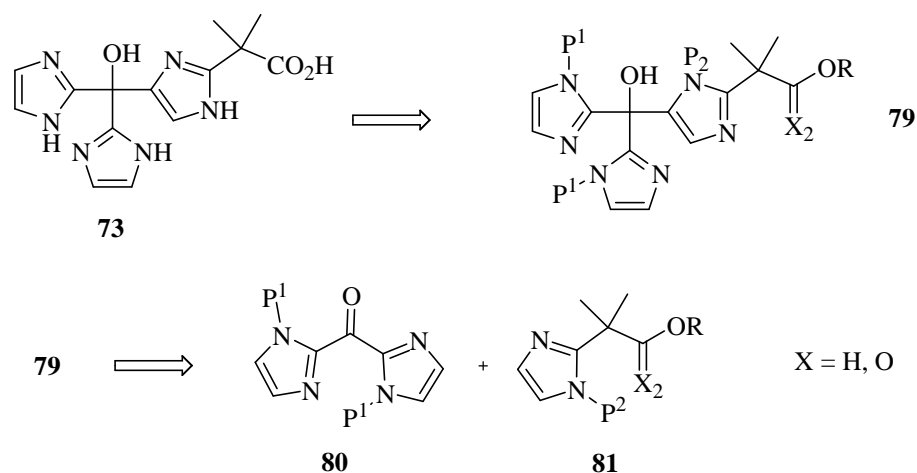
The second approach (scheme 3.2), a complementary route, envisioned the addition of two equivalents of nucleophiles **77** to an imidazole ester bearing the pendant arm **78**.



Scheme 3.2

Both of these routes are aiming at a 4-TIC analogue as the ultimate target. The synthesis of a model substrate **73**, a mixed tripod with a C4 and two C2 linkages, was initially considered by the simplified path delineated in scheme 3.3. This approach was a model study to the more complex target and, as shown in the retrosynthetic scheme below, one of the obvious advantages of such a strategy is

the absence of C2 reactive positions on the ketone **80**, therefore by-passing a protection-deprotection sequence.

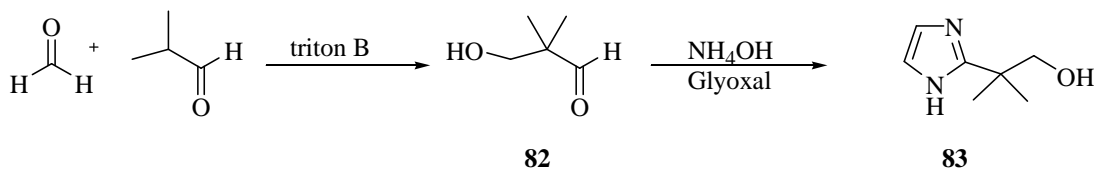


Scheme 3.3

3.2 Synthesis of precursors **80** and **81**

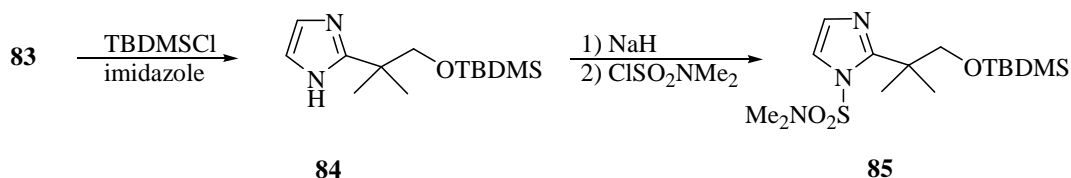
3.2.1 Synthesis of protected imidazole **85**

Reports of 2-functionalized imidazoles with the desired oxidation state on the side-chain were not available at the time of the synthetic work, but the known 2-(1H-imidazol-2-yl)-2-methyl-propan-1-ol **83** (scheme 3.4) seemed to display all the required features for an initial test of the proposed synthetic route. The compound is readily available in gram quantity in two steps (37% yield overall) and makes for a good starting point. Condensation of formaldehyde and iso-butyraldehyde led to the hydroxy aldehyde **82** which once condensed with glyoxal and ammonium hydroxide, gave the imidazole alcohol **83**.¹⁴²



Scheme 3.4

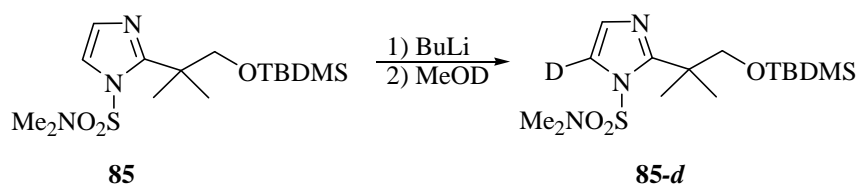
The alcohol **83** was then protected with TBDMS-Cl in methylene chloride in the presence of imidazole, as a base, in excellent yield (94% yield) (scheme 3.5). The white product was easily purified by recrystallization from acetonitrile and characterized by NMR spectroscopy. The ^1H NMR signals of the TBDMS group and their relative integration supported the assignment of the product. The identity of **84** was also confirmed by ^{13}C spectroscopy and mass spectrometry. *N*-protection performed at room temperature with NaH and *N,N*-dimethylsulfamoyl chloride yielded the desired compound **85** in good yield (72%). The characterization of **85** was simplified by the appearance of two doublets, δ 7.19 ppm and δ 6.95 ppm with a coupling constant of $J= 1.5$ Hz from the imidazole ring protons and the resonances of the sulfamoyl protecting group. Further characterization by ^{13}C NMR spectroscopy supported the *N*-protection of the imidazole.



Scheme 3.5

The pro-nucleophile was thus rapidly prepared in four steps in an overall yield of 25% from iso-butyraldehyde. Lithiation at the C5-position was probed by addition

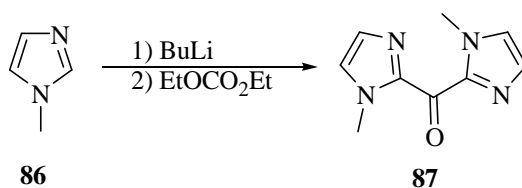
of BuLi at -78 °C and quenching with deuterated methanol. Complete deuteration of the 5-position was observed by ^1H NMR spectroscopy (scheme 3.6). The characteristic doublets of the aromatic ring in **85** became a singlet in **85-d**, confirming the quantitative lithiation at the desired position. With these results established we then turned our attention to the electrophilic partner of the reaction.



Scheme 3.6

3.2.2 Synthesis of symmetrical bis-imidazolyl ketones **87-89**

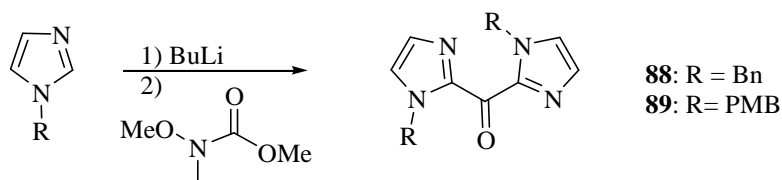
Symmetrical 2-imidazolyl-ketones are known and some preparations have been published. We settled for C-2 ketones as model substrates due to their availability and the N-methyl protected ketone **87** was easily prepared in large quantity according to the known procedure illustrated in scheme 3.7.¹⁴³



Scheme 3.7

One of the problems encountered with ketone **87** was its low solubility in aprotic solvents such as THF, which rendered its handling in reactions where BuLi was used rather difficult. In order to address this obstacle other ketones were also

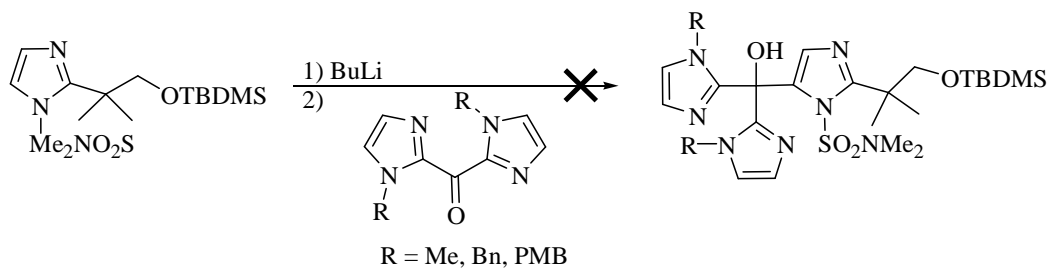
prepared. The known ketones capped by a benzyl (Bn) **88**¹⁴⁴ or a para-methoxybenzyl (PMB) **89** protecting group¹⁴⁵ showed increased solubility in organic solvents. The preparations of these two ketones were carried out according to the published procedures *via* the formation of a Weinreb amide and were utilized as electrophilic partners in the addition reaction (scheme 3.8). Ketones **88** and **89** were obtained in 81% yield and 92% yield respectively, as white solids and were characterized by ¹H and ¹³C NMR spectroscopy.



Scheme 3.8

3.2.3 Addition attempts of **85** to **87-89**

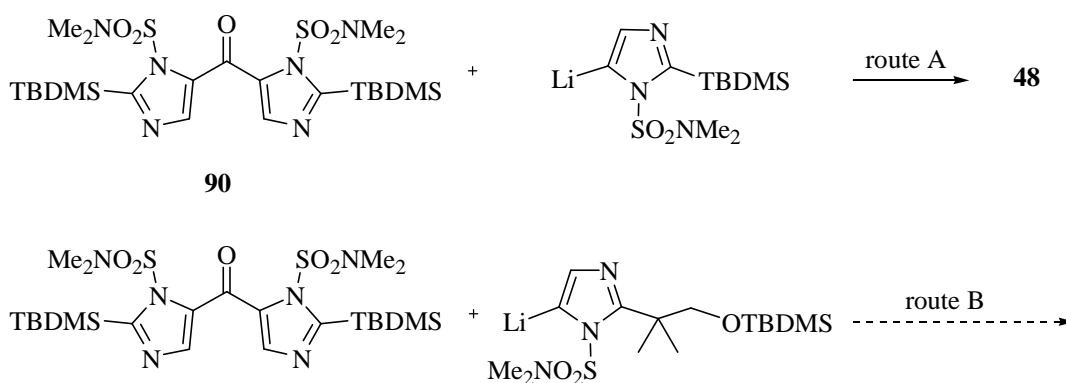
All three synthesized ketones **87-89** were used in addition attempts (scheme 3.9). Initially, the 1-methyl-imidazolyl ketone was added to the reaction mixture *via* cannula where the nucleophilic partner was preformed at -78 °C with one equivalent of BuLi. ¹H NMR analysis of the crude mixture confirmed a lack of the expected product and the formation of a myriad of imidazole-containing products. Although the failure to obtain the expected product was initially blamed on the poor solubility of the reactant **87**, reactions carried out with electronically equivalent substrates such as benzyl **88** and PMB **89** protected imidazoles did not differ in their outcomes.



Scheme 3.9

3.2.4 Conclusion

These surprising results presented us with a rather difficult problem since no obvious reasons for these failed attempts could be put forward. The initial simplification of the synthetic route using a 2-imidazolyl-ketone seemed unlikely to be responsible for this lack selectivity. Despite the negative results we turned our attention to the preferred substrate **90** (= **75** with P¹ = SO₂NMe₂ and P³ = TBDMS) (scheme 3.10) hoping that our success in forming **48** in the synthesis of 4-TIC (scheme 2.10) would translate to this slightly modified version. A direct parallel could be drawn between routes A and B as an intermediary ketone was presumably formed on the way to **48** (route A),

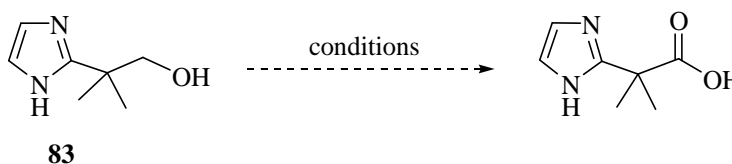


Scheme 3.10

3.3 Modification and optimization of precursor syntheses

3.3.1 Introduction: oxidation attempts of alcohol **83**

Oxidation of the alcohol (scheme 3.11) to the carboxylic acid was also probed on the model compound¹⁴⁶⁻¹⁴⁸. This oxidation proved to be more complex than anticipated initially since purification of the zwitterionic product was complicated by its water solubility. Only the oxidizing system involving 2,2,6,6-tetramethylpiperidine 1-oxyl (TEMPO) and iodobenzene diacetate (BAIB) seemed to produce any crude products that included the desired target, as determined by *in situ* ¹H NMR spectroscopy. No optimization or isolation of the product was successful given the complexity of the mixtures.



Scheme 3.11

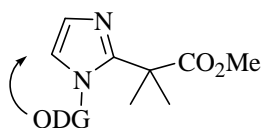
Entry	catalyst	Stoichiometric oxidant	Additives
1	RuCl ₃ ·3H ₂ O	TCCA	TBAB, Na ₂ CO ₃
2	TEMPO	BAIB	n/a
3	TEMPO	TCCA	n/a

Table 3.1: Reactions of scheme 3.11

3.3.2 Modifications and synthesis of precursor **54**

The nucleophilic imidazole component **85** even though practical for its ease of preparation, presented the major drawback of having its side chain in the wrong

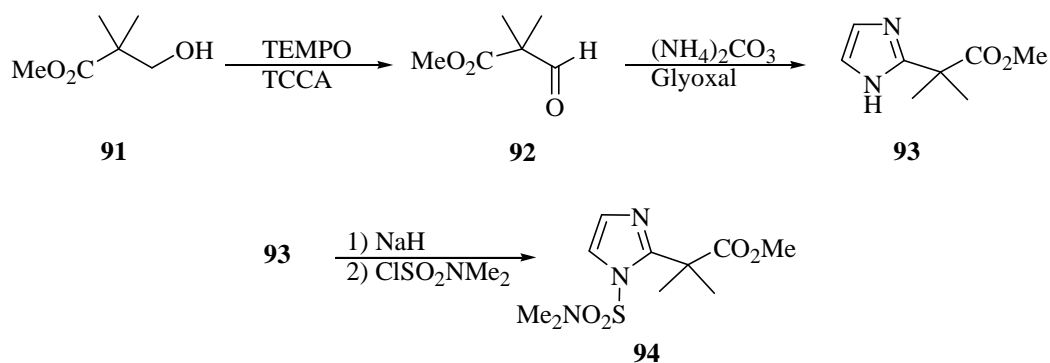
oxidation state. This side chain was initially incorporated to prevent too many late stage chemical transformations but was not the best possible option. A more effective strategy would be to carry through the entire synthesis the desired tether in its correct oxidation state as an ester (scheme 3.12). Adding such an electrophilic site in the precursor was apparently trading one problem for another as the compound must be deprotonated by the nucleophilic base BuLi. We therefore envisioned the use of an ortho-directing group (ODG) on the imidazole nucleus, which along with the sterically encumbered vicinal gem-dimethyl unit, would prevent any side reactions at the carboxyl group.



Scheme 3.12

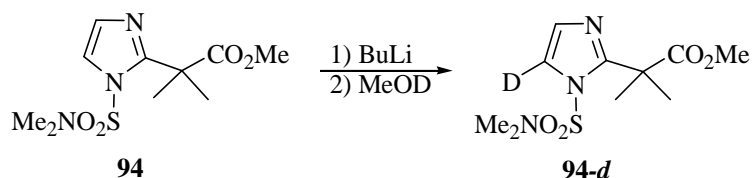
The desired new compound **94** was expeditiously synthesized by the oxidation of hydroxymethyl pivalate¹⁴⁹ **91** to **92** and without purification, engaged in the condensation to the imidazole derivative **93** (scheme 3.13) in 63% overall yield. The compound was easily purified by precipitation from EtOAc and fully characterized by NMR spectroscopy with three resonances at δ 6.99 ppm (s, 2H), δ 3.72 ppm (s, 3H) and δ 1.66 ppm by ¹H NMR and a more informative ¹³C NMR spectrum. The structure assignment was also supported by IR spectroscopy ($\nu(\text{CO})= 1729 \text{ cm}^{-1}$) and mass spectrometry (ESI +: exact mass calculated for C₈H₁₃N₂O₂ [M + H]⁺ 169.0972. Found 169.0962). Protection of the imidazole was carried out with *N,N*-dimethylsulfamoyl chloride and NaH to furnish the required precursor **94** in 60% yield. This white solid was again characterized by ¹H NMR

spectroscopy and the diagnostic appearance of two doublets of an N-substituted imidazole at δ 7.11 ppm and δ 7.01 ppm with coupling constant $J= 1.5$ Hz. The ^{13}C NMR and mass spectrometry confirmed the presence of the protecting group.



Scheme 3.13

The regioselectivity of the lithiation of the compound and its stability to nucleophiles was tested in a deuteration experiment (scheme 3.14). Complete incorporation of deuterium at C5, indicated by the disappearance of the aromatic doublets and appearance of a single aromatic singlet, allowed us to confirm the quantitative lithiation of **94** within the detection limit of ^1H NMR spectroscopy. No apparent decomposition of the methyl ester was detected by ^1H NMR analysis of the crude product **94-d**, confirming its use as competent precursor.

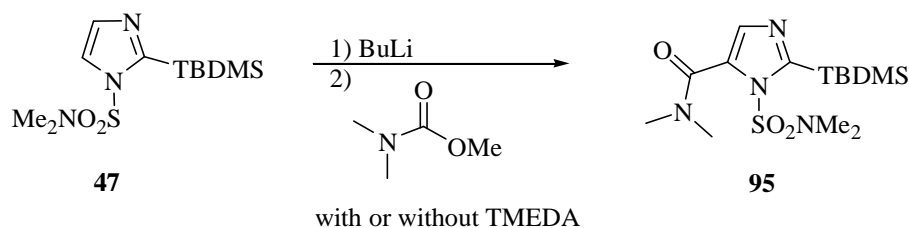


Scheme 3.14

3.4 Synthesis of bis-imidazolyl ketone **90**

3.4.1 First approach

Since our true goal was to obtain a 4-TIC derivative, the symmetrical ketone **90** of routes A and B (scheme 3.10) was a desired intermediate and could potentially be beneficial to the addition reaction by involving the presumed intermediate in the condensation of tripod **48**. The synthesis of the ketone **90** was more challenging than expected as the known procedures to form the desired product were quite ineffective. The simple transposition of the procedure, used to synthesize *N*-alkyl and *N*-benzyl symmetrical ketones **87-89**, to imidazole **47** (scheme 3.15), yielded only the undesired amide **95** and the starting material **47** as determined by ¹H NMR analysis. Attempts to modify the procedure by adding TMEDA or using Weinreb's amide did not improve the reactivity. This reactivity was observed either at the C2 (**47**) or the C5 (**46**) position and further confirmed prior findings by Katritzky¹⁵⁰ and Brown¹⁵¹.

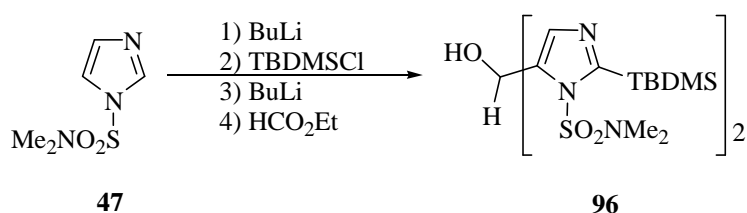


Scheme 3.15

3.4.2 Second approach

The inability to form the desired ketone **90** was circumvented by a two step procedure (scheme 3.16). First sulfonamide **47** was added to 0.5 equivalent of ethyl formate, using a “one pot procedure”, to yield the secondary symmetrically

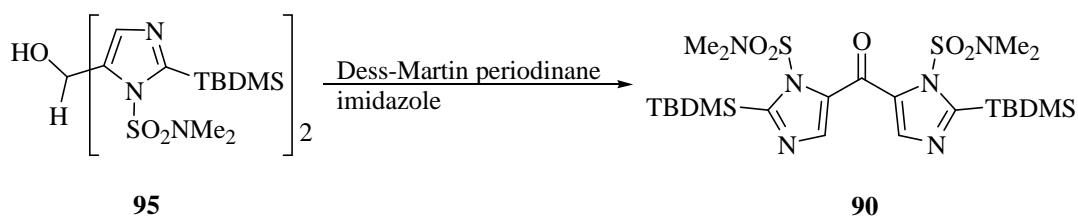
substituted alcohol **96**, in 51% yield. The compound was characterized by ^1H NMR spectroscopy and featured a doublet from the methine proton at δ 5.53 ppm and a doublet from the hydroxy proton at δ 3.58 ppm with $J= 3.6$ Hz. The composition of **96** was further supported by mass spectrometry (ESI+) through a diagnostic peak at $[\text{M}+\text{H}]^+ = 607.2$.



Scheme 3.16

The conditions for oxidation of the secondary alcohol were surveyed using different known methodologies. General conditions reported with PCC, DDQ, tempo/TCCA¹⁵², I₂/tempo¹⁴⁹, MnO₂¹⁵³, IBX^{154,155} all failed to produce ketone **90** from the alcohol and led to decomposition products. A milder oxidant was sought in the Dess-Martin periodinane reagent which proved indeed to be more effective. NMR analysis of the reaction mixture clearly indicated the clean formation of the product but also its decomposition when the conversion of the reactants reached an acceptable level. The release of protons during the oxidation was identified as a potential catalyst for a decomposition pathway, but no improvements were observed when an inorganic solid base such as sodium bicarbonate (NaHCO₃) was added. However the decomposition stopped almost completely when imidazole was added to the reaction mixture (scheme 3.17) and **90** was isolated in 60% yield and characterized by ^1H and ^{13}C NMR. The diagnostic deshielded aromatic protons

were observed at δ 7.55 ppm supporting the oxidation of the secondary alcohol to the ketone **90**.

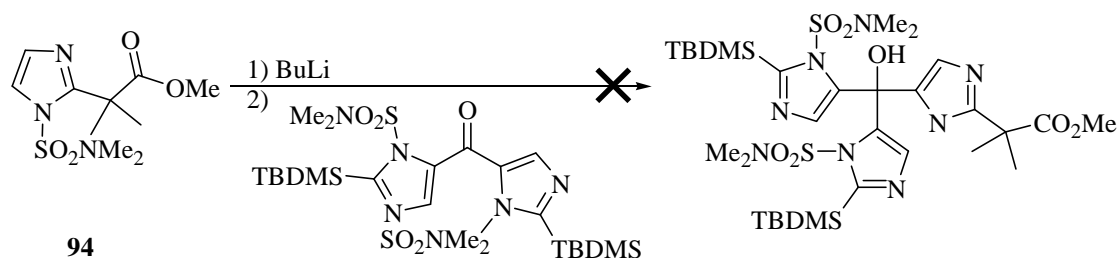


Scheme 3.17

Similarly to H_2O and $t\text{BuOH}$ ¹⁵⁶, imidazole was thought to act as a ligand rather than a base; replacing imidazole by $t\text{BuOH}$ led to comparable results.

3.4.3 Addition attempts with the new precursors **90** and **94**

With the two exact desired precursors **90** and **94** in our hands, attempts to conclude the synthesis by performing the required condensation were carried out (scheme 3.18). It was regrettably found that the reaction did not yield the expected product and the two starting materials were completely recovered with no decomposition. According to the ^1H NMR spectrum of the crude reaction mixture only the reactants were detectable with no formation of other compounds; hence it appears that no reaction occurred.



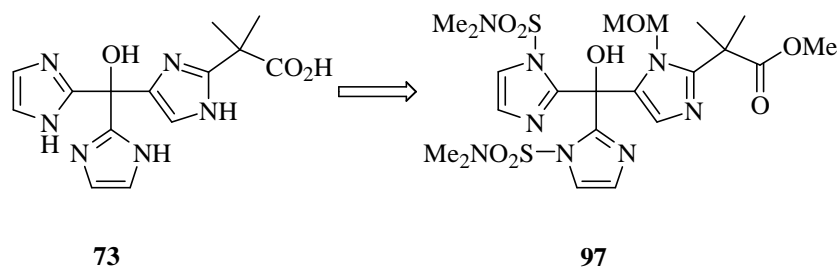
90
Scheme 3.18

The formation of the 5-lithio-imidazolyl starting material from **94** (scheme 3.18) was confirmed multiple times by deuteration and no reason has been found for the lack of reactivity of the reactants. It is all the more remarkable that a clear parallel can be drawn between route A (scheme 3.10), assumed to occur during the preparation of **48**, and B, this reaction. One can speculate on the electronic differences of the two pathways which could result in a potential energy mismatch of the reactants. The opposite inductive effects of the silyl group on **46** and carboxyl group on **94**, at the 2-position, could explain the difference in behavior. Indeed, TBDMS, an electron releasing group used in the synthesis of **48**, is directly attached to the aromatic ring, whereas the carboxyl group, inductively withdrawing, could deactivate the nucleophile **94** rendering it inefficient. As more unexpected results from such addition reactions were observed, attempts to model and understand the reactivity of the imidazole containing molecules by computational analysis is provided later.

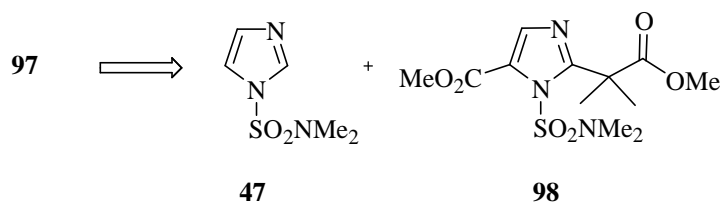
3.5 Second and third approach of a build-in carboxylate tether

3.5.1 Introduction: retrosynthetic analysis

As the first approach of the appended tripod failed to produce a viable route, a second look at the retrosynthetic analysis led us to investigate the synthesis of the target **73** (scheme 3.19.1) as the direct regioselective addition product of two equivalents of sulfonamide **47** to **98** (scheme 3.19.2). The necessary compound should easily be prepared as most of the chemistry required for a proper probe has been developed or is only a few steps removed from current known materials.



Scheme 3.19.1

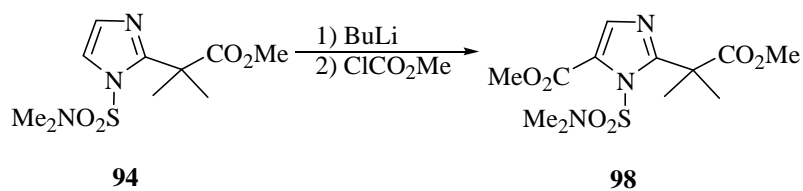


Scheme 3.19.2

3.5.2 Synthesis of precursor **98**

3.5.2.1 Synthesis of diester **98**

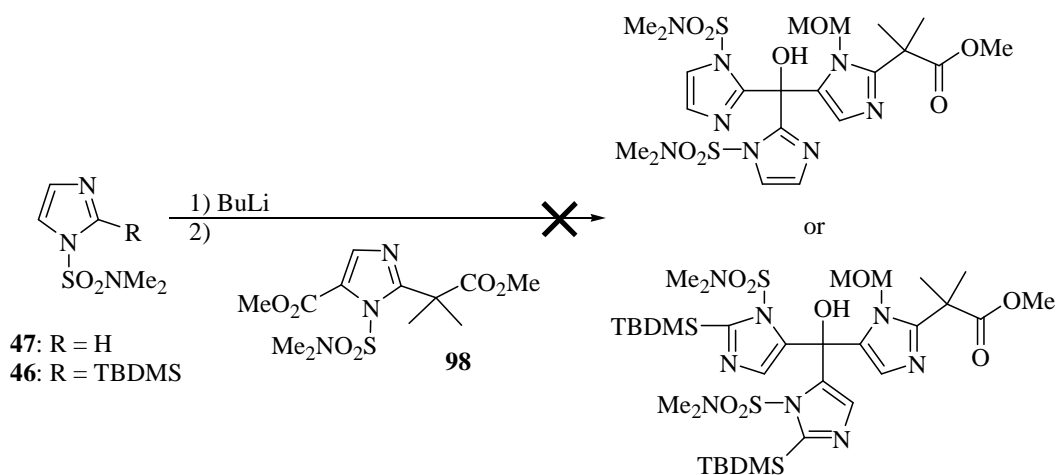
This new electrophile was simply obtained by deprotonation at the C5-position of **94** and quenching with methyl chloroformate (scheme 3.20). The product was easily purified and modification of the aromatic resonances (two doublets) in the ^1H NMR spectrum to a more deshielded singlet at δ 7.61 ppm confirmed the addition of the carboxyl group on the imidazole ring. The compound was fully characterized by ^{13}C NMR spectroscopy and its composition verified by mass spectrometry (ESI+).



Scheme 3.20

3.5.2.2 Addition attempts

Two reactions were attempted on the diester **98** (scheme 3.21). First, the addition reaction of the 2-lithio-N-sulfonamide imidazole, obtained from **47**, showed by ^1H NMR and TLC analysis the presence of numerous products in the crude reaction mixture. After aqueous work-up, reactant **47** was clearly detectable but **98** did not seem to have survived the reaction. This conclusion was further corroborated by the reaction of the 5-lithio-2-TBDMS-imidazole, obtained from **46**, with **98** with similar results. After aqueous work-up, no apparent consumption of **46** and no recovery of the electrophile **98** were detected by ^1H NMR analysis of the crude mixture.

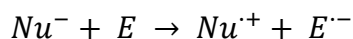


Scheme 3.21

3.5.2.3 Conclusion

These observations were difficult to explain and a hypothesis was formulated. The sulfamoyl protecting group used could be responsible for such a contrarian behavior of the reactions. This was circumstantially supported by the radical modification of the nucleophilicity of imidazoles, as the organo-lithium

species could not be added to amides (scheme 3.15) as observed by Katritzsky¹⁵⁰, Brown¹⁵¹ and us. In the present case the strong electron withdrawing ability of the sulfamoyl protecting group could facilitate electron transfer from the organolithiums **46-47** to **98** to form a stable radical anion (equation 3.1).



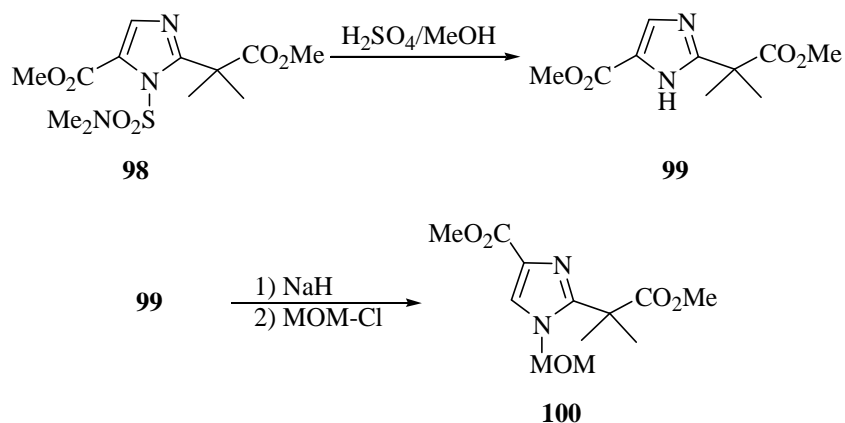
Equation 3.1

In order to test this hypothesis, we decided to modify the electronic character of the imidazole diester **98** by introducing a more electron rich protecting group.

3.5.3 Third approach of a build-in carboxylate tether

3.5.3.1 Synthesis of MOM-protected imidazole **100**

Introduction of a MOM protecting group on **98**, chosen for the ease of its removal under acidic conditions, was simply accomplished in two steps by a deprotection/protection sequence (scheme 3.22). The sulfonamide protecting group was promptly removed in methanol with catalytic amount of sulfuric acid to yield **99** in 85% yield, which displays a very broad singlet for the aromatic proton. The signal was sharpened by protonating **99** with deuterated trifluoroacetic acid. The compound **99** fully characterized spectroscopically and then regioselectively protected using one equivalent of NaH and chloromethyl methyl ether (MOM-Cl) to give **100** in 90% yield.



Scheme 3.22

The C4 location of the ester was established by a NOESY experiment. Irradiation of the methylene group of the MOM protecting group allowed us to detect the methyl group of the MOM and gem-dimethyl unit by NOE but more importantly the resonance of the aromatic proton was also enhanced (Figure 3.1: NOESY experiment on **100**).

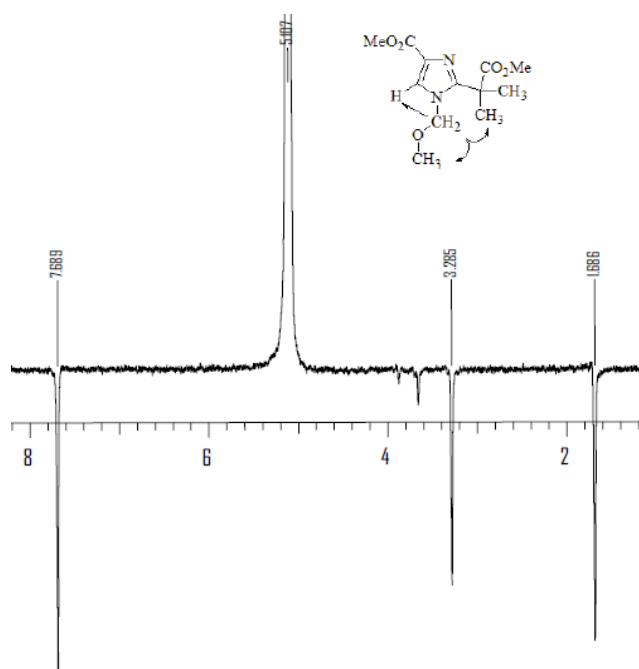
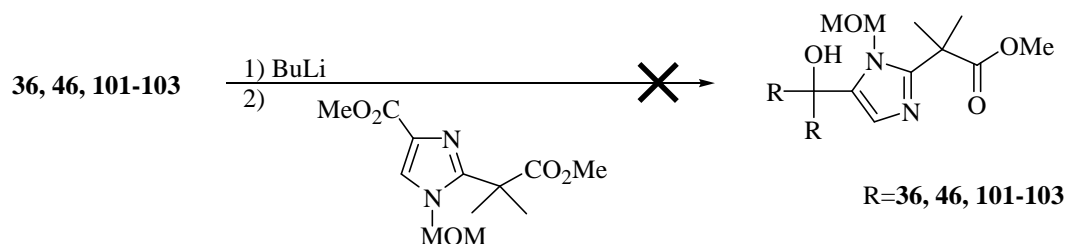


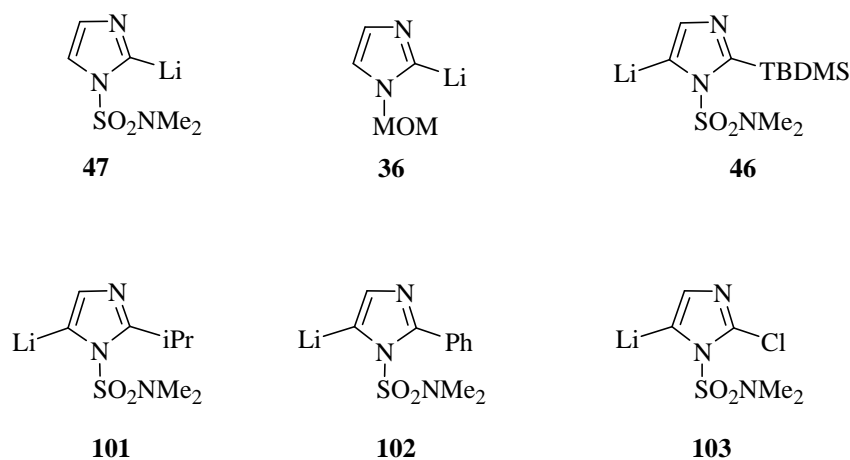
Figure 3.1: NOESY experiment on **100**

3.5.3.2 Addition attempts to **100** and synthesis of **73**

With compound **100** readily available we then tested the addition reactions (scheme 3.23) with the different lithiated pro-nucleophiles **36**, **46**, **47** and **101-103** (scheme 3.24):



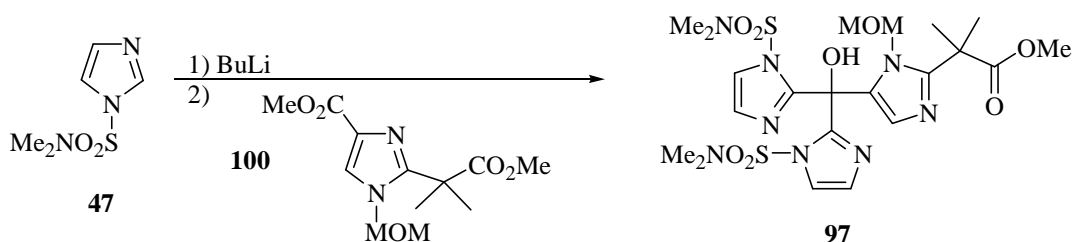
Scheme 3.23



Scheme 3.24

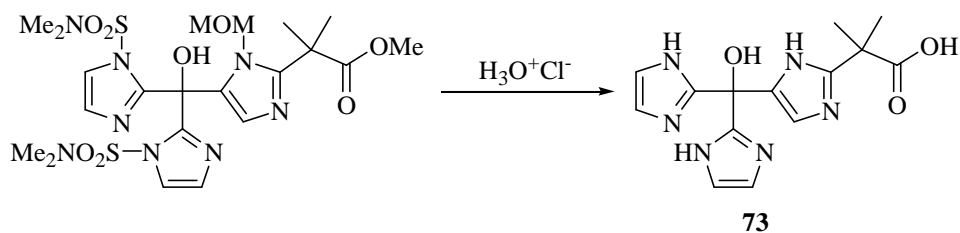
All the pro-nucleophiles **36**, **46**, and **101-103** were recovered after aqueous work up of the reaction mixture, but as previously described the electrophile **100** was completely consumed and could not be recovered (scheme 3.23). Only one substrate **47** was found to be effective for the double addition to **100** (scheme 3.25).

Though completely specific to a single reactant, one should emphasize that this reaction proceeded smoothly to the desired compound **97** in 74% yield. The expected two doublets of the nucleophilic imidazole protons at δ 7.31 ppm and δ 6.93 ppm with a coupling constant $J= 1.5$ Hz were detected by ^1H NMR spectroscopy along with the singlet of the electrophilic imidazole proton shifted upfield by 1.15 ppm at δ 6.54 ppm.



Scheme 3.25

The synthesis could thus be completed by hydrolysis of the protecting groups, sulfamoyl and MOM, and the ester in 6N HCl to give after purification by cation exchange chromatography the mixed tripod **73** in 85% yield (scheme 3.26).



Scheme 3.26

As determined by ^1H NMR, the compound displayed the expected three resonances at δ 7.17 ppm (4H), δ 6.81 ppm (1H) and δ 1.55 ppm (6H). The white solid was found to be soluble only in methanol and water most likely due to the presence of

its zwitterionic form. Full characterization by ^{13}C NMR, IR spectroscopy and mass spectrometry confirmed the structure of **73**.

3.6 Computational Studies

3.6.1 The influence of the protecting groups in terms of electron affinity

The successful addition of **47** and only **47** to the diester **100** was investigated in greater depth as to better understand what the required characteristics of an effective nucleophile were. We were especially interested in understanding why compounds **36**, **46**, and **101-103** were not competent nucleophiles. Computational chemistry was used to examine the frontier orbitals to try to elucidate the reasons for such a narrow scope and to develop a predictive model to identify which reaction partners would combine effectively.

The LUMOs of **98** and **100** were calculated using the density functional method (DFT) at the B3LYP 6-311+G(d,p)//6-31+G(d) level and are displayed below (figure 3.2). As expected, the strong electron withdrawing capacity of the sulfonamide **98** shows a more extensive delocalization of the LUMO (orbital accepting an electron) on the aromatic ring (on the C2 carbon) than the MOM protected imidazole **100**; hence a greater ability to stabilize a radical anion by **98**.

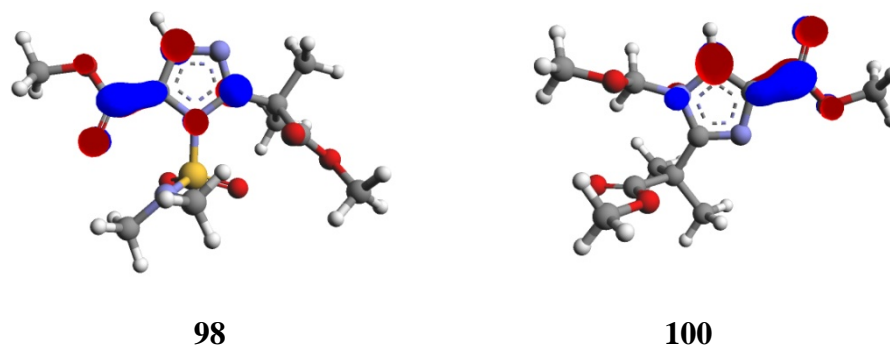
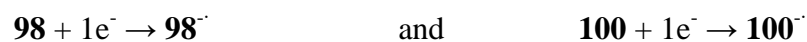


Figure 3.2: LUMOs of **98** and **100**, isocontour at 0.08 au

The vertical electron affinities were calculated at the same level of theory from equations 3.1 ($\Delta H_{\text{reaction}} = -EA$)¹⁵⁷ and interestingly showed a slightly exothermic process for the sulfonamide **98** whereas it is endothermic for the MOM protected imidazole **100** (table 3.2).



Equations 3.1

	98	100
$\Delta H = (-)\text{vertical EA (eV)}$	-0.03	0.49

Table 3.2: (-)Vertical EA (eV)

The opposite signs for the enthalpy of reaction reinforced the notion that the protecting group was at least partially responsible for the observed reactivity. As organolithiums can be considered good reducing agents, the ease with which the electrophilic partner accepts a single electron might be responsible for promoting

side reactions and their decomposition. This explanation was obviously not complete and one needed to address the limited number of competent nucleophiles discovered for this transformation.

3.6.2 Ionization of the nucleophiles **36**, **46**, **47**, **101-103**

If the model is consistent one should observe that stronger reducing reactants are ill suited nucleophiles for the addition to the MOM-protected imidazole. This trend was verified by calculating the energy of the HOMO of each nucleophile engaged in the reaction, using the DFT method with the B3LYP 6-31+G(d) level (table 3.3).

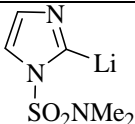
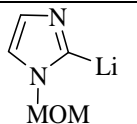
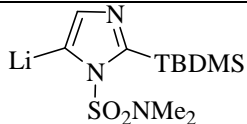
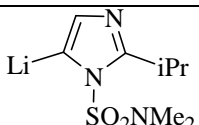
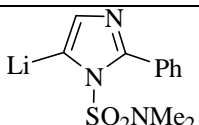
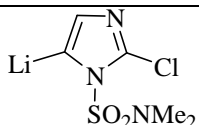
Nucleophiles			
Energy in eV (HOMO)	-6.01	-5.74	-5.72
Nucleophiles			
Energy in eV (HOMO)	-5.57	-5.46	-5.83

Table 3.3: HOMO energies of selected nucleophiles

Satisfyingly, the only imidazole capable of addition of **47** is also the weakest reducing agent (lower energy of HOMO), as Koopman theorem states that the average orbital (HOMO) energy is equal to the ionization potential. However, these calculations are not complete as many assumptions were made and used to simplify the model. The first and probably the most important is the physical state of the

nucleophiles themselves as the aggregation state of the substrate was assumed to be monomeric, which may not be accurate. Moreover calculations of enthalpies of reactions are notorious for their basis set dependence and a more accurate determination is usually achieved by a G2 or G3 calculation which was not available to us at the time. And last but not least the calculations are done in the gas phase not representative of the true reaction conditions in solution.

To conclude the reaction is partially explained in terms of ionization potential and electron affinity. We can therefore speculate that a competent nucleophile must have its HOMO energy at least equal to or lower than that of the 2-lithio-*N*-sulfonamide imidazole obtained from **47** (≈ -6 eV). If correct in our interpretation, the energy of the HOMO of the nucleophile can be used as a condition necessary, but not sufficient for a successful addition.

3.6.3 Conclusion

We developed an effective synthesis of a mixed tripod C2 and C4 with a carboxylate tether in 8 steps (longest linear sequence) with an overall yield of $\sim 15\%$ from hydroxy pivalate methyl ester, a cheap commercially available compound. Moreover we also provide a rationale for the limited substrate scope observed in the addition reaction to **100**. Our calculations should provide guidelines in the choice of protecting groups and nucleophiles. The sulfamoyl protecting group should not be used in the presence of strong reducing agent and the HOMO of the lithiated compound should have its energy approximately equal to or lower than 6 eV.

3.7 Coordination chemistry and metal ion complexation by **73**

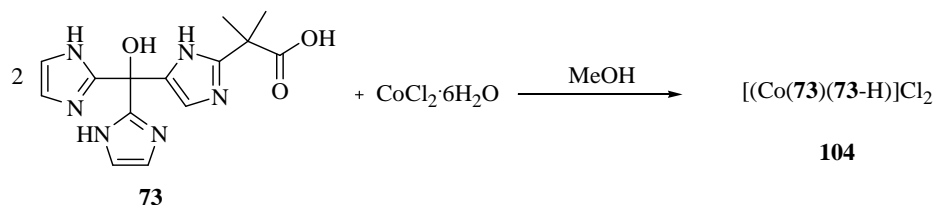
3.7.1 Addition of base and its effect

All complexation attempts with **73** were carried out in either water or methanol with the addition of an external inorganic base such as sodium bicarbonate. The choice of these polar protic solvents was dictated by the solubility of tripod **73** and all reactions led to the formation of insoluble amorphous solids which could not be redissolved. This behavior was observed with all the following metal salts: $\text{FeCl}_2 \cdot 6\text{H}_2\text{O}$, $\text{Fe}(\text{acac})_3$, $\text{Fe}(\text{NO}_3)_3 \cdot 9\text{H}_2\text{O}$, CuCN , $\text{Cu}(\text{acetate})_2 \cdot \text{H}_2\text{O}$, $\text{Cu}(\text{CH}_3\text{CN})_4\text{PF}_6$, $\text{Zn}(\text{OTf})_2$. As a general rule the precipitation of solid products presumed to be oligomers with bridging imidazoles and carboxylates always appeared after addition of a base.

3.7.2 Synthesis of cobalt (III) complex under neutral conditions

The metal salts and protonated ligands are soluble and attempts to characterize the coordination properties of the ligand was achieved by complexation of cobalt (III). For example, the reaction between **73** and $\text{CoCl}_2 \cdot 6\text{H}_2\text{O}$ in methanol open to the air led to the isolation of a dark red solid Co^{III} complex (scheme 3.27), $[\text{Co}(\mathbf{73})(\mathbf{73-H})]\text{Cl}_2$ **104**, which was characterized spectroscopically by ^1H NMR and its structure established by X-ray diffraction (figure 3.3). The octahedral geometry about the cobalt atom in **104** is provided by two 2-imidazole-1-carboxylate subunits of the ligands coordinated in a meridional fashion, with the third imidazole of each ligand free to engage in a short (2.68 Å) imidazole-H-imidazolium hydrogen bond (N23B-H-N23A). The methyl groups of the pendant arm are inequivalent and have a chemical shift of δ 1.55 ppm and 1.70 ppm.

Moreover three signals are found for the imidazole protons: 1) two resonances are shifted upfield by the proximal aromatic systems at δ 5.20 ppm (1H) and 6.77 ppm (1H) with a coupling constant of $J= 2.1$ Hz, 2) one broad singlet at δ 6.90 ppm (2H) and 3) a singlet at δ 8.17. ppm (1H). Due to their coordination to cobalt (III) all three imidazoles are inequivalent and this was reflected in the three different resonances detected for the imidazoles NHs. Finally the proton involved in the short hydrogen bond was located at approximately δ 13 ppm in the baseline (see experimental).



Scheme 3.27

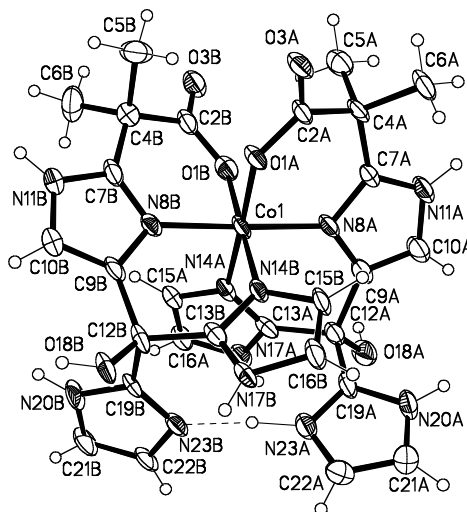


Figure 3.3: X-ray ORTEP diagram for the dication of **104**

Selected bond lengths (Å): Co(1)-O(1B)= 1.888(5); Co(1)-N(8A)= 1.895(5); Co(1)-N(8B)= 1.908(5); Co(1)-N(14A)= 1.910(5). Selected angles (°): O(1B)-Co(1)-O(1A)= 91.21(17); O(1B)-Co(1)-N(8A)= 89.00(19).

3.8 Conclusion

After careful analysis we determined that the ligand itself might not possess the correct architecture for an N_3O -coordination in an octahedral environment. The ligand was initially conceived as a tripod plus a pendant arm (figure 3.4 (a) and (b)), but this was not an accurate indication of its coordinating properties. The carboxylate functionality of the tether is the strongest coordinative bond in the ligand and its strong electrostatic interaction with the positively charged metal most likely controls the coordination mode of the ligand. The crystal structure of the cobalt complex seems to indicate a preference for a meridional coordination with one carboxylate and two imidazoles. The preferred coordination mode of the ligand is therefore better described as a 2-imidazole-1-carboxylate unit plus one imidazole (figure 3.4 (c)).

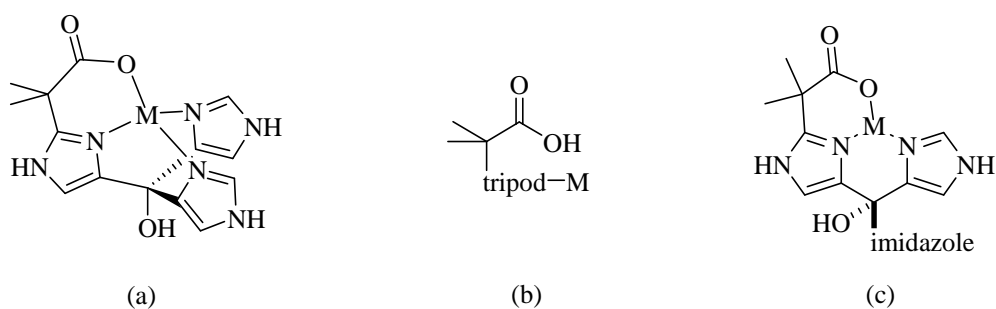


Figure 3.4: Binding modes of **73**

In the particular case of the cobalt complex **104** a greater gain in energy is achieved by coordinating a second ligand, with little steric repulsion or strain, rather than coordinating the third imidazole. As iron and nickel coordinations were considered primary goals and the more technical problems encountered (oligomerization) could also stem from poor coordination behavior, we turned our attention to designing a new ligand with the appropriate feature to a tetradentate N_3O -coordination in an octahedral environment.

3.9 Experimental

Compounds **46**¹³², **83**^{142,158}, **87**¹⁴³, **88**¹⁵⁹, **89**¹⁴⁵, MOM-Cl¹⁶⁰, **36**¹⁶¹ were prepared by known procedures and matched all spectroscopic data available.

Oxidation attempts of **83** were carried out according to the published procedures.¹⁴⁶⁻

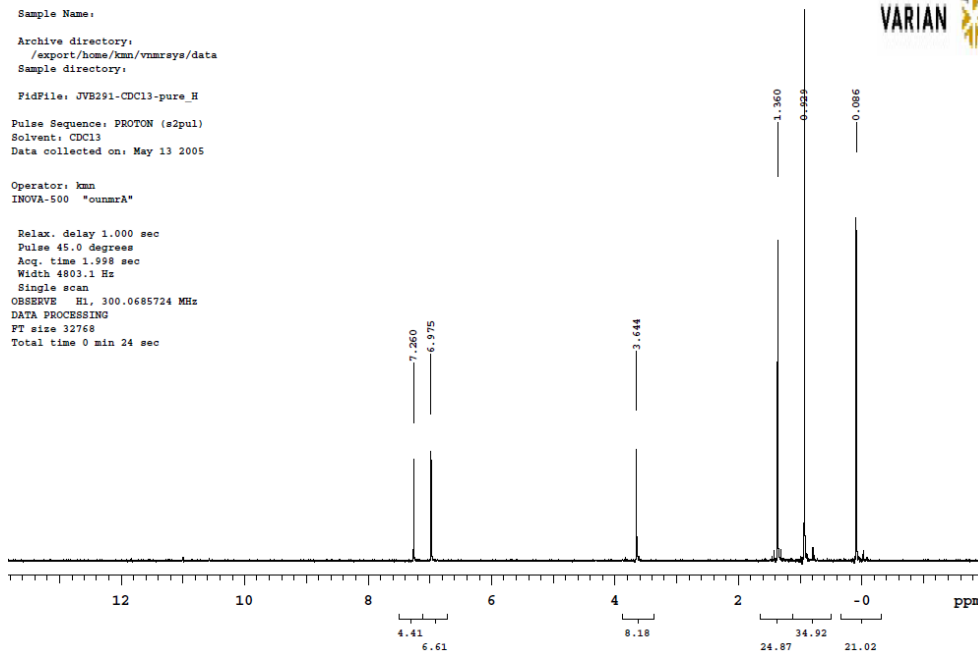
148

2-[2-(tert-Butyl-dimethyl-silanyloxy)-1,1-dimethyl-ethyl]-1H-imidazole **84**

Compound **83** (2.00 g, 14.3 mmol) and imidazole (1.94 g, 28.5 mmol, 2.0 eq.) were dissolved in dry CH₂Cl₂ (60 mL) and stirred at room temperature, TBDMSCl (2.58 g, 17.1 mmol, 1.2 eq.) was then added and left at room temperature overnight. The reaction mixture was diluted with EtOAc (100 mL) and washed with saturated NaHCO₃ (2 × 25 mL), brine (25 mL) and dried over MgSO₄. The organic solvents were partially removed by rotary evaporation and a white solid precipitated which was filtered to yield compound **84** (3.40 g, 94% yield). ¹H (300 MHz, CD₃OD) δ 6.98 (s, 2H), 3.64 (s, 2H), 1.36 (s, 6H), 0.93 (s, 9H), 0.09 (s, 6H); ¹³C (75.5 MHz, CDCl₃) δ 154.9, 73.1, 39.7, 26.4, 24.2, 19.2, -5.4; MS (ESI +): exact mass calculated for C₁₃H₂₇N₂OSi [M + H]⁺ 255.19. Found 255.19.

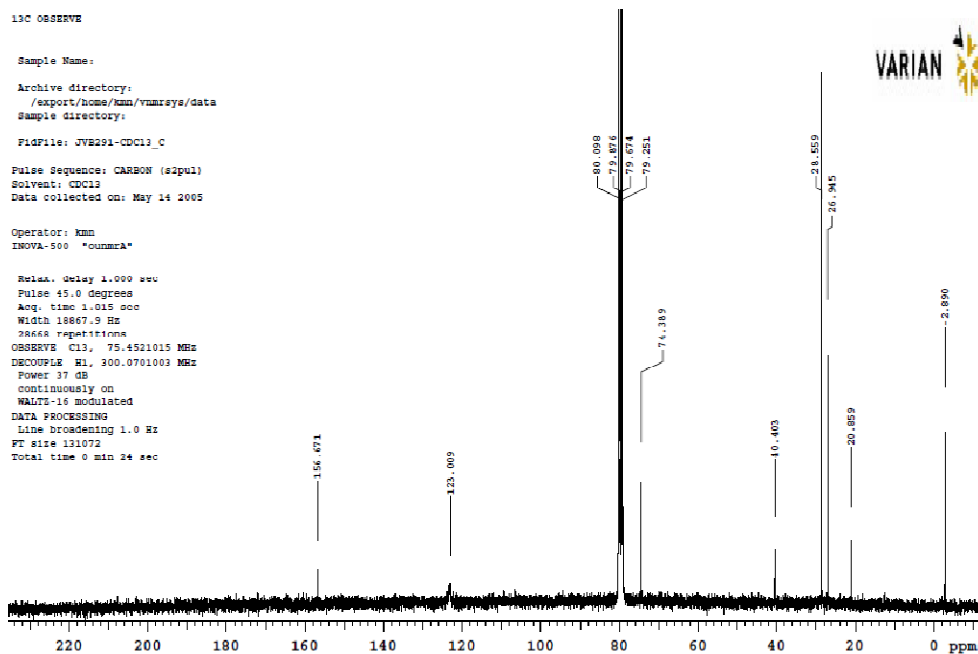
STANDARD 1H OBSERVE

Sample Name:
Archive directory:
/export/home/knn/vnmrsws/data
Sample directory:
FidFile: JVB291-CDCl3-pure_H
Pulse Sequence: PROTON (s2pul)
Solvent: CDCl3
Data collected on: May 13 2005
Operator: knn
INNOVA-500 "oumrA"
Relax. delay 1.000 sec
Pulse 45.0 degrees
Acq. time 1.998 sec
Width 4803.1 Hz
Single scan
OBSERVE H1, 300.0685724 MHz
DATA PROCESSING
FT size 32768
Total time 0 min 24 sec



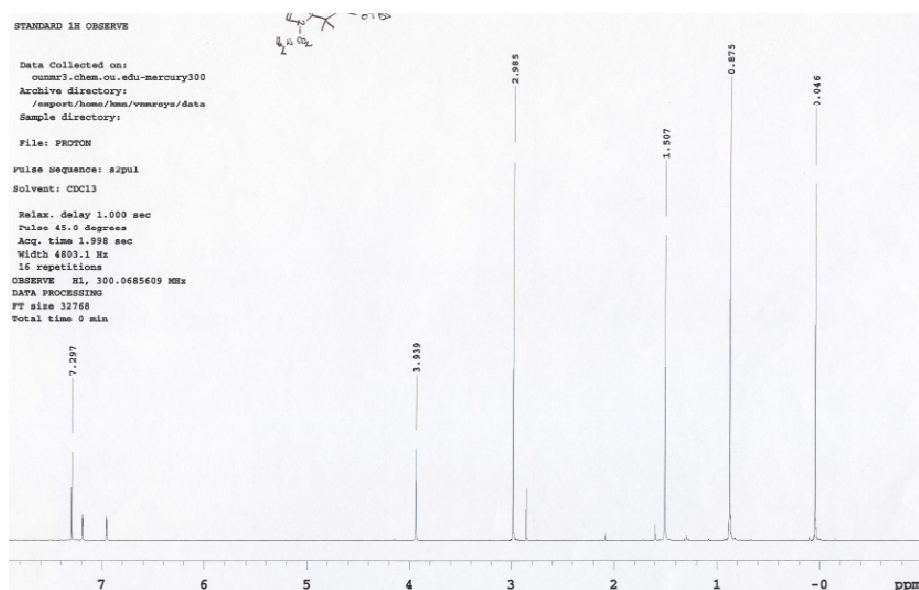
13C OBSERVE

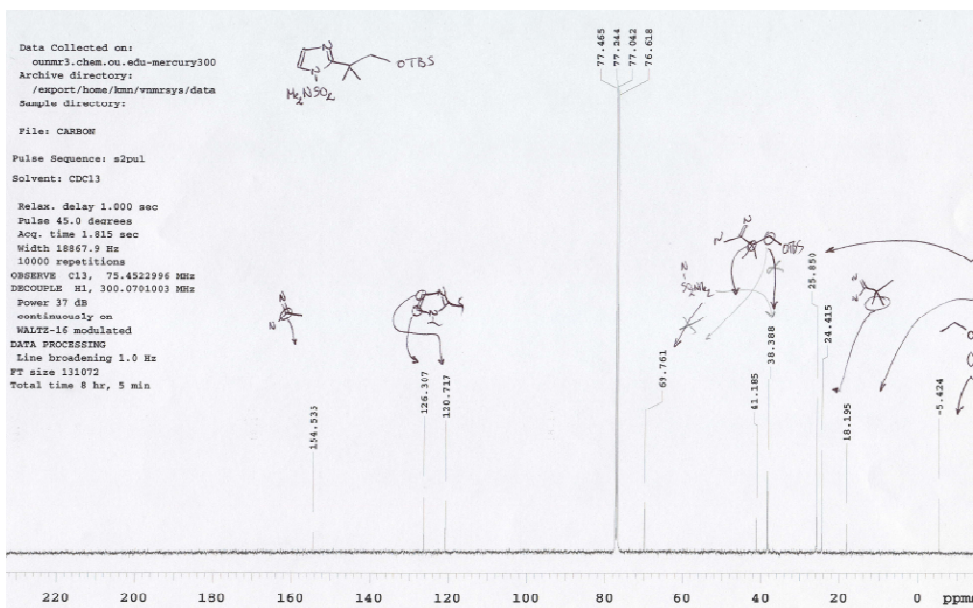
Sample Name:
Archive directory:
/export/home/knn/vnmrsws/data
Sample directory:
FidFile: JVB291-CDCl3_C
Pulse Sequence: CARBON (s2pul)
Solvent: CDCl3
Data collected on: May 14 2005
Operator: knn
INNOVA-500 "oumrA"
Relax. delay 1.000 sec
Pulse 45.0 degrees
Acq. time 1.015 sec
Width 18667.9 Hz
28668 repetitions
OBSERVE C13, 75.4921015 MHz
DECOUPLE H1, 300.0701003 MHz
Power 37 dB
continuously on
WALTZ-16 modulated
DATA PROCESSING
Line broadening 1.0 Hz
FT size 131072
Total time 0 min 24 sec



2-[2-(tert-Butyl-dimethyl-silyloxy)-1,1-dimethyl-ethyl]-1-sulfamoyl-1H-imidazole **85**

To a stirred solution of **84** (1.01 g, 4.0 mmol) in dry THF (10 mL) cooled to 0 °C, NaH (0.64 g 60% dispersion in mineral oil, 16 mmol, 4 eq.) was added portion-wise over 30 min and left at room temperature for 30 min. N,N-dimethylsulfamoyl chloride was then added neat (0.51 mL, 4.8 mmol, 1.2 eq.) and the solution was refluxed for 3 h. The reaction was quenched with H₂O and ethyl acetate was added (50 mL). The organic phase was then washed with saturated NaHCO₃ (2 × 25 mL), brine (25 mL) and dried over MgSO₄. The organic solvents were removed under vacuum and the crude material purified by flash column chromatography (7 AcOEt: 3 Hexanes) to yield the desired compound as a white solid (1.03 g, 60% yield). ¹H (300 MHz, CDCl₃) δ 7.15 (d, *J*= 1.5 Hz, 1H), 6.91 (d, *J*= 1.5 Hz, 1H), 3.89 (s, 3H), 2.94 (s, 6H), 1.46 (s, 6H), 0.83 (s, 9H), 0.00 (s, 6H); ¹³C (75.5 MHz, CDCl₃) δ 154.5, 126.3, 120.7, 69.8, 45.8, 41.2, 38.4, 25.9, 24.4, 18.2, -5.42;





Bis-(3-sulfamoyl-3H-imidazol-4-yl)-methanone **90**:

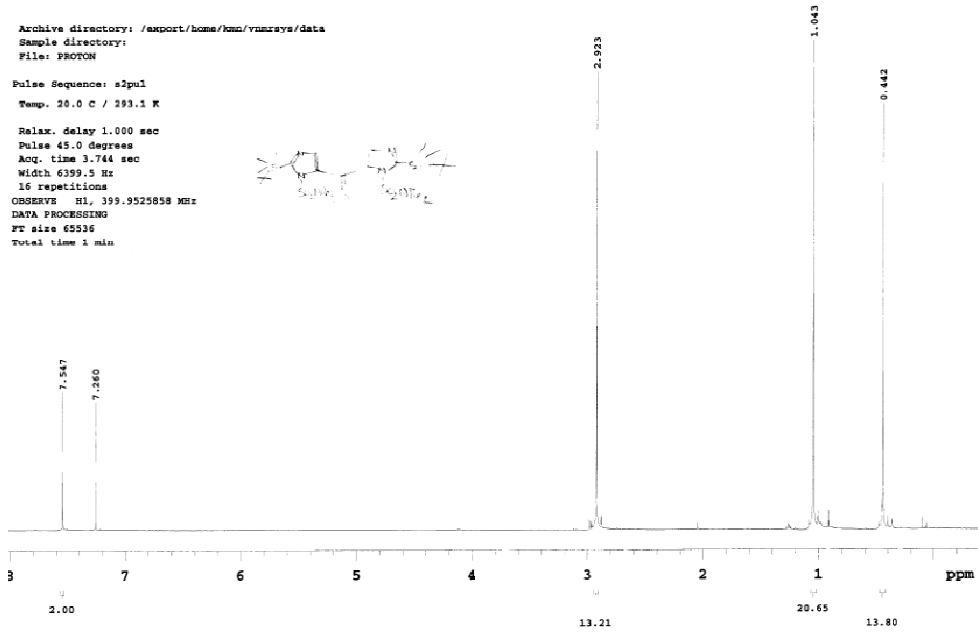
To a cooled solution of Dess-Martin periodinane (0.740 mg, 1.73 mmol) and imidazole (0.120 g, 1.73 mmol) in CH_2Cl_2 (30 mL) **96** (0.700 g, 1.15 mmol, 1 eq.) was added in one portion. The reaction mixture was warmed to room temperature and left to stir for one h. The reaction was then quenched with saturated $\text{Na}_2\text{S}_2\text{O}_3$, NaHCO_3 (20 mL) and Et_2O (30 mL) and stirred for 1 h. The solution was then washed with saturated NaHCO_3 (20 mL). The organic solvent was removed under vacuum and the crude residue was purified by flash column chromatography (8 Hexanes: 2 AcOEt) to yield **90** as a white solid (0.42 g, 60% yield). IR (KBr) 2933, 2890, 2851, 1671, 1513, 1389, 1169, 980; ^1H (300 MHz, CDCl_3) δ 7.55 (s, 2H), 2.92 (s, 12H), 1.04 (s, 18H), 0.44 (s, 12H); ^{13}C (100.6 MHz, CDCl_3) δ 171.0, 162.9, 140.4, 132.9, 38.4, 27.2, 18.6, -3.6.

STANDARD 1H OBSERVE

Archive directory: /export/home/knn/vnmrsws/data
Sample directory:
File: PROTON

Pulse Sequence: s2pul
Temp. 20.0 C / 293.1 K

Relax. delay 1.000 sec
Pulse 45.0 degrees
Acq. time 3.744 sec
Width 6399.5 Hz
16 repetitions
OBSERVE H1, 399.9525858 MHz
DATA PROCESSING
FT size 65536
Total time 1 min

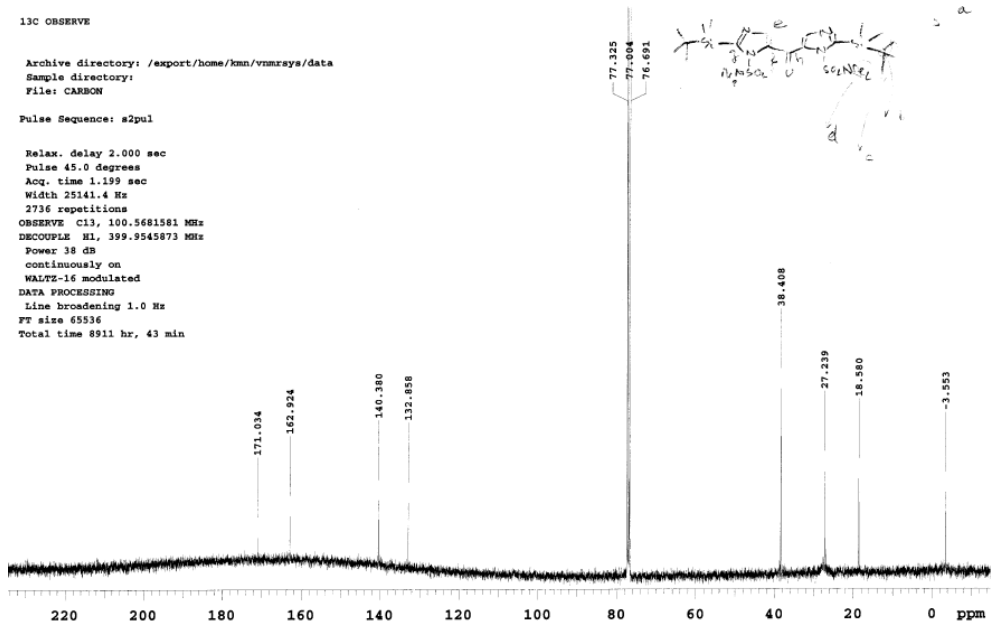


13C OBSERVE

Archive directory: /export/home/knn/vnmrsws/data
Sample directory:
File: CARBON

Pulse Sequence: s2pul

Relax. delay 2.000 sec
Pulse 45.0 degrees
Acq. time 1.199 sec
Width 25141.4 Hz
2736 repetitions
OBSERVE C13, 100.5681581 MHz
DECOUPLE H1, 399.9545873 MHz
Power 38 dB
continuously on
WALTZ-16 modulated
DATA PROCESSING
Line broadening 1.0 Hz
FT size 65536
Total time 8911 hr, 43 min

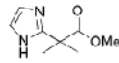


2-(1H-Imidazol-2-yl)-2-methyl-propionic acid methyl ester 93:

To a solution of hydroxypivalic methyl ester (10.00 g, 75.7 mmol) in dichloromethane (150 mL), trichloroisocyanuric (19.38 g, 83.4 mmol, 1.10 eq.) of acid was added. The suspension thus obtained was cooled to 0 °C before adding TEMPO (150 mg, 0.96 mmol, 0.010 eq.). The reaction mixture was stirred at 0 °C for 15 min before being warmed to room temperature and stirred for 3.5 h. The suspension was then filtered through celite and subsequently washed with saturated Na₂CO₃ (100 mL), 1N HCl and brine respectively. The organic layer was then dried over MgSO₄ and the solvent removed under vacuum. The crude mixture was dissolved in methanol (60 mL) and cooled to 0 °C. Concentrated aqueous ammonia (16 mL) was added at 0 °C and the solution was stirred for 30 min at room temperature. A solution of aqueous glyoxal (40 wt % in H₂O, 10.98 g, 75.7 mmol, 1 eq.) in methanol (20 mL) was added drop-wise over 2.5 h. The reaction was left at room temperature overnight. The methanol was then evaporated under reduced pressure and the remaining solution was dissolved in warm ethyl acetate (200 mL). The organic phase was washed with brine (3 × 20 mL) and dried over MgSO₄. Upon evaporation of the solvent an off white solid precipitates which was filtered to yield the desired product (7.98 g, 63% yield). Melting point: 148-150 °C; IR (KBr) 3439, 3115, 2956, 1887, 1729, 1555, 1453, 1374, 1262, 1196, 1162, 1104, 903, 768; ¹H (300 MHz, CDCl₃) δ 6.99 (s, 2H), 3.72 (s, 3H), 1.66 (s, 6H); ¹³C (75.5 MHz, CDCl₃) δ 176.2, 149.6, 122.0, 52.8, 43.9, 25.9; HRMS (ESI +): exact mass calculated for C₈H₁₃N₂O₂ [M + H]⁺ 169.0972. Found 169.0962.

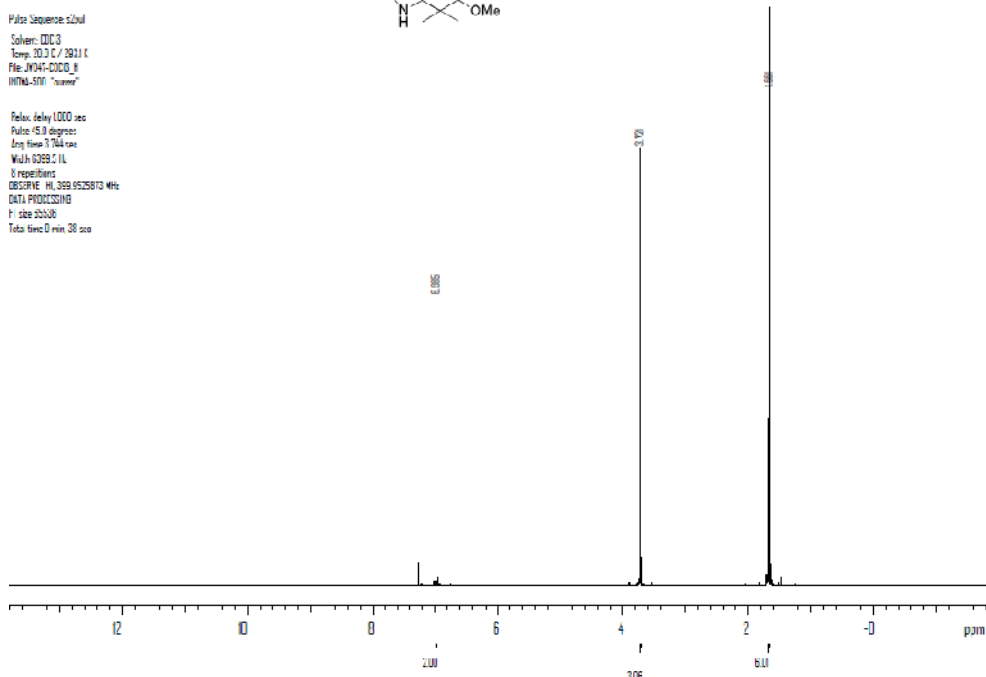
STANDARD OBSERVE

Archive directory: /export/home/kmm/mmrzys/data
 Sample directory:



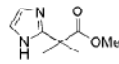
Pulse Sequence: zgpg30
 Solvent: CDCl3
 Temp: 30.3 C / 281.1 K
 File: J0047-0003_8
 INYU-500 "name"

Relax delay: 1.000 sec
 Pulse: 45.0 degree
 Acq time: 3.744 sec
 Width: 6329.0 Hz
 0 repetitions
 OBSERVE: H1, 399.6525813 MHz
 DATA PROCESSING
 FT size: 32000
 Total time: 0 min, 38 sec



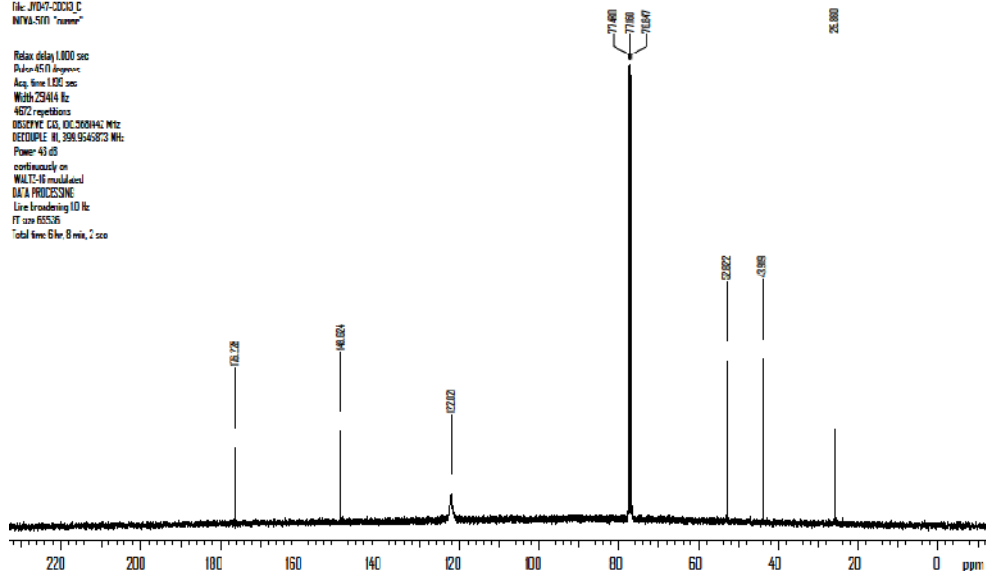
13C UNUSUAL

Archive directory: /export/home/kmm/mmrzys/data
 Sample directory:



Pulse Sequence: zgpg30
 Solvent: CDCl3
 Temp: 20.0 C / 283.1 K
 File: J0047-0003_C
 INYU-500 "name"

Relax delay: 1.000 sec
 Pulse: 45.0 degree
 Acq time: 1.000 sec
 Width: 2594.6 Hz
 40/2 repetitions
 OBSERVE: C13, 100.6260442 MHz
 DECOUPLE: H1, 399.6545873 MHz
 Power: 43 dB
 continuously on
 WALTZ-16 modulated
 DATA PROCESSING
 Line broadening: 10 Hz
 FT size: 65536
 Total time: 6 hr, 8 min, 2 sec



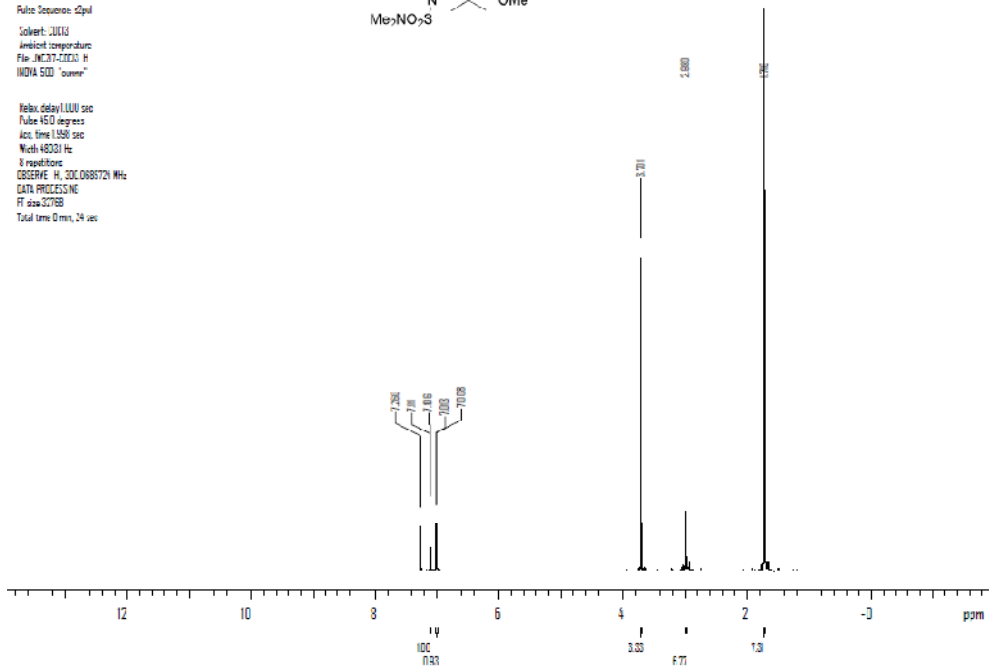
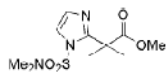
2-(1-Dimethylsulfamoyl-1H-imidazol-2-yl)-2-methyl-propionic acid methyl ester

94:

To a solution of 2-(1H-imidazol-2-yl)-2-methyl-propionic acid methyl ester **93** (5.00 g, 29.7 mmol) in dry THF (150 mL) cooled to 0 °C, NaH (1.80 g, 60% dispersion in mineral oil, 45 mmol, 1.5 eq.) was added portion-wise over 30 min. and left stirring at room temperature for 30 min. *N,N*-dimethylsulfamoyl chloride was then added neat (3.8 mL, 35 mmol, 1.2 eq.) and the solution was refluxed for 3 h. The reaction was quenched with H₂O and ethyl acetate was added (150 mL). The organic layer was then washed with saturated NaHCO₃ (2 × 25 mL), brine (25 mL) and dried over MgSO₄. The organic solvents were removed at reduced pressure and the crude purified by flash column chromatography (75 AcOEt: 25 Hexanes) to yield the desired compound as a white solid (4.91 g, 60% yield). Melting point: 83-85 °C; IR (KBr) 3154, 2992, 1742, 1536, 1491, 1380, 1281, 1262, 1097, 981; ¹H (300 MHz, CDCl₃) δ 7.11 (d, *J*= 1.5 Hz, 1H), 7.01 (d, *J*= 1.5 Hz, 1H), 3.70 (s, 3H), 2.90 (s, 6H), 1.71 (s, 6H); ¹³C (75.5 MHz, CDCl₃) δ 175.6, 152.1, 127.8, 118.5, 52.4, 45.8, 38.4, 26.5; HRMS (ESI +): exact mass calculated for C₁₀H₁₇N₃O₄S [M + H]⁺ 276.1013. Found 276.1006.

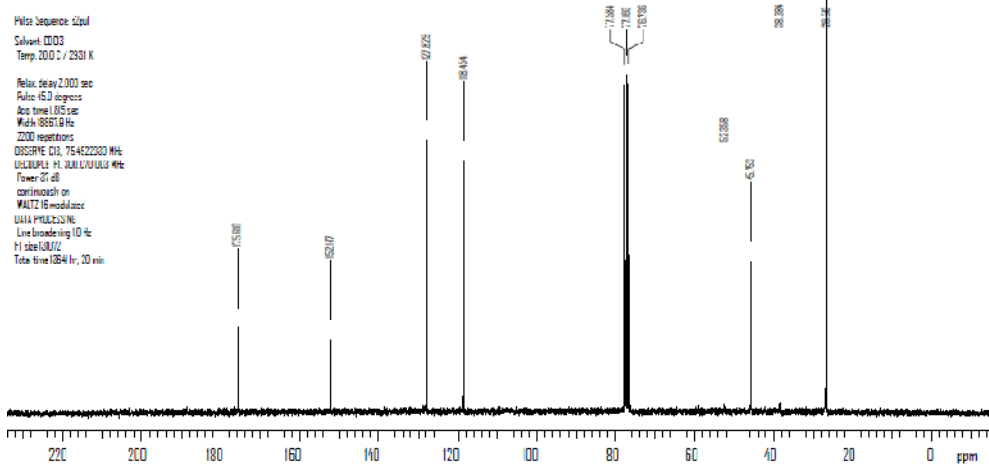
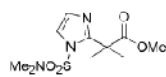
STANDARD 1H NMR

Arbino directory / export / name / name / name / data
 Sample directory
 Pulse Sequence: zgpg30
 Solvent: CDCl3
 Acquisition temperature: 300.2 K
 File: JNC07-00033.H
 NMR: 500.136 MHz



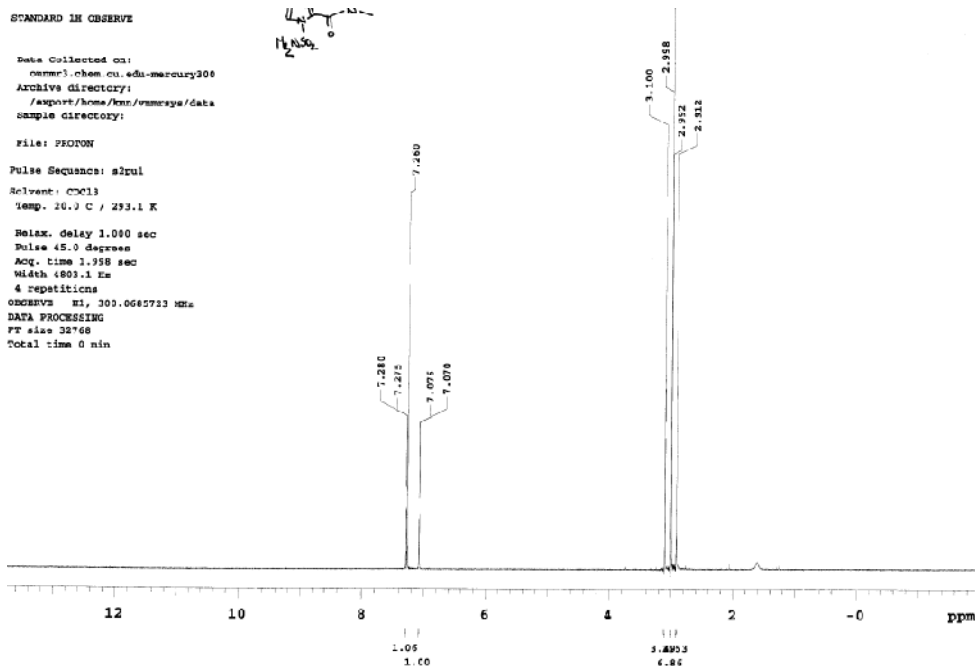
13C NMR

Data Collected on:
 sum3-chem-oxidu-memam-200
 Arbino directory
 / export / name / name / name / data
 Sample directory
 File: JNC09-00033.C



3-*N,N*-Dimethylsulfamoyl-3H-imidazole-4-carboxylic acid dimethylamide 95

To a stirred solution of **47** (1.00 g, 3.45 mmol, 1 eq.) in THF (120 mL) at -78 °C under a positive pressure of Ar, BuLi in pentane (2.0 mL, 1.90 M, 1.1 eq.) was added drop-wise. The solution was left 30 min at -78 °C before ClCONMe₂ (0.155 mL, 1.69 mmol, 0.5 eq.) was added neat. The reaction was warmed to room temperature and left stirring overnight. The mixture was then quenched with saturated NaHCO₃ and ethyl acetate (30 mL) was added. The organic phase was washed with saturated NaHCO₃ (2 × 25 mL), brine (25 mL) and dried over MgSO₄. The organic solvent was removed under vacuum and the crude product was analyzed by ¹H NMR spectroscopy. In order to confirm the assignment 100 mg of crude product was purified by preparative TLC (1 Hexanes: 1 AcOEt) to yield of the desired product as a white solid (20 mg) along with the starting material **47**. ¹H (300 MHz, CDCl₃) δ 7.28 (d, *J*= 1.5 Hz, 1H), 7.07 (d, *J*= 1.8 Hz, 1H), 3.10 (s, 3H), 3.00 (s, 6H), 2.91 (s, 3H); MS (ESI +): exact mass calculated for C₁₅H₃₂N₄O₃SSiNa [M + Na]⁺ 399.19. Found 399.20.



Bis-(3-*N,N*-dimethylsulfamoyl-3H-imidazol-4-yl)-methanol **96**:

To a stirred solution of sulfonamide **47** (1.807 g, 10.3 mmol) in anhydrous THF (90 mL) at -78 °C under a positive pressure of Ar, BuLi in pentane (5.4 mL, 2.10M, 11 mmol, 1.1 eq.) was added drop-wise. The solution was left 30 min at -78 °C before TBDMSCl (1.86 g, 12.4 mmol 1.2 eq.) dissolved in THF (2 mL) was cannulated in the reaction mixture. The reaction mixture was then warmed to room temperature and left to stir for 3 h. The reaction was cooled back down to -78 °C and ethylformate (415 µL, 5.20 mmol, 0.5 eq) was added neat. The reaction was slowly warmed to room temperature overnight. The mixture was then quenched with saturated NaHCO₃ and ethyl acetate (100 mL) is added. The organic layer was washed with saturated NaHCO₃ (2 × 50 mL), brine (50 mL) and dried over MgSO₄. The organic solvent was removed under vacuum and the crude was purified by flash column chromatography (9 CH₂Cl₂: 1 Acetone) to yield the desired product as a white solid (1.60 g, 51% yield). The compound matched the reported

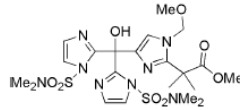
spectroscopic data: ^1H (300 MHz, CDCl_3) δ 7.07 (d, 2H, $J= 0.6$ Hz), 6.53 (d, 1H, $J= 3.6$ Hz), 3.58 (d, 1H, $J= 3.6$ Hz), 2.81 (s, 6H), 1.01 (s, 18H), 0.43 (s, 6H), 0.43 (s, 6H); MS (ESI +): exact mass calculated for $\text{C}_{23}\text{H}_{47}\text{N}_6\text{O}_5\text{S}_2\text{Si}_2$ $[\text{M} + \text{H}]^+$ 607.3. Found 607.2.

2-{4-[Bis-(1-*N,N*-dimethylsulfamoyl-1H-imidazol-2-yl)-hydroxy-methyl]-1-methoxymethyl-1H-imidazol-2-yl}-2-methyl-propionic acid methyl ester **97**:

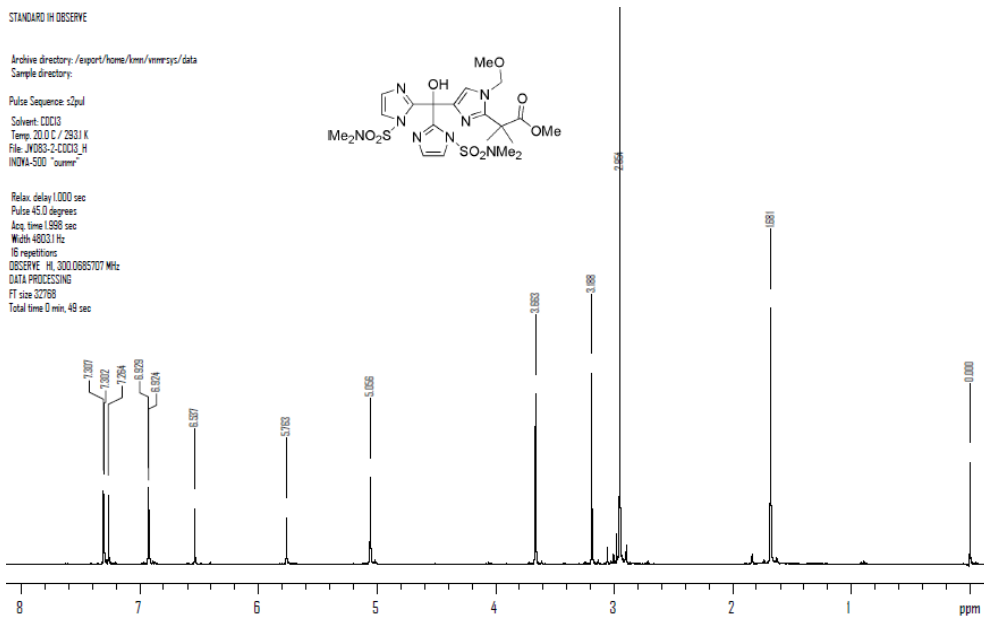
1-*N,N*-dimethylsulfamoyl-imidazole **47** (800 mg, 4.6 mmol, 1 eq.) was dissolved in dry THF (45 mL) and stirred under a positive pressure of Ar. The temperature was lowered to -78 °C and a solution of *n*-BuLi in pentane (5.1 mmol, 2.8 mL of a 1.81 M solution, 1.1 eq.) was added drop-wise. After stirring for 30 min, a solution of **100** (617 mg, 2.3 mmol, 0.5 eq.) in dry THF (5 mL) was added *via* cannula. The reaction was then left overnight to slowly warm up to room temperature. EtOAc (50 ml) was added and the organic phase was washed with of saturated NaHCO_3 (2×30 mL), brine (30 mL) and dried over MgSO_4 . The organic solvents were removed under vacuum and the crude was purified by flash column chromatography (95 CH_2Cl_2 : 5 MeOH) to yield product **97** as a white solid (0.99 g, 74% yield). Melting point: decomposes at 60-65 °C; IR (KBr) 3439, 3122, 2941, 1737, 1389, 1266, 1177, 1153, 980; ^1H (300 MHz, CDCl_3) δ 7.30 (d, $J= 1.5$ Hz, 2H), 7.92 (d, $J= 1.5$ Hz, 2H), 6.54 (s, 1H), 5.76 (s, 1H), 5.06 (s, 2H), 3.66 (s, 3H), 3.19 (s, 3H), 2.95 (s, 6H), 1.68 (s, 6H); ^{13}C (75.5 MHz, CDCl_3) δ 175.9, 150.4, 147.9, 139.3, 126.4, 121.9, 119.8, 77.7, 73.1, 56.2, 52.6, 44.1, 38.5, 25.9; HRMS (ESI +): exact mass calculated for $\text{C}_{21}\text{H}_{32}\text{N}_8\text{O}_8\text{S}_2\text{Na}$ $[\text{M} + \text{Na}]^+$ 611.1677. Found 611.1663.

STANDARD 1H OBSERVE

Archive directory: /export/home/kmm/nmr/sys/data
 Sample directory:
 Pulse Sequence: s2pul
 Solvent: CDCl3
 Temp: 20.0 C / 293.1 K
 File: JN053-2-CDCl3_H
 INOVA-500 "summr"

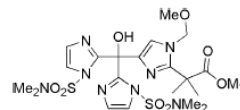


Relax. delay: 1.000 sec
 Pulse: 45.0 degrees
 Acq. time: 1.998 sec
 Width: 4803.1 Hz
 16 repetitions
 OBSERVE: H1, 300.0685707 MHz
 DATA PROCESSING
 FT size: 32768
 Total time: 0 min, 49 sec

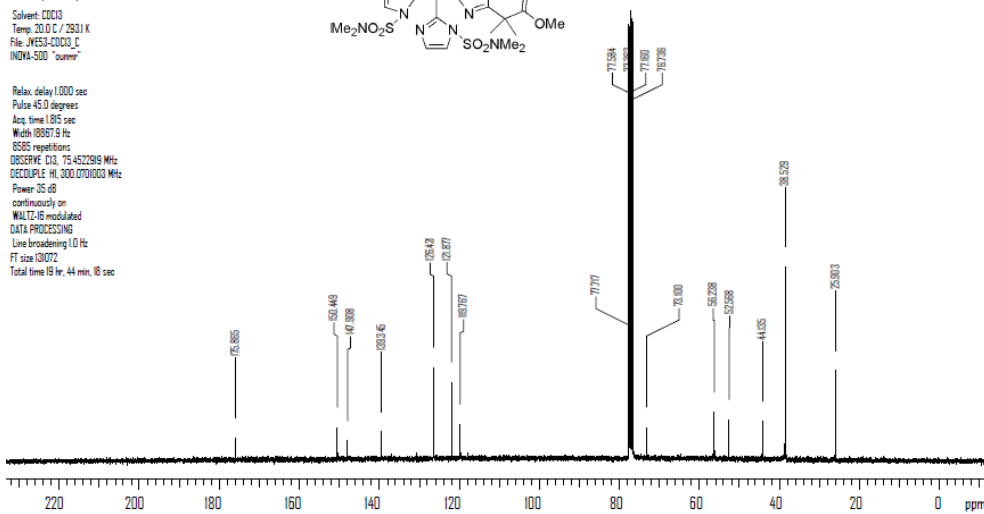


13C OBSERVE

Archive directory: /export/home/kmm/nmr/sys/data
 Sample directory:
 Pulse Sequence: s2pul
 Solvent: CDCl3
 Temp: 20.0 C / 293.1 K
 File: JN053-2-CDCl3_C
 INOVA-500 "summr"



Relax. delay: 1.000 sec
 Pulse: 45.0 degrees
 Acq. time: 1.815 sec
 Width: 18867.3 Hz
 6565 repetitions
 OBSERVE: C13, 75.4522919 MHz
 DECOUPLE: H1, 300.0701003 MHz
 Power: 25 dB
 continuously on
 WALTZ-16 modulated
 DATA PROCESSING
 Line broadening: 1.0 Hz
 FT size: 13072
 Total time: 19 hr, 44 min, 18 sec

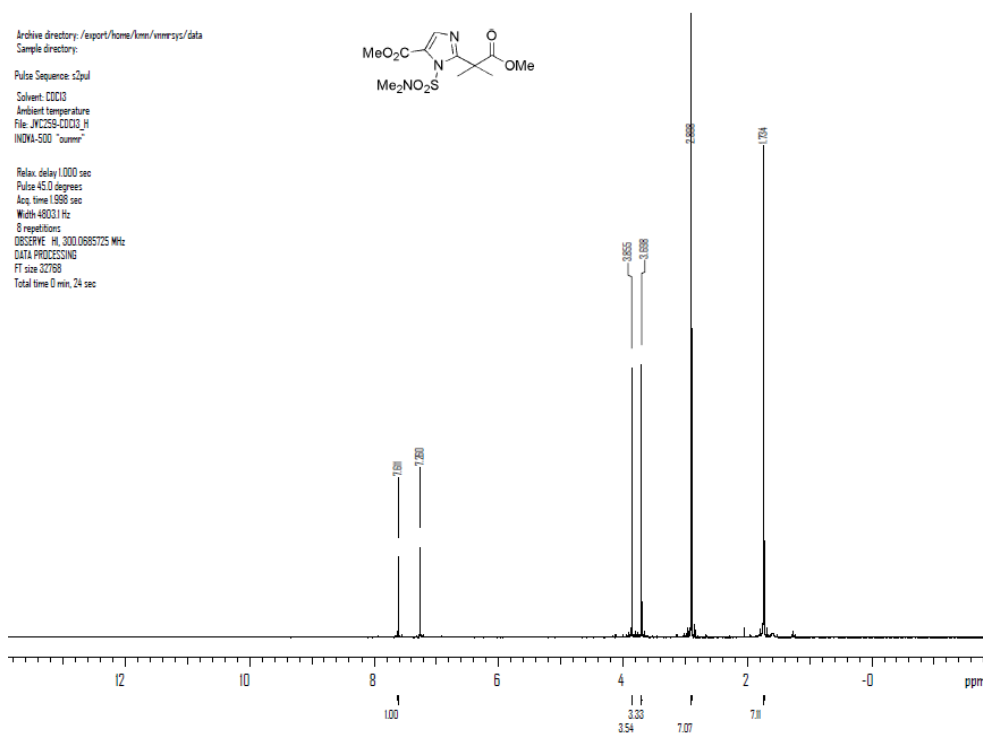
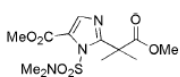


3-*N,N*-Dimethylsulfamoyl-2-(1-methoxycarbonyl-1-methyl-ethyl)-3H-imidazole-4-carboxylic acid methyl ester **98**:

To a stirred solution of **94** (4.00 g, 14.5 mmol) in THF (120 mL) at -78 °C under a positive pressure of Ar, BuLi in pentane (16.0 mmol, 9.7 mL, 1.65M, 1.1 eq.) was added drop-wise. The solution was left 30 min at -78 °C before methyl chloroformate (2.3 mL, 30 mmol, 2.1 eq.) was added neat. The reaction was warmed to room temperature and left stirring for 2 h. The mixture was then quenched with saturated NaHCO₃ and ethyl acetate (100 mL) was added. The organic phase was washed with saturated NaHCO₃ (2 × 50 mL), brine (50 mL) and dried over MgSO₄. The organic solvent was removed under vacuum and the crude was purified by flash column chromatography (9 CH₂Cl₂: 1 AcOEt) to yield the desired product as a white solid (4.65 g, 96% yield). Melting point: 92-95 °C; IR (KBr) 3003, 2956, 1745, 1490, 1386, 1262, 1200, 1154, 980; ¹H (300 MHz, CDCl₃) δ 7.61 (s, 1H), 3.86 (s, 3H), 3.70 (s, 3H), 2.90 (s, 6H), 1.73 (s, 6H); ¹³C (75.5 MHz, CDCl₃) δ 175.1, 158.8, 158.6, 136.8, 124.9, 118.5, 52.3, 52.3, 47.4, 38.3, 27.0; HRMS (ESI +): exact mass calculated for C₂₀H₁₉N₃O₆SNa [M + Na]⁺ 356.0892. Found 356.0946.

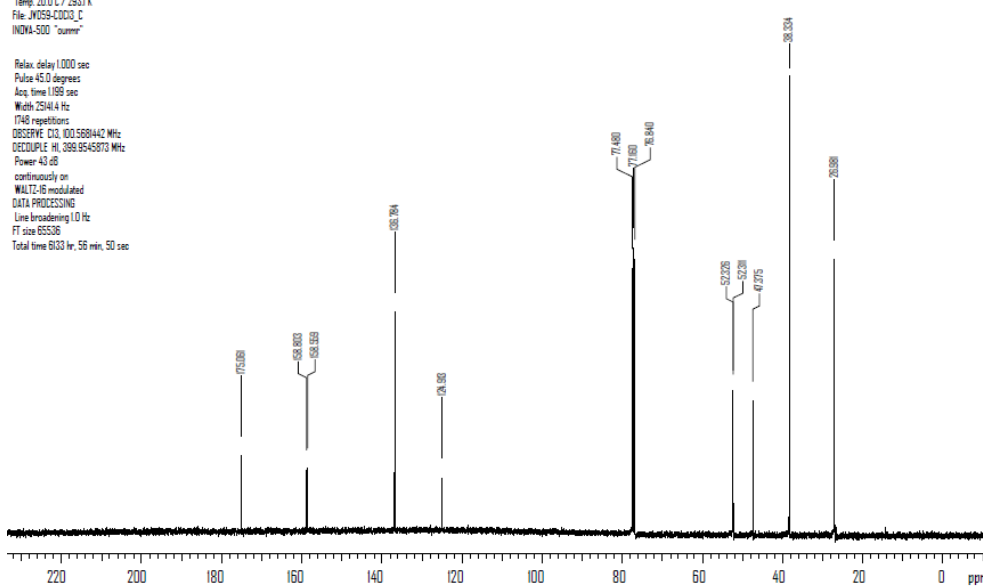
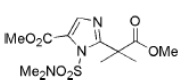
STANDARD IN OBSERVE

Archive directory: /export/home/kmm/vnmrsys/data
 Sample directory:
 Pulse Sequence: zgpg30
 Solvent: CDCl3
 Ambient temperature
 File: JVC259-CDCl3_H
 INOVA-500 "oumr"



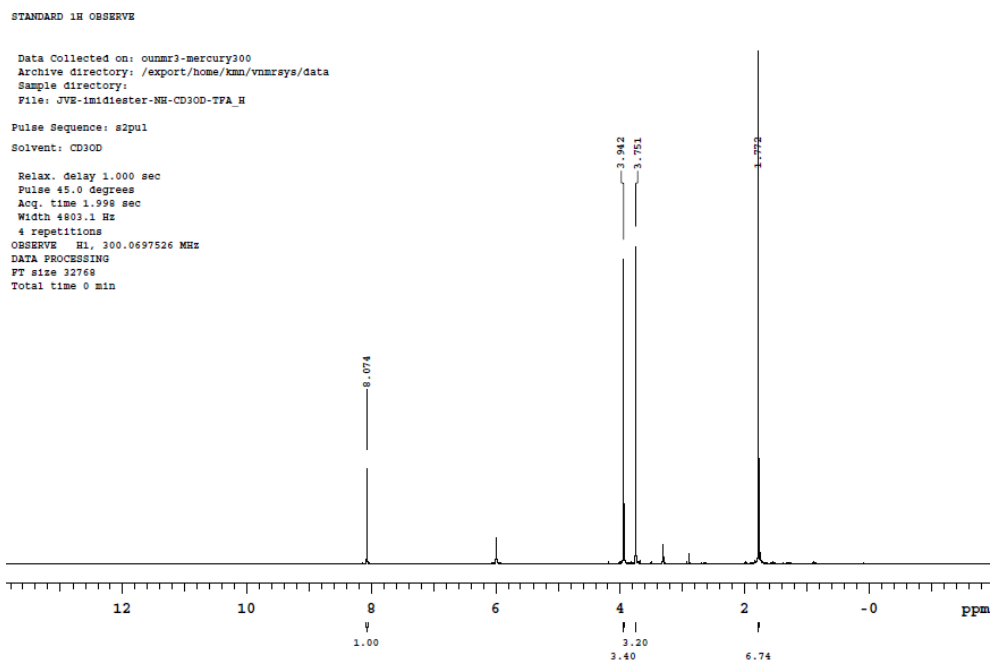
13C OBSERVE

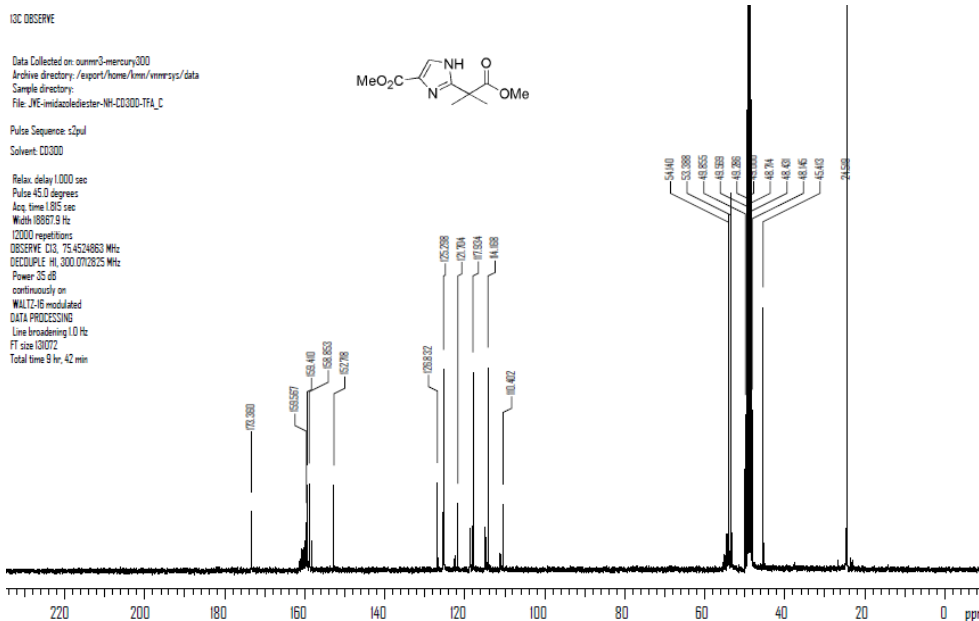
Archive directory: /export/home/kmm/vnmrsys/data
 Sample directory:
 Pulse Sequence: zgpg30
 Solvent: CDCl3
 Temp: 20.0 C / 293.1 K
 File: JVC259-CDCl3_C
 INOVA-500 "oumr"



2-(1-Methoxycarbonyl-1-methyl-ethyl)-3H-imidazole-4-carboxylic acid methyl ester **99**:

To a cooled solution of **98** (4.55 g, 13.6 mmol) in dry methanol (120 mL), concentrated H₂SO₄ (1 mL) was added and the solution was refluxed for 20 h. The solution was then cooled to room temperature and 1N NaOH (40 mL) was added. The aqueous layer was extracted with CH₂Cl₂ (3 × 100 mL) Removal of the organic solvent yielded compound **99** in a pure form as a white solid (2.61 g, 85% yield). Melting point: 148-149 °C; IR (KBr) 3003, 2956, 1741, 1725, 1528, 1443, 1347, 1262, 1200, 1169, 1108; ¹H (300 MHz, MeOD:TFA (4:1, v:v)) δ 8.07 (s, 1H), 3.94 (s, 3H), 3.75 (s, 3H), 1.77 (s, 6H); ¹³C (75.5 MHz, CDCl₃) δ 173.4, 159.6, 152.7, 126.8, 125.3, 54.1, 53.4, 45.4, 24.5; HRMS (ESI +): exact mass calculated for C₁₀H₁₄N₂O₄Na [M + Na]⁺ 249.0860. Found 249.0851.



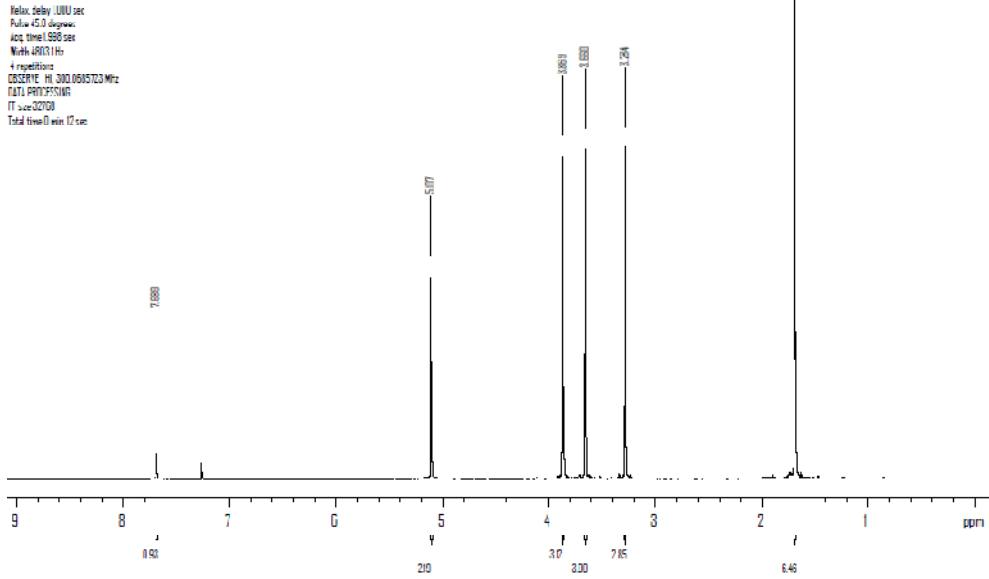
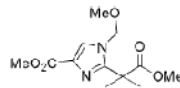


2-(1-Methoxycarbonyl-1-methyl-ethyl)-1-methoxymethyl-1H-imidazole-4-carboxylic acid methyl ester **100**:

To a stirred solution of **99** (1.00 g, 3.7 mmol) in THF (60 mL) at 0 °C, NaH (60% mineral oil, 220 mg, 5.50 mmol, 1.5 eq.) was added portion-wise and warmed to room temperature. MOM-Cl (410 μ L, 5.40 mmol, 1.5 eq.) was then added neat and the reaction was left stirring overnight. After adding ethyl acetate (50 mL), the organic phase was washed with saturated NaHCO₃ (2 \times 30 mL), brine (50 mL) and dried over MgSO₄. The solvents were removed under vacuum and the crude residue purified by flash column chromatography (6 AcOEt: 4 Hexanes) to yield the desired compound **100** as a white solid (1.08 g, 90% yield). Melting point: 45-46 °C; IR (KBr) 3138, 2991, 2953, 1737 1552 1509, 1443, 1351, 1270, 1235, 1200, 1157, 1123, 1092, 1011; ¹H (300 MHz, CDCl₃) δ 7.69 (s, 1H), 5.11 (s, 2H), 3.87 (s, 3H), 3.66 (s, 3H), 3.28 (s, 3H), 1.69 (s, 6H); ¹³C (75.5 MHz, CDCl₃) δ 175.5, 163.4, 150.8, 131.3, 128.0, 56.6, 52.7, 51.9, 44.2, 25.8; HRMS (ESI +): exact mass calculated for C₁₂H₁₉N₂O₅ [M + H]⁺ 271.1288. Found 271.1258.

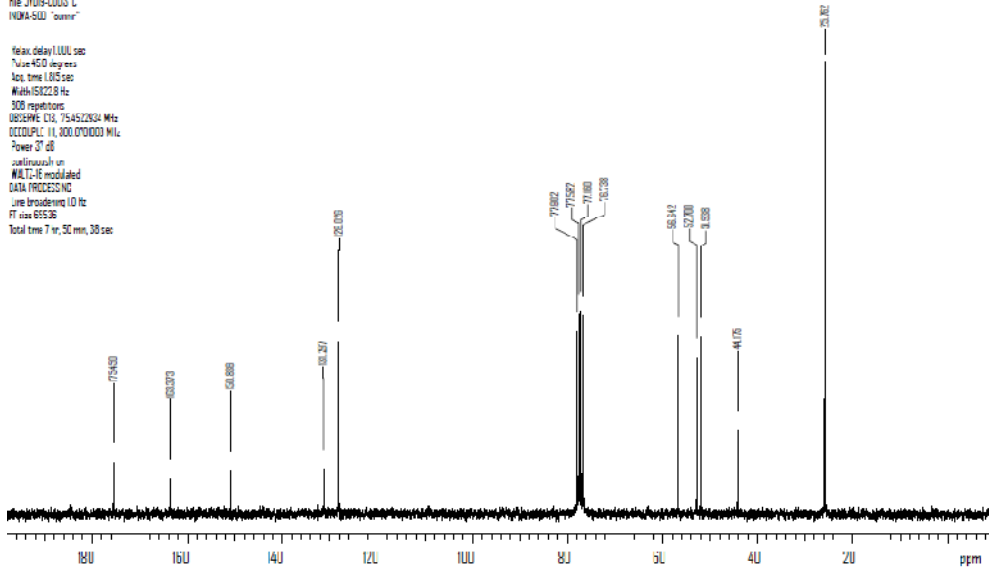
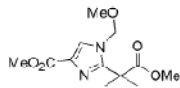
STANDARD OBSERVE

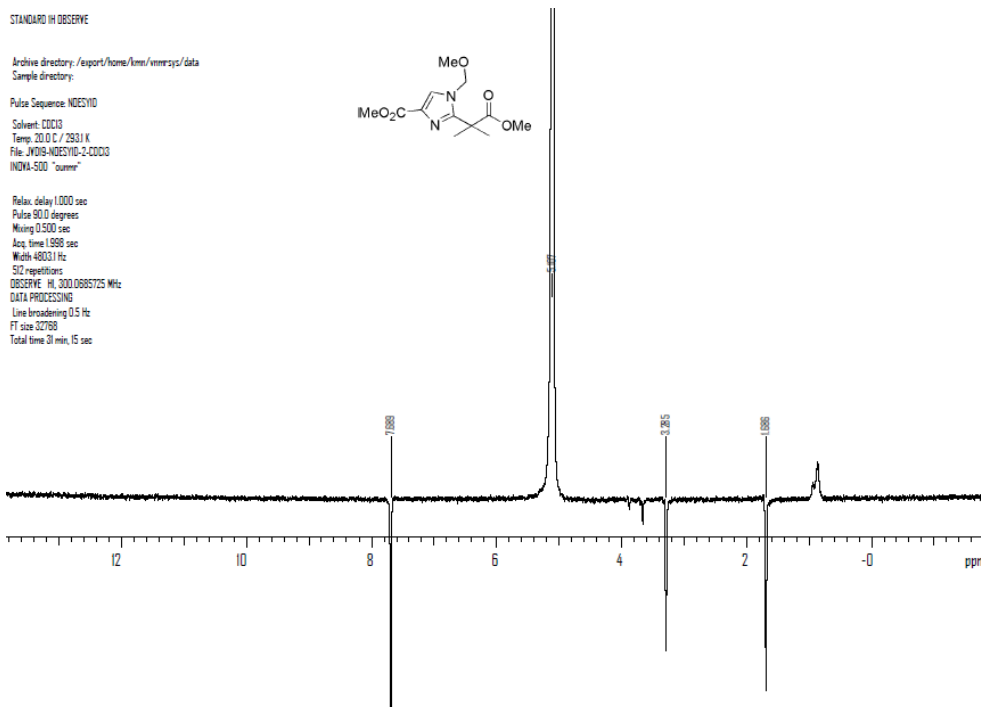
Archive directory /export/home/chem/chemistry/data
 Sample directory:
 Pulse Sequence: zgpg30
 Solvent: CDCl3
 Temp: 300.0 / 293.1 K
 File: NMR5-CDCl3_9
 NMR-500 "summer"



¹³C OBSERVE

Archive directory /export/home/chem/chemistry/data
 Sample directory:
 Pulse Sequence: zgpg30
 Solvent: CDCl3
 Temp: 200.0 / 293.1 K
 File: J139-13003 C
 NMR-500 "summer"

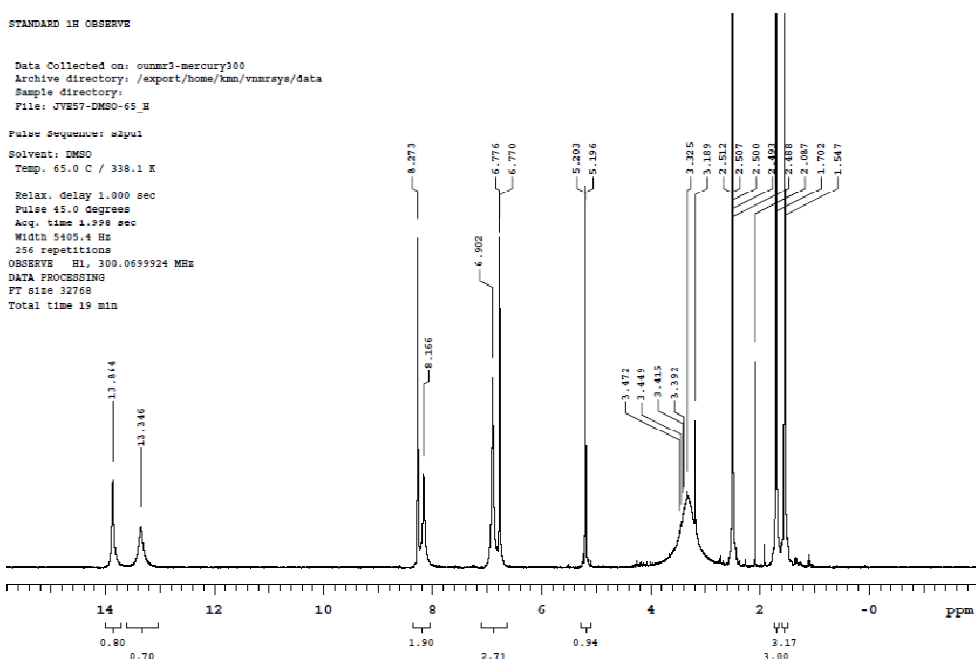




2-{4-[Hydroxy-bis-(1H-imidazol-2-yl)-methyl]-1H-imidazol-2-yl}-2-methylpropionic acid **73**:

A solution of **97** (0.94 g, 1.60 mmol) in 6N HCl (40 mL) was refluxed for 6 h. The solvent was evaporated under reduced pressure. The crude product was loaded onto a column chromatography Dowex 50WX8-100 resin (10 mL) and washed with water. The product was eluted with 6% aqueous ammonia. After removing almost all the solvent addition of acetone precipitated an off-white solid (0.43 g, 85% yield). Melting point: decomposes at 130 °C; IR (KBr) 3458, 3207, 2983, 1660, 1617, 1567, 1532, 1447, 1404, 1355, 1115, 1077, 1027; ¹H (300 MHz, CD3OD) δ 7.17 (s, 4H), 6.81 (s, 1H), 5.76 (s, 1H), 1.55 (s, 6H); ¹³C (75.5 MHz, CD3OD) δ 181.1, 155.6, 149.7, 138.7, 122.5, 117.8, 119.8, 71.0, 46.7, 38.5, 26.1; HRMS (ESI +): exact mass calculated for C₁₄H₁₇N₆O₃ [M + H]⁺ 317.1357. Found 317.1296.

red crystals were washed with acetone and dried under vacuum. Melting point: decomposes at 195-200 °C; IR (KBr) 3425, 3146, 3003, 2933, 1591, 1477, 1405, 1378, 1351, 1119, 1088, 1061, 889, 772; ¹H (300 MHz, DMSO-*d*₆, 65 °C) δ 13.86 (bs, 2H), 13.35 (bs, 2H), 8.27 (s, 2H), 8.17 (bs, 2H), 6.90 (bs, 4H), 6.77 (d, *J* 1.8 Hz, 2H), 5.20 (d, *J*= 2.1 Hz, 2H), 1.70 (s, 6H), 1.55(s, 6H); MS (ESI +): exact mass calculated for C₂₈H₃₀N₁₂O₆Co [M - H]⁺ 689.17. Found 689.00.



We acknowledge and thank Dr. D. Powell for his expertise in determining the crystal structure of **104**.

Table 3.4: Crystal data and structure refinement for **104**

Empirical formula	C ₂₉ H ₄₅ Cl ₂ Co N ₁₂ O ₁₂
Formula weight	883.60
Crystal system	Triclinic
Space group	$P\bar{1}$
Unit cell dimensions	$a= 12.381(12) \text{ \AA}$, $\alpha= 72.897(9)^\circ$ $b= 12.735(12) \text{ \AA}$, $\beta= 69.379(11)^\circ$ $c= 15.117(14) \text{ \AA}$, $\gamma= 67.594(11)^\circ$
Volume	2027(3) \AA^3
Z, Z'	2, 1
Density (calculated)	1.448 Mg/m ³
Wavelength	0.71073 \AA
Temperature	100(2) K
$F(000)$	920
Absorption coefficient	0.627 mm ⁻¹
Absorption correction	Semi-empirical from equivalents
Max. and min. transmission	0.959 and 0.832
Theta range for data collection	2.02 to 26.00°
Reflections collected	19401
Independent reflections	7901 [R(int)= 0.1622]
Data / restraints / parameters	7901 / 1 / 524
$wR(F^2 \text{ all data})$	$wR2= 0.2609$
$R(F \text{ obsd data})$	$R1= 0.0864$
Goodness-of-fit on F^2	1.014
Observed data [$I > 2\sigma(I)$]	4537
Largest and mean shift / s.u.	0.000 and 0.000
Largest diff. peak and hole	1.364 and -1.040 e/ \AA^3
$wR2= \{ \sum [w(F_o^2 - F_c^2)^2] / \sum [w(F_o^2)^2] \}^{1/2}$ $R1= \sum F_o - F_c / \sum F_o $	

Computational procedures:

The DFT calculations were performed using Becke's three parameter hybrid functional with the correlation of Lee, Yang and Parr (B3LYP)¹⁶²⁻¹⁶⁵. The geometries were calculated with the 6-31+G(d) basis set and a single point was performed on **98** and **100** with an augmented basis set 6-311+G(d,p).

Addition attempt of **85** to **87-89** (scheme 3.9)

The protected imidazole **85** (800 mg, 2.21 mmol, 1 eq.) was dissolved in dry THF (45 mL) under a positive pressure of Ar. The temperature was lowered to -78 °C and a solution of *n*-BuLi in pentane (2.43 mmol, 1.4 mL of a 1.80 M solution, 1.1 eq.) was added drop-wise. After stirring for 30 min, a solution of **87** (418 mg, 2.20 mmol, 1 eq.) in dry THF (5 mL) was added *via* cannula. The reaction was then left overnight to slowly warm up to room temperature. EtOAc (50 ml) was added and the organic phase was washed with saturated NaHCO₃ (2 × 30 mL), brine (30 mL) and dried over MgSO₄. The organic solvents were removed under vacuum. The crude mixture was analyzed by TLC and ¹H NMR spectroscopy and only starting material **87** was detected with numerous by-products. Procedures for **88** and **89** were carried out in a similar way.

Addition attempt of **94** to **90** (scheme 3.18)

The ester **94** (502 mg, 1.82 mmol, 1 eq.) was dissolved in dry THF (50 mL) under a positive pressure of Ar. The temperature was lowered to -78 °C and a solution of *n*-BuLi in pentane (2.00 mmol, 1.0 mL of a 1.92 M solution, 1.1 eq.)

was added drop-wise. After stirring for 30 min, a solution of **90** (907 mg, 1.80 mmol, 1 eq.) in dry THF (5 mL) was added *via* cannula. The reaction was then left overnight to slowly warm up to room temperature. EtOAc (100 ml) was added and the organic phase was washed with saturated NaHCO₃ (2 × 30 mL), brine (30 mL) and dried over MgSO₄. The organic solvents were removed under vacuum. The crude mixture was analyzed by TLC and ¹H NMR spectroscopy and only starting materials **94** and **90** without any by-product.

Addition attempts of **47** and **46** to **98** (scheme 3.21)

1-*N,N*-dimethylsulfamoyl-imidazole **47** (300 mg, 1.71 mmol, 1 eq.) was dissolved in dry THF (45 mL) under a positive pressure of Ar. The temperature was lowered to -78 °C and a solution of *n*-BuLi in pentane (1.71 mmol, 0.86 mL of a 1.98 M solution, 1.1 eq.) was added drop-wise. After stirring for 30 min, a solution of **98** (569 mg, 1.71 mmol, 1 eq.) in dry THF (3 mL) was added *via* cannula. The reaction was then left overnight to slowly warm up to room temperature. EtOAc (30 ml) was added and the organic phase was washed with saturated NaHCO₃ (2 × 20 mL), brine (20 mL) and dried over MgSO₄. The organic solvents were removed under vacuum. The crude mixture was analyzed by TLC and ¹H NMR spectroscopy and only starting material **47** was detected with numerous by-products. The procedure for **46** was carried out in a similar way.

Addition attempts of **36** and **101-103** to **100** (scheme 3.23):

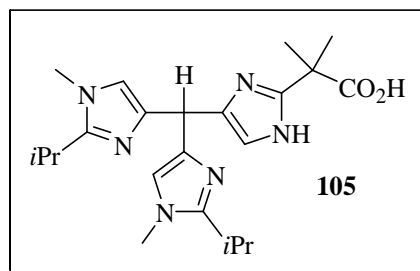
1-Methoxymethyl-1H-imidazole **36** (83 mg, 0.74 mmol, 1 eq.) was dissolved in dry THF (10 mL) under a positive pressure of Ar. The temperature was lowered to -78 °C and a solution of *n*-BuLi in pentane (0.74 mmol, 0.42 mL of a 1.78 M solution, 1.1 eq.) was added drop-wise. After stirring for 30 min, a solution of **100** (100 mg, 0.37 mmol, 0.5 eq.) in dry THF (1 mL) was added *via* cannula. The reaction was then left overnight to slowly warm up to room temperature. EtOAc (10 ml) was added and the organic phase was washed with saturated NaHCO₃ (2 × 10 mL), brine (10 mL) and dried over MgSO₄. The organic solvents were removed under vacuum. The crude mixture was analyzed by TLC and ¹H NMR spectroscopy and only starting material **36** was detected with numerous by-products. The procedures for **46**, **101-103** were carried out in a similar way and yielded the same result: recovery of the pro-nucleophiles and consumption of the electrophile **100**.

Complexation experiments of **73**:

The short side-chain tripod **73** (50 mg, 0.16 mmol, 1 eq.) was dissolved in MeOH (3 mL) and 1 equivalent of metal salt is added. After stirring for 15 min the NaHCO₃ (15 mg, 0.20 mmol, 1.2eq) was added and a precipitate formed. Attempts to redissolve it in organic solvents failed. Metal salts used: FeCl₂·6H₂O, Fe(acac)₃, Fe(NO₃)₃·9H₂O, CuCN, Cu(acetate)₂·H₂O, Cu(CH₃CN)₄PF₆, Zn(OTf)₂.

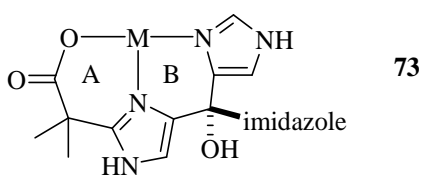
Chapter 4

Synthesis of the Carboxylate-Functionalized *Tris*[4-(*N*-Methyl-2-Isopropyl-Imidazolyl)]Methane **105** and its Copper (II) Complex



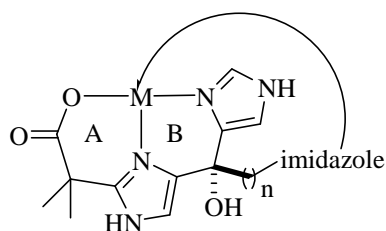
4.1 Introduction: Ligand design and retrosynthesis

As concluded in the previous chapter, **73** behaved as a tridentate ligand (meridional coordination) rather than the desired tetradentate N_3O -donor and should be considered, in terms of its coordination mode, as a 2-imidazole-1-carboxylate unit plus one (non-coordinating) imidazole. Careful analysis of the 2-imidazole-1-carboxylate unit revealed important geometric details of the structure (Scheme 4.1). Chelate rings A and B, respectively 6 and 5 membered rings, possess four carbon and two nitrogen atoms sp^2 hybridized, enforcing two nearly planar rings. In order to bring the remaining imidazole in closer proximity to the metal center, to enable its coordination, two options were considered.



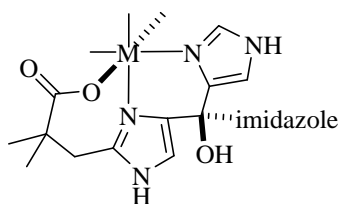
Scheme 4.1

The first was to extend the linker between the third imidazole and the central carbon (scheme 4.2). Though very attractive this option was deemed more time consuming to achieve since a new methodology for the synthesis of the ligand would have to be developed.



Scheme 4.2

The second plan considered a chain extension of the tether (scheme 4.3). This type of modification could enforce a facial coordination of the 2-imidazole-1-carboxylate unit as an extra methylene group has to be accommodated, thus forcing the third imidazole closer to the metal center.



106

Scheme 4.3

This analysis was supported by PM3 modeling of putative neutral iron (III) metal neutral complexes with two chloride ions and either ligand **73** (short side chain, figure 4.1) or **106** (extended side chain, figure 4.2).

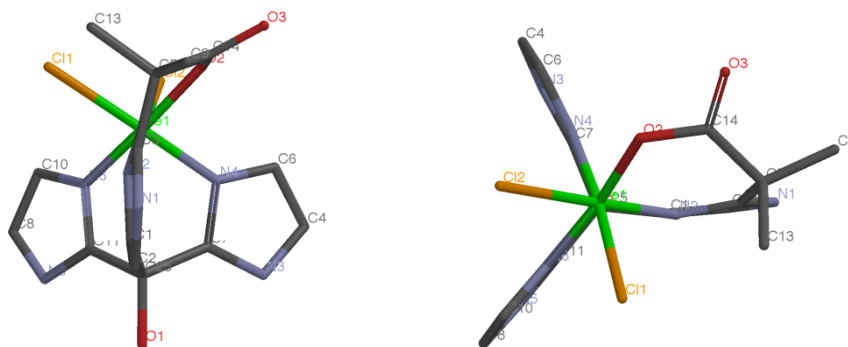


Figure 4.1: Side and top views of the PM3-minimized structure of **73**·FeCl₂

Selected dihedral angle (°): C2-N1-C3-C5= -164.4; C1-N2-C3-C5= 163.4

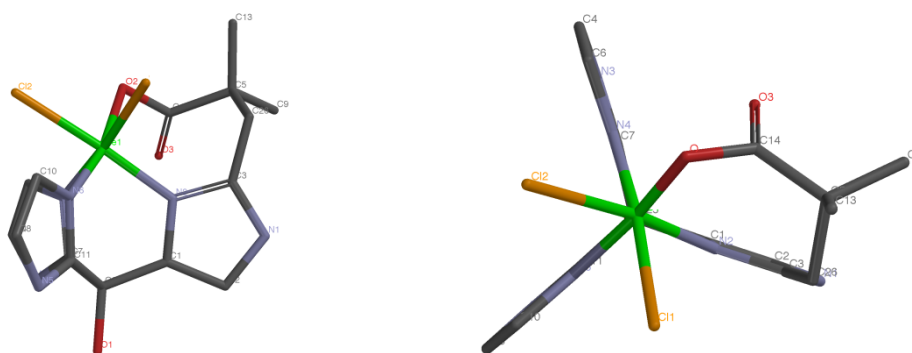
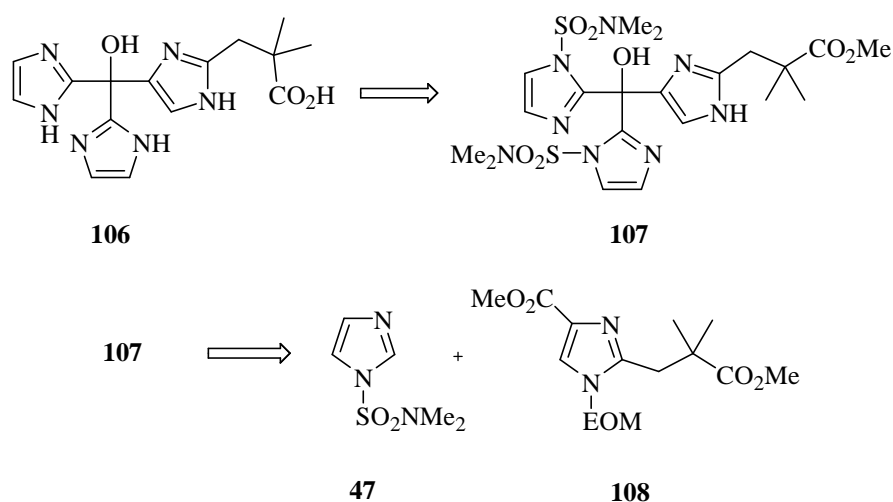


Figure 4.2: Side and top views of the PM3-minimized structure of **106**·FeCl₂

Selected dihedral angle (°): C2-N1-C3-C26= -177.6; C1-N2-C3-C26= 177.0

After geometry minimization of the model complexes, the dihedral angles of the complexed ligands were analyzed. The short side chain ligand **73** seemed to display considerable ruffling of the imidazole ring bearing the carboxylate, with C5 being almost 16° out of the plane of the imidazole ring. This ruffling was much less pronounced with the newly proposed ligand **106**, as C26 was only 3° out the plane of the imidazole ring. This more acceptable dihedral angle should alleviate some of the strain and allow for its N₃O-coordination in an octahedral environment.

Moreover, this strategy has the advantage of capitalizing on the previously successful synthesis used and, provided that the added methylene group is sufficiently impervious to the basic conditions, minor changes in the synthetic plan were expected. Analogous to the preceding route the following retrosynthetic path from **106** was devised (scheme 4.4), with the critical step being the formation of **107** by adding two equivalents of **47** to **108**.

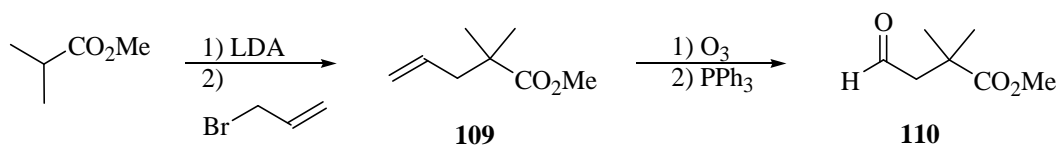


Scheme 4.4

4.2 Synthesis of the tripod **81** with an extended side-chain

4.2.1 Synthesis of **108** by analogy

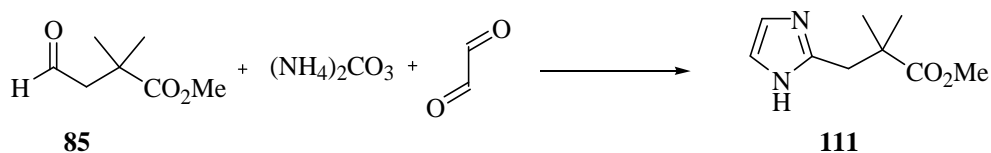
The initial approach to the diester **108** was envisioned by simple transposition of the previous route of the parent compound (scheme 4.5).



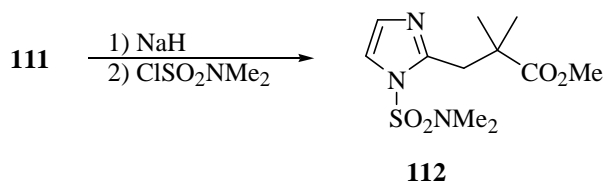
Scheme 4.5

The preparation of the known aldehyde-ester **110** was carried out in two steps from methyl isobutyrate. Deprotonation by one equivalent of LDA followed by addition of allyl bromide gave the alkene **109** in good yields (80%). The product was submitted to ozonolysis and followed by a reduction with triphenylphosphine to give **110** in 60% yield.¹⁶⁶

The condensation of the aldehyde with glyoxal and ammonium carbonate on gram scale produced the expected imidazole^{167,168} **111** which was purified by recrystallization (scheme 4.6.1) in 64 % yield. The structure of product **111** was confirmed by ¹H NMR spectroscopy which displayed all the expected singlets at δ 6.92 ppm (2H), 3.66 ppm (3H), 2.96 ppm (2H), 1.20 ppm (6H), and was further characterized by ¹³C NMR. Ester **111** was then protected with *N,N*-dimethyl sulfamoyl chloride under the usual conditions and purified by flash column chromatography yielding **112** in 93% yield (scheme 4.6.2). The side-chain extension facilitated the protection step by decreasing the steric crowding from the geminal dimethyl unit and the protected imidazole was characterized by ¹H NMR spectroscopy. The diagnostic appearance of two aromatic doublets at δ 7.12 ppm and 6.87 ppm with a coupling constant $J= 1.5$ Hz indicated the successful addition of the protecting group. This was further confirmed by the resonance of dimethyl sulfamoyl group and the ¹³C NMR spectrum.

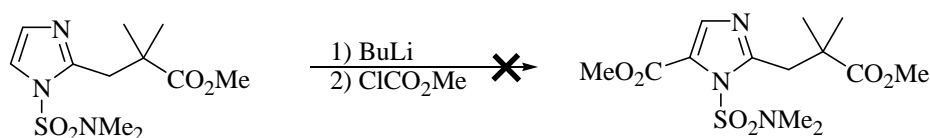


Scheme 4.6.1



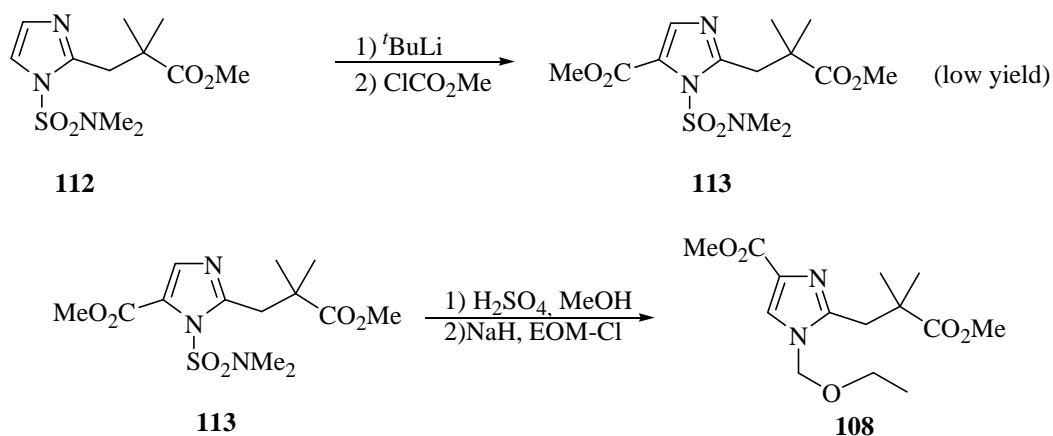
Scheme 4.6.2

Unfortunately, as feared, the lithiation of the protected imidazole **112** did not occur with the desired selectivity (scheme 4.7). When treated with one equivalent of BuLi and methyl chloroformate, the starting material was recovered along with numerous by-products after aqueous workup. In order to prevent the presumed deprotonation of the added methylene group we turned our attention to ^tBuLi, a base sterically more hindered than BuLi (scheme 4.8).



Scheme 4.7

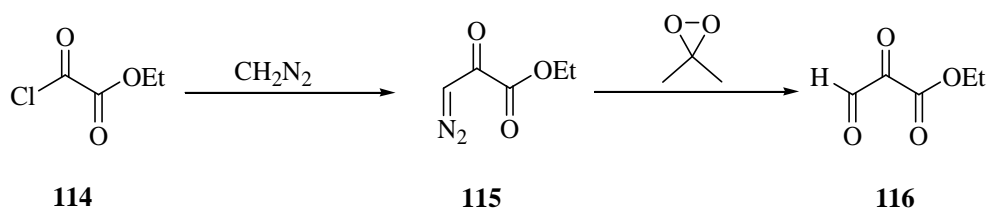
However the added bulk was not sufficient to prevent side reactions and only partial conversion of **112** was achieved to yield **113** along with numerous unidentified by-products which rendered its purification difficult (scheme 4.8). Enough was isolated to be hydrolyzed and without purification to be protected by ethoxymethyl chloride (EOM-Cl) in a 15% overall yield. The protected diester **108** was carefully purified by chromatography and characterized by its ¹H NMR spectrum which displayed the ethyl resonances of the EOM protecting group and by mass spectrometry [(M+H)⁺= 299.18].



Scheme 4.8

4.2.2 Modified and improved synthesis of **108**

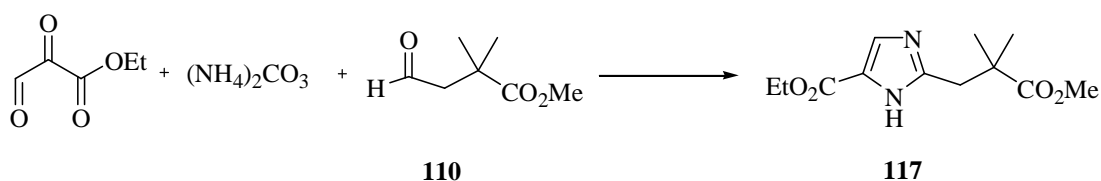
Given the difficulty in introducing the second carboxyl group on the C5 position, we considered the possibility of introducing it further upstream before the condensation of the imidazole nucleus. The tri-carbonyl compound **116**¹⁶⁹ (scheme 4.9), which contains formyl, a keto and a carboxyl group on three adjacent carbons, has been reported¹⁶⁹ and its interesting reactivity properties exploited. We therefore decided to investigate its viability within our synthetic plan for producing **108**.



Scheme 4.9

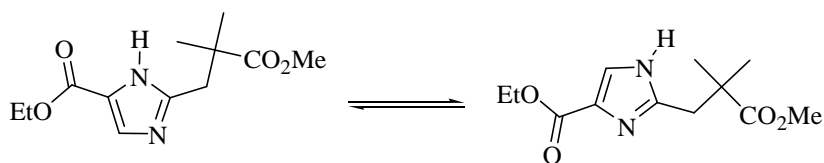
The addition of diazomethane to ethyl chlorooxoacetate **114** led in moderate yield ($\approx 40\%$) to the diazo compound **115**¹⁷⁰. Its oxidation by a solution of dimethyldioxirane in acetone gave the vicinal tricarbonyl product with acetone and

nitrogen gas as the only by-products. This feature allowed us to form the tri-carbonyl compound **116** *in situ* and without further purification used it directly in the subsequent condensation step with ammonium carbonate^{167,168} and the aldehyde **110** (scheme 4.10).



Scheme 4.10

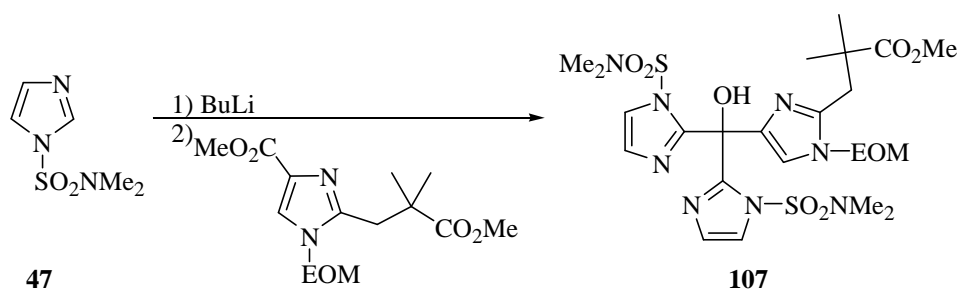
The imidazole **117** was thus obtained in 56% yield and characterized by ^1H NMR spectroscopy and mass spectrometry. Interestingly in deuterated chloroform two isomers were detected in an approximate ratio of 6:1, with two sets of resonances (scheme 4.11). Two aromatic protons were observed at δ 7.63 ppm with a coupling constant of $J= 2.7$ Hz and at δ 7.57 ppm, with a coupling constant of $J= 1.8$ Hz; the C5 isomer is most likely stabilized by an internal hydrogen bond.



Scheme 4.11

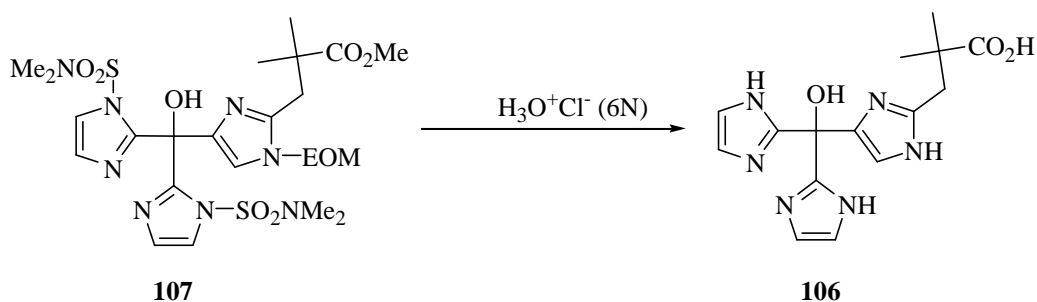
4.2.3 Addition of **47** to **108** and synthesis of the desired target **106**

With our new starting materials in hand, the addition reaction of lithiated **47** to **108** was carried out and successfully produced the desired tripod with an extended chain **107**, though its complete purification on silica gel was not possible in our hands (scheme 4.12).



Scheme 4.12

The crude product **107** was therefore used without purification and successfully deprotected by acidic hydrolysis, in refluxing 6N HCl for 6 hours, to **106**. The compound was obtained in its neutral form after purification by cation exchange chromatography with NH_4OH in 27% yield from **47** (scheme 4.13). The product was fully characterized by ^1H and ^{13}C NMR spectroscopy.



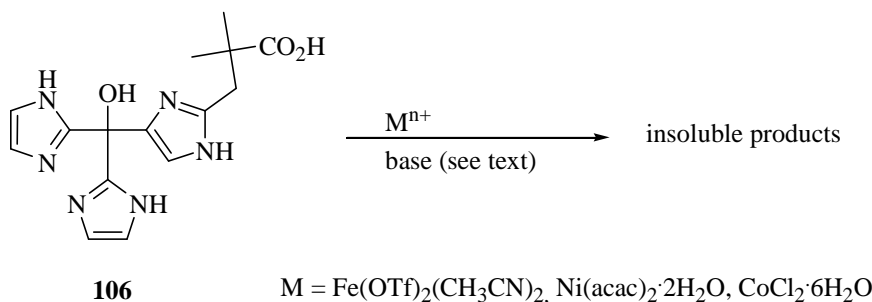
Scheme 4.13

4.2.4 Conclusion

We successfully developed a second synthesis of a 3-imidazole-1-carboxylate tetrad in six linear steps with an extended side chain. This new ligand **106** was specifically designed to serve as an N₃O-donor in an octahedral environment and its coordinating properties were tested.

4.3 Complexation studies and lessons learned

In order to probe the binding capabilities of **106** different metal salts were used. However, very disappointingly all experiments carried out with Fe(OTf)₂(CH₃CN)₂¹⁷¹, Ni(acac)₂·2H₂O and CoCl₂·6H₂O failed to provide tractable mononuclear complexes (scheme 4.14). As previously observed the addition of any type of base (*N,N*-diisopropylethylamine with iron (II), acac with Ni (II) and NaHCO₃ with the cobalt (II)) led to the formation of intractable and insoluble products, presumed to be oligomeric.



Scheme 4.14

Similar behaviors observed with the short or the extended chain pointed to other problems imbedded within the ligands themselves. It clearly appeared that more dramatic changes of the ligands would be necessary if any characterizable

mononuclear complexes were to be produced. We therefore identified all the common features of **73** (short side arm) and **106** (long side-arm) potentially responsible for the formation of intractable solids and decided to incorporate in our last attempt all preemptive measures possible. After careful consideration of the previous results, three specific points were targeted. First, the insolubility of the ligands in polar aprotic organic solvents greatly limited their use and our ability to easily purify them. Secondly, the presence of the N-Hs in the ligands was potentially detrimental to the discrete nature of the desired products. Upon binding to metal ions a depressed pKa of the imidazole NH¹²⁰ could potentially lead to bridging imidazolate ligands¹⁷² and therefore oligomerization. Third, we also were aware of the potential unwanted coordination to metal ions by the hydroxo group of the carbinol; as its coordination for example with copper (II) in similar ligands is well documented.^{173,174}

4.4 Synthesis of the carboxylate-functionalized tris[4-(N-methyl-2-isopropyl-imidazolyl)methane

4.4.1 Design and retrosynthesis of an optimal ligand for a structural model of the 3-His-1-carboxylate motif

In order to prevent side reactions which could derive from the identified shortcomings of the ligands, an optimal design was proposed (figure 4.3 (a) and (b)). Protection of all N-Hs was envisioned with an alkyl group, which should prevent oligomerization and also improve the solubility of the ligands. Moreover introduction of steric bulk with an isopropyl unit at the C2 position should favor the formation of discrete 1:1 complexes and also further improve the solubility of the

tripods. Last, the deoxygenation of the hydroxy group, result from the addition reaction, would leave our ligands with only the required hetero-atoms for the coordination chemistry. We believed that these pre-emptive measures would provide us with a well behaved system and the desired N₃O tetradentate ligands.

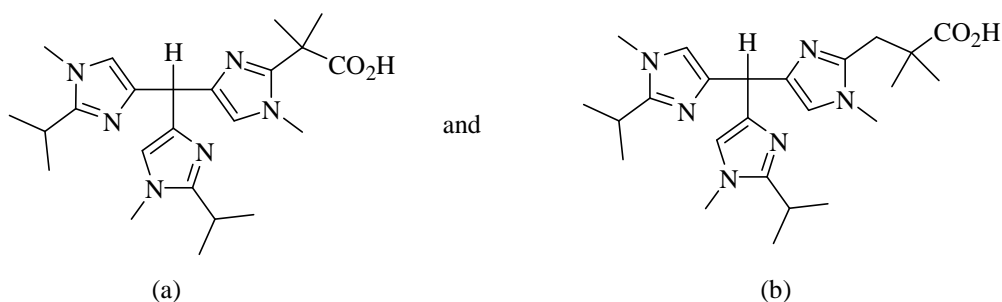
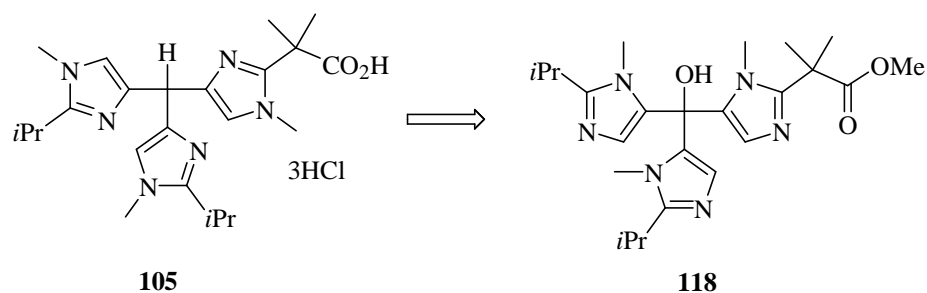
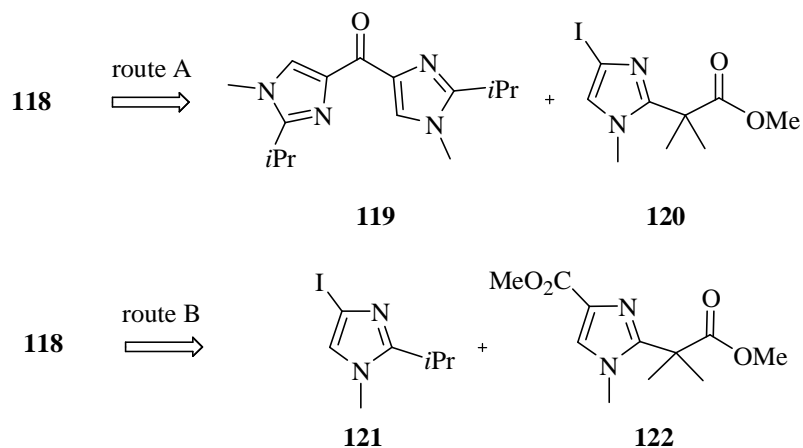


Figure 4.3: New design of the N₃O-donor ligand

This new design (scheme 4.15.1) was not without challenges as the chemistry used until now had to be extended to new building blocks. A recent report¹⁷⁵ on the synthesis of a new sterically hindered tris(imidazolyl)carbinol led us to consider a modified version of our synthetic approach by the utilization of (4)-iodo-imidazoles **97** and **98** as pro-nucleophiles (scheme 4.15.2). Given the changes proposed, we decided to focus first on the short side chain parent compound as the syntheses of the required precursors were easier.



Scheme 4.15.1



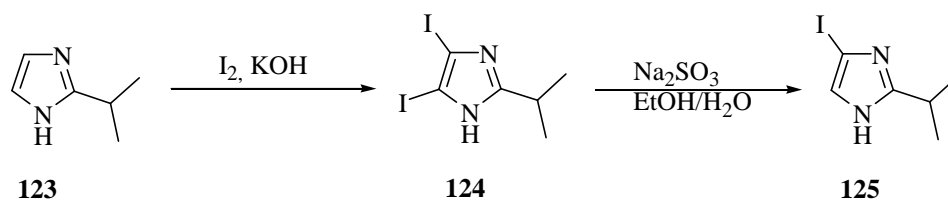
Scheme 4.15.2

The target could again be obtained by two paths already well explored. Route A would use the addition of (4)-iodo-imidazole **120** to the symmetrical ketone of imidazoles **119**. Route B would utilize the successful disconnect previously used in the synthesis of **106** and, as such, we decided it to be our best option.

4.4.2 Synthesis of the optimal ligand **105**

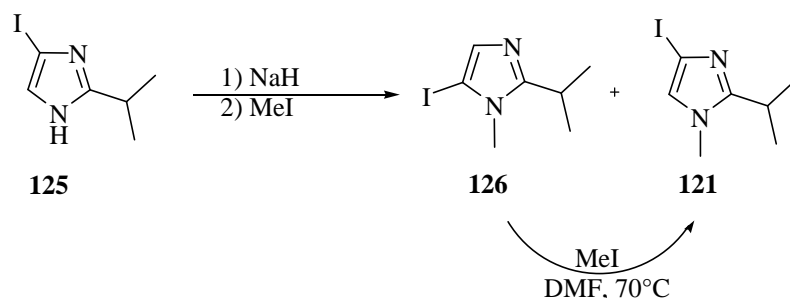
4.4.2.1) Synthesis of 4-iodo-N-methylimidazole **121**

As organomagnesium reagents are known to be less reducing than organolithiums, they should also be less prone to single electron transfer. This is indeed partially verified as they were used by Collman¹²² and Fujii¹⁷⁵. The pro-nucleophile necessary for our purpose must incorporate the iodine atom at the 4-position in order to produce a chelating tripod **105**. Its preparation^{175,176} was achieved by a known procedure (scheme 4.16) starting from imidazole **123** which was initially per-iodinated (**124**) and subsequently reduced back to the mono-iodoimidazole **125** by sodium sulfite in aqueous ethanol, in approximately 50% overall yield.



Scheme 4.16

The protection of iodo imidazole **125** by MeI gave two regioisomers in approximately equal amount (scheme 4.17) in an 82% yield. Fortunately, the undesired regioisomer **126** can be isomerized¹⁷⁶ to the desired 4-iodo-N-methyl imidazole **121** in DMF with a small amount of iodomethane at 70 °C.

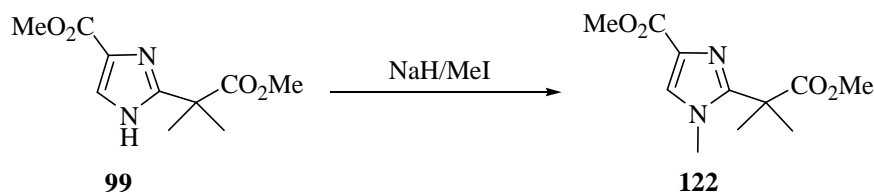


Scheme 4.17

4.4.2.2 Synthesis of the imidazole diester **122**

The synthesis of **122** was achieved from a common intermediate, **99**, from the previous method (scheme 3.22) using sodium hydride and iodomethane (scheme 4.18). The reaction proceeded as expected producing a fully characterized white solid. The five expected ¹H NMR resonances were detected as singlets and the structure was confirmed by ¹³C NMR. The regioselectivity of the protection was determined by a NOESY experiment and supported the C4 substitution. The

germinal dimethyl unit and the aromatic proton resonance were enhanced when the methyl group was irradiated (figure 4.4).



Scheme 4.18

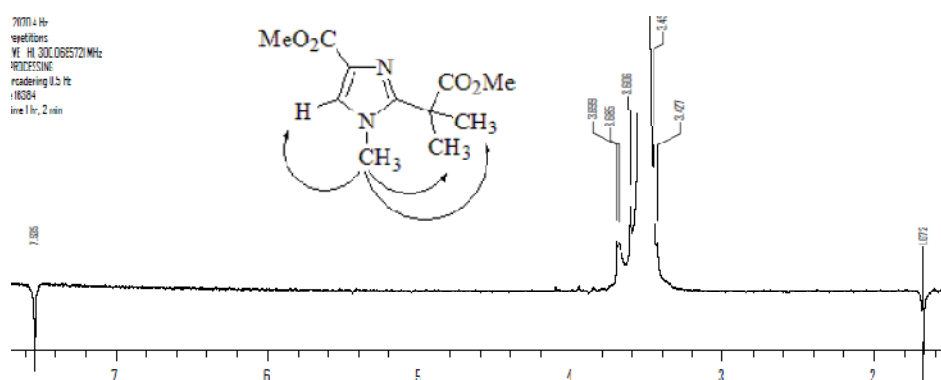
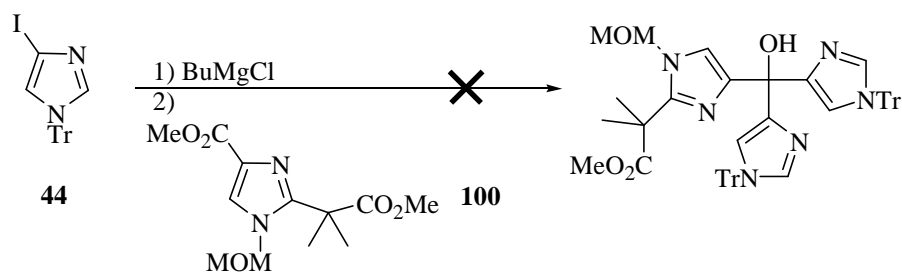


Figure 4.4: NOESY experiment on **122**

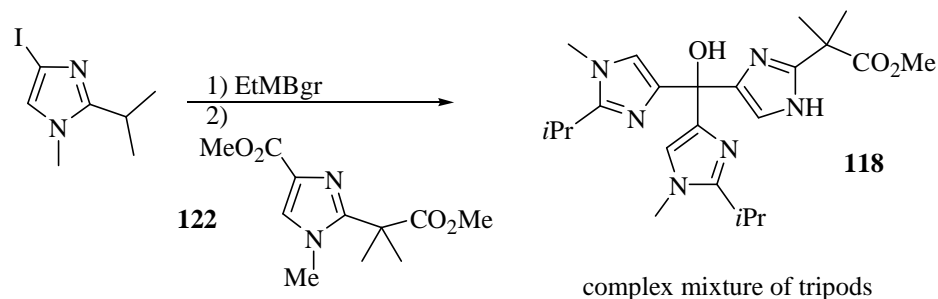
4.4.2.3 Addition of **121** to **122**

With our two building blocks readily synthesized, we probed the addition of Grignard reagents to the diesters **100** and **122**. Initial attempts to use trityl-protected intermediate **44** were not successful when metallated with butylmagnesium chloride (scheme 4.19). The de-iodinated imidazole trityl-protected **44** and its electrophilic partner were both recovered and the desired product was not detected by ^1H NMR analysis of the crude mixture.



Scheme 4.19

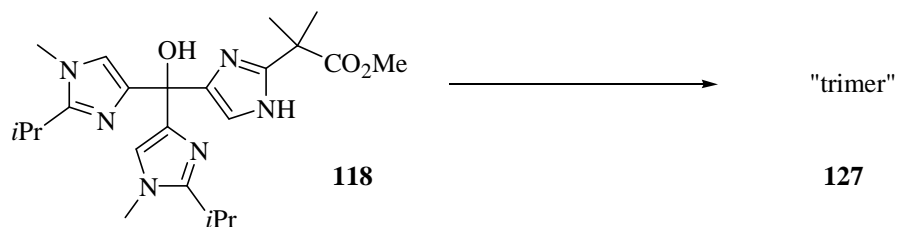
However, since the chloride derivative is not the commonly used nucleophile, we therefore used ethyl magnesium bromide to perform the metal halogen exchange. The formation of the Grignard occurred smoothly at room temperature but the addition of the electrophilic partner **122** to the Grignard solution led to a complex mixture of products as determined by ^1H NMR (scheme 4.20).



Scheme 4.20

After a great amount of time spent on purification the imidazole-containing products, they were tentatively assigned as atropoisomers by ^1H NMR spectroscopy which showed three sets of resonances all consistent with structure **118** (scheme 4.20). Unfortunately, they could not be separated from each other and even though the compound was not homogeneous, complexation of the mixture with tetrakis

(acetonitrile) copper hexafluorophosphate confirmed one of our concerns (scheme 4.21).



Scheme 4.21

Crystals obtained from a concentrated solution in methanol (figure 4.5) allowed us to isolate the copper complex **127**. The unrefined crystal structure clearly indicated the anticipated coordination of the alkoxy group of the tripod bridging two copper centers. Moreover, the syn relation of the three nitrogen-donor atoms to the hydroxy group in the crystallized atroposomer was evidence of the undesired geometry of the ligand.

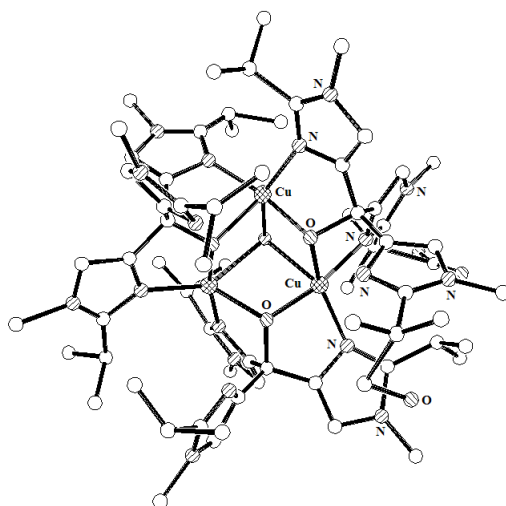
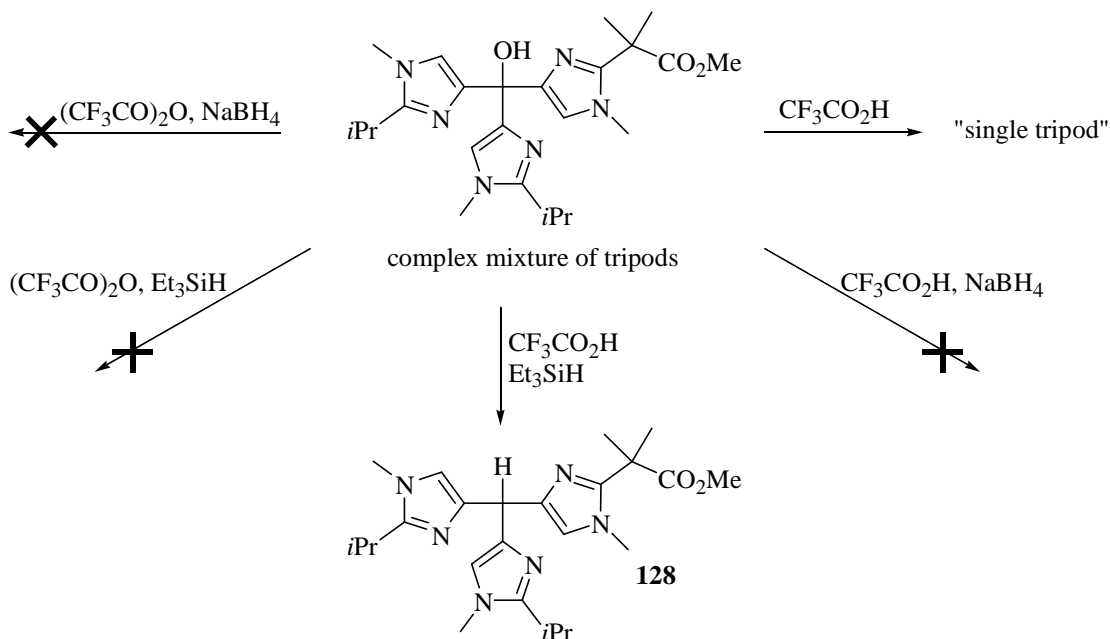


Figure 4.5: X-ray ORTEP diagram of **127** (unrefined)

The protection of the hydroxy by a methoxy group, a common tactic used to prevent its coordination, seemed to be a poor option as the mixture of atropoisomers could remain and most likely give low yields of the desired atropoisomer. The reduction of the carbinol to the hydrocarbon on the other hand appeared to be a better option.

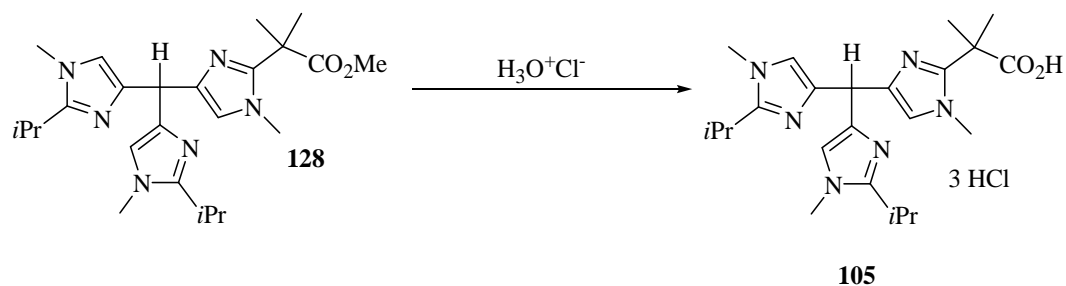
4.4.2.4 Reduction of carbinols **118** and synthesis of **105**

Different conditions for the reduction of the carbinol were tested and are summarized below (scheme 4.22). Activation of the alcohol by trifluoroacetic anhydride proved to be unproductive, but addition of trifluoroacetic acid converted all atropoisomers to a single one. This result was determined by ^1H NMR analysis of the crude mixture. Prior to the addition of trifluoroacetic acid (TFA), three sets of two resonances (s, 1H and 2H) in the aromatic region were detected, corresponding to the imidazole protons. These three imidazole-containing products, after 20 hours at room temperature in CH_2Cl_2 with 3 equivalents of TFA, converged to a single one as indicated by detection of only two singlets by ^1H NMR spectroscopy. This result suggested the clean and reversible formation of the carbocation. Its reduction was attempted with sodium borohydride but did not proceed cleanly producing numerous products by ^1H NMR analysis of the crude mixture. However, complete and clean conversion was achieved with triethylsilane and TFA in refluxing dichloroethane.



Scheme 4.22

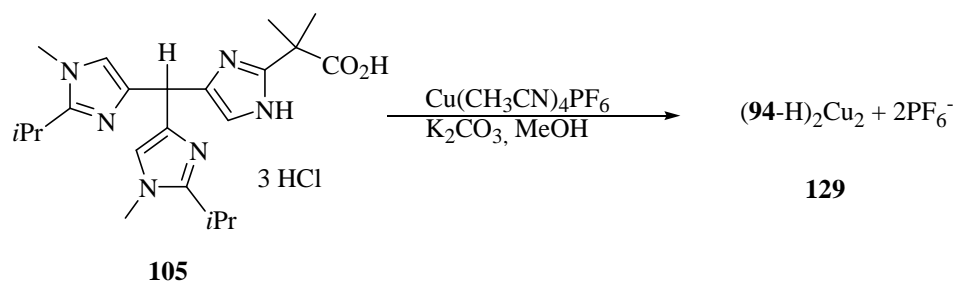
The purification of **128** was rather difficult, but could be achieved with an alumina column (activity grade II) to give **128** in a good purity, in 53% yield over two steps. The orange oil displayed all the required signals by ^1H NMR spectroscopy with two resonances at δ 6.55 ppm (s, 1H), 6.51 ppm (s, 1H) for the aromatic protons and the reduction was indicated by a new proton resonance for the methine group at δ 5.27 (s, 1H). The tripod was also characterized by ^{13}C NMR. With ester **128** in hand, its quantitative hydrolysis in refluxing 6N HCl led to the pure carboxylic acid as a trihydrochloride salt **105** (scheme 4.23). The compound was fully characterized by ^1H NMR spectroscopy which confirmed the hydrolysis of the ester. The protonated state was evidenced by the deshielded signals of the imidazole protons at δ 7.61 ppm (s, 1H), 7.45 ppm (s, 2H), and the methine proton δ 6.00 ppm (s, 1H). The structure of the acid was further established by ^{13}C NMR, mass spectrometry (ESI+) and the carboxylic acid group was detected by IR spectroscopy with a broad band at $\approx 3100\text{-}2300\text{ cm}^{-1}$ and a carbonyl absorption at 1741 cm^{-1} .



Scheme 4.23

4.5 Synthesis of a structural model complex of Cu-dependent 2,3- quercetin dioxygenase

The newly formed tripod **105**, even though a tri-hydrochloride carboxylic acid salt, seemed to be stable in air and no particular precautions were taken to protect it from moisture. Moreover, the compound proved to be soluble in methylene chloride in the presence of an organic base such as triethylamine. These observations led us to believe that our analysis of the potential problems with our previous ligands were at least partially correct. Acid **105** was used in different complexation reactions. As we believed that the mono-anionic short side-chain ligand **105** would have a better chance to form 1:1 complexes with a mono-cationic metal to access to tetrahedral coordination environment, we chose tetrakis (acetonitrile) copper (I) hexafluorophosphate as a metal ion source. When the ligand was mixed in methanol with two equivalents of potassium carbonate and copper (I), no insoluble compounds were formed (scheme 4.24). The solution was exposed to air and turned green. After removing methanol under reduced pressure and redissolving the crude products in methylene chloride, the filtered solution was left overnight in the freezer to yield green crystals suitable for X-ray crystallography (figure 4.6).



Scheme 4.24

This dimer of copper (II) presented a distorted square pyramidal geometry around the copper center, with two PF_6^- counter ions (not shown). The complex displays an expected five coordinate copper (II) center and can directly be compared to the active site of 2,3-querctin dioxygenase (*Aspergillus japonicus*) with coordinated querctin (figure 4.8 and table 4.1 and 4.2). The distances are similar with the exception of longer Cu-E73 and apical H68 in the enzyme structure than in complex **129**. The angles around the copper center are different, especially the angles N-Cu-N, as it is probably due to the tripod of imidazoles, better suited for a facial coordination in an octahedral environment.

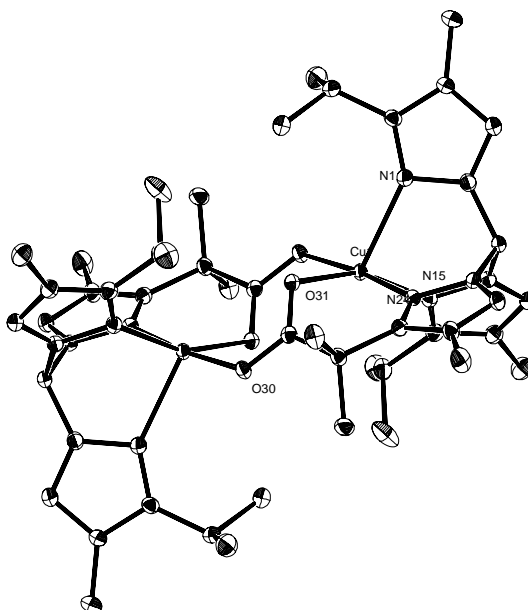


Figure 4.6: X-ray ORTEP diagram of **129**

Selected bond lengths and angles of (2,3-quercetin dioxygenase–quercetin) complex (2,3-QD·QUE) and of **129**

Distances (Å)	2,3-QD·QUE ²⁷	Complex 129
Cu-H66/Cu-N15 (trans to O31)	2.11 (0.03)	2.0409(15)
Cu-H68/Cu-N1 (apical)	2.12 (0.05)	2.2873(16)
Cu-E73/Cu-O31	2.28 (0.09)	2.0278(13)
Cu-H112/Cu-N24	2.05 (0.03)	1.9490(15)
Cu-quercetin/Cu-O30	2.29 (0.06)	1.9534(13)

Table 4.1: Selected distances of 2,3-QD·QUE and **129**

Angles (°)	2,3-QD·QUE	Complex 107
H66-Cu-H68	104(3)	86.40(6)
H66-CuE73	169(3)	156.62(6)
H66-Cu-H112	100(2)	86.40(6)
H68-Cu-E73	86(1)	110.87(5)
E73-Cu-H112	77(2)	83.91(6)

Table 4.2: Selected angles of 2,3-QD·QUE and **129**

However, since each monomer is formally positively charged, we believe that displacement of the bridging carboxylate is possible and would provide us with an excellent monomeric structural model for the 3-His-1-carboxylate tetrad with copper (II). Preliminary experiments showed a color change upon addition of two equivalents of flavonol, a quercetin model, to a solution of **129** in methylene chloride. Further investigations are underway in our laboratory as we believe that complex **129** will also provide us with a functional model.

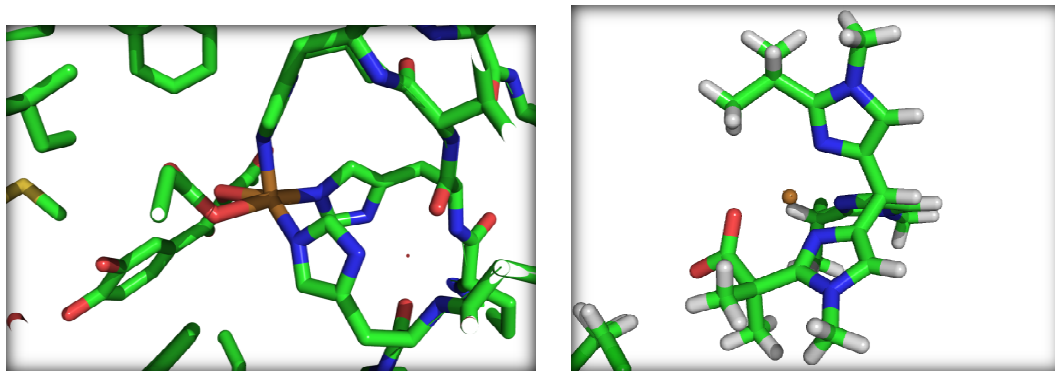
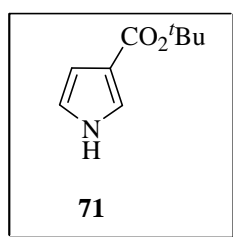


Figure 4.7: Views 2,3-QD·QUE (left) and **129** (right)

Conclusion

We have developed an effective synthesis of a short arm tripod chelator in nine steps, containing the 4-TIC motif, and proved its coordinating properties with copper (II). To the best of our knowledge this compound is the first tetradentate tripodal ligand incorporating three imidazoles and a carboxylate function. Further studies are underway in order to determine the type of coordination, if any, between flavanol and complex **129**. The reactivity and catalytic activity of our complex will also be examined as the difference of ligand environment with the previously reported complexes will surely have a dramatic effect. Finally this is the most accurate structural model²⁹⁻³⁸ of copper-dependent quercetin 2,3-dioxygenase as it incorporates all the desired ligands of the first coordination sphere.

Moreover we have explored the functionalization of the 2 position on imidazole utilizing Itoh's chemistry and discovered a mechanistically interesting rearrangement of activated imidazolines. The imidazolines synthesized, bearing electron withdrawing groups on the nitrogen atoms, underwent a ring contraction to give 3-substituted pyrroles such as **71** (scheme 4.26).

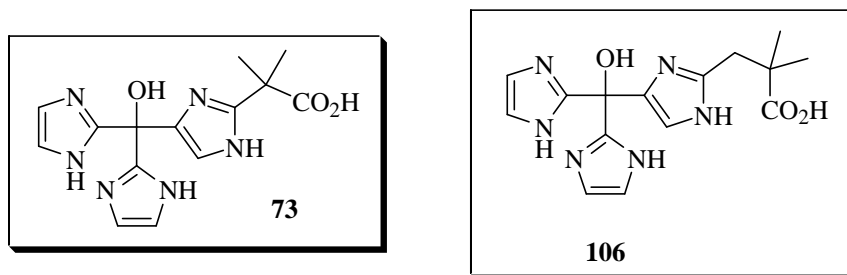


Scheme 4.26

The synthesis of two carboxylate-functionalized tripods of imidazoles also brought some new and interesting discoveries. First, we have shown by computational studies and confirmed experimental reports that the sulfamoyl protecting group modifies dramatically the imidazole reactivity. Indeed, the addition of one electron to the sulfamoyl protected imidazole was calculated to be thermodynamically favorable contrary to more electron rich MOM-imidazole. Moreover, this computational study was further extended to the difficult addition reaction of lithio-imidazoles to the ester of imidazole **100**. The rationalization of the observed narrow scope in competent nucleophiles was based on the ionization potential of the lithio-imidazoles.

Second, we have been able to synthesize a mixed tris(imidazolyl)carbinol with a short side-chain **73** and analyze its coordinating properties with cobalt (III). However, the ligand only formed intractable solids under basic conditions and

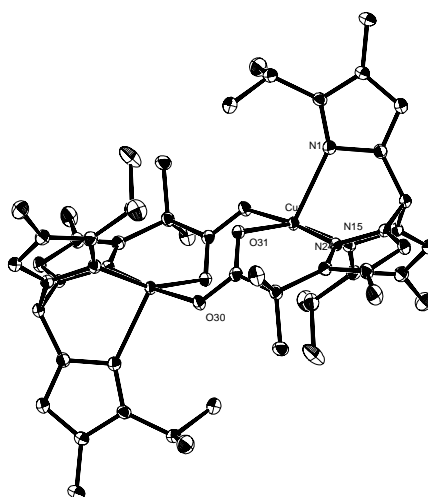
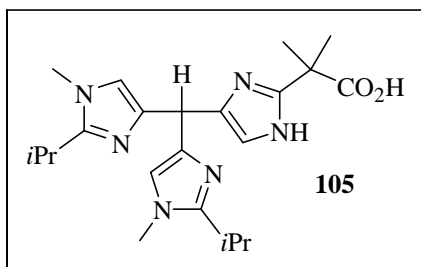
formed a 2:1 adduct, $(\mathbf{73})(\mathbf{73-H})\text{:Co}^{\text{III}}$, under neutral conditions. The cobalt complex **104** displayed a preferred meridional coordination which led us to develop and synthesize a longer side-chain carbinol **106**. The synthetic route capitalized on the former approach and underwent only slight modifications and optimizations. Regrettably, the two ligands **73** and **106** (scheme 4.27) displayed similar behavior in their coordination chemistries (i.e. formation of intractable solids under basic conditions).



Scheme 4.27

Since, the geometric concerns had been addressed by the longer side-chain, we considered the common features which could be responsible for the formation of intractable solids and three potential problems were identified: 1) the presence of potentially acidic imidazole N-H, especially in the presence of metals, could lead to bridging imidazolates 2) the lack of solubility of the ligand in polar aprotic solvents and 3) the presence of a hydroxyl group known to coordinate metal ions. These three specific points were addressed by first providing a methyl protecting group on the imidazole removing completely the imidazole N-H and presumably increasing the solubility. Addition of steric bulk with an isopropyl unit was carried out in order to promote 1:1 complexes and also increase solubility. Last but not least, the

hydroxyl group was reduced and the N₃O methane **105** derivative thus obtained proved to be a good ligand (scheme 4.28).



Scheme 4.28

This was demonstrated by the formation and characterization of the first 3-imidazole-1-carboxylate copper (II) complex, a structural mimic of copper-dependent 2,3-querctine dioxygenases. This excellent structural mimic will be spectroscopically studied and its catalytically activity probed. The synthesis of ligand **105** is a first step in the generalization of structurally accurate ligands for the 3-His-1-carboxylate binding motif. The short side-chain likely to form four or five coordinate biorelevant complexes just establishes the synthetic steps. The extension

of the chemistry to long side-chain will allow for a larger set of metal ions in an octahedral environment to be coordinated in particular Mn, Fe, Co and Ni. As we discussed, the dioxygenases are only a subset of the entire population of enzymes utilizing the 3-His-1-carboxylate tetrad, the cupin superfamily for example, and the study of their biomimetic complexes and in particular their reactivity should provide us with a better understanding of the mechanism considered. Moreover, these new complexes should provide us with interesting new catalysts and therefore new synthetically useful chemistries.

4.7 Experimental

Compounds **110**¹⁶⁶, **116**¹⁶⁹ and **121**¹⁷⁵ were prepared by the reported procedures.

3-{4-[Hydroxy-bis-(1H-imidazol-2-yl)-methyl]-1H-imidazol-2-yl}-2,2-dimethyl-propionic acid **106**

To a solution of sulfonamide **47** (0.655 mg, 3.74 mmol, 1 eq.) in THF (40 mL) at -78 °C under a positive pressure of Ar, BuLi in pentane (1.95 mL, 2.12 M, 4.13 mmol, 1.1 eq.) was added drop-wise. The solution was left 30 min at -78 °C before a solution of **108** (0.560 g, 1.88 mmol, 0.5 eq.) in dry THF (5 mL) was transferred *via* cannula. The reaction was warmed to room temperature and left stirring overnight. The mixture was then quenched with saturated NaHCO₃ and ethyl acetate (50 mL) was added. The organic layer was washed with saturated NaHCO₃ (2 × 50 mL), brine (50 mL) and dried over MgSO₄. The organic solvent was removed under vacuum and the crude was purified by flash column chromatography (95 CH₂Cl₂: 5 MeOH) without success. The crude product was therefore dissolved in 6N HCl (40 mL) and refluxed for 6 h. The crude product was loaded onto an ion exchange column chromatography (Dowex 50WX8-100 resin, 10 mL) and washed with water. The product was then eluted with 6% aqueous ammonia. After removing almost all the solvent addition of acetone precipitated an off-white solid (0.167 g, yield: 27% overall). ¹H (300 MHz, CD₃OD) δ 7.10 (s, 4H), 6.82 (s, 1H), 3.70 (s, 3H), 2.91 (s, 2H), 1.15 (s, 6H); ¹³C (75.5 MHz, CD₃OD) δ 181.9, 148.4, 147.1, 138.3, 121.3, 116.3, 69.6, 43.1, 37.7, 24.8;

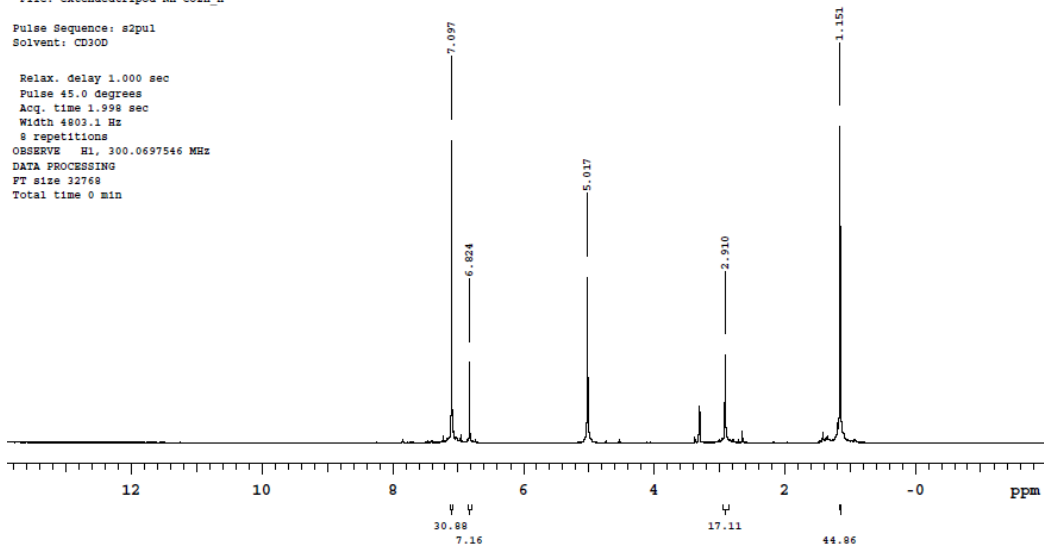
STANDARD 1H OBSERVE

Data Collected on:
oumr4-mercury300
Archive directory:
/export/home/km/vmrsys/data
Sample directory:

File: extendedtripod-NH-CO2H_H

Pulse Sequence: s2pul
Solvent: CD3OD

Relax. delay 1.000 sec
Pulse 45.0 degrees
Acq. time 1.998 sec
Width 4803.1 Hz
8 repetitions
OBSERVE H1, 300.0697546 MHz
DATA PROCESSING
FT size 32768
Total time 0 min



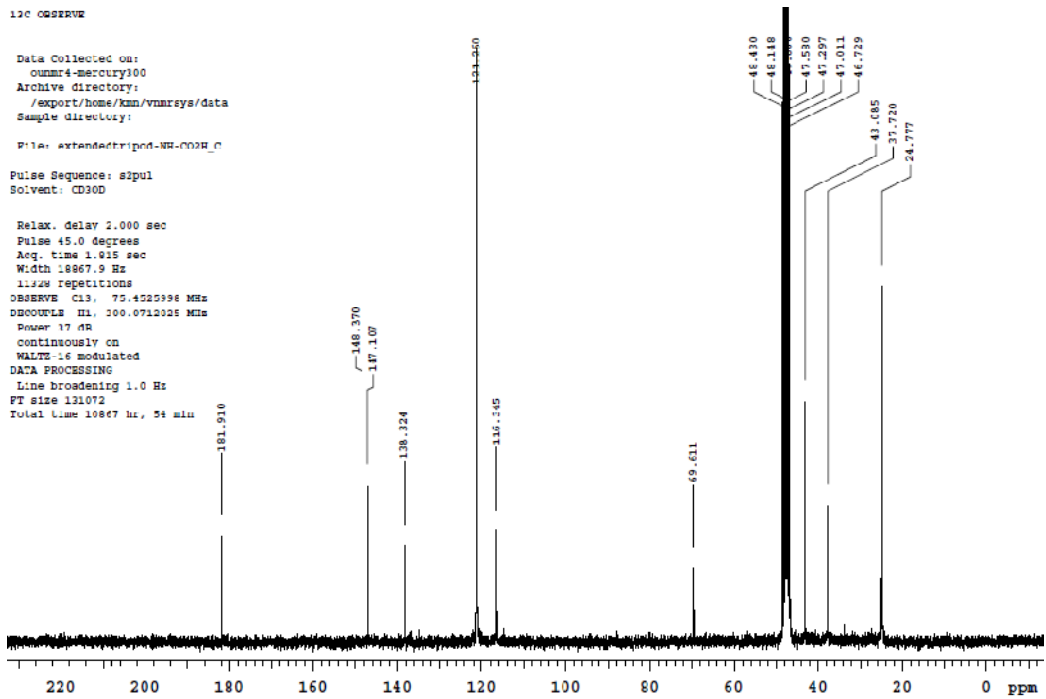
13C OBSERVE

Data Collected on:
oumr4-mercury300
Archive directory:
/export/home/km/vmrsys/data
Sample directory:

File: extendedtripod-NH-CO2H_C

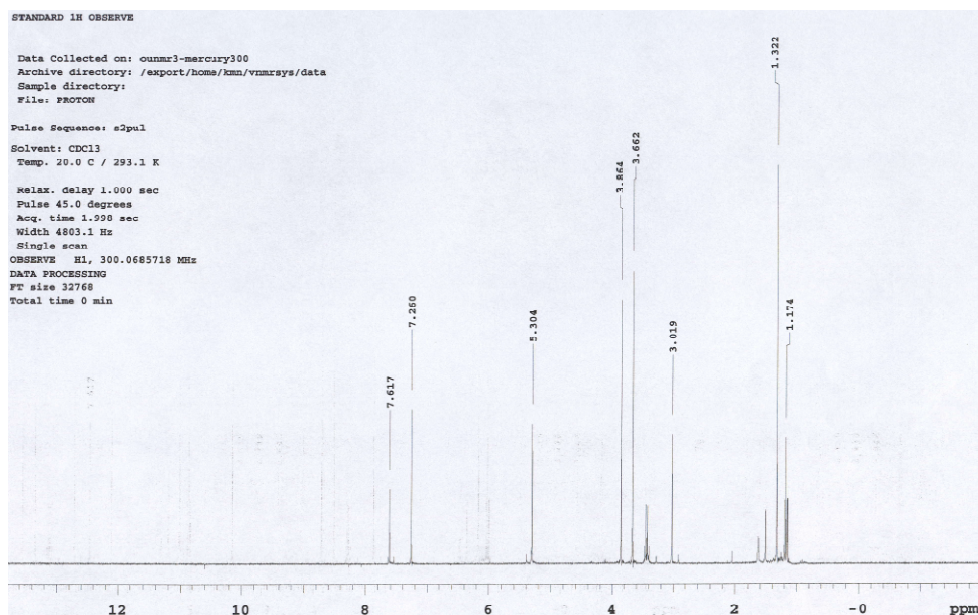
Pulse Sequence: s2pul
Solvent: CD3OD

Relax. delay 2.000 sec
Pulse 45.0 degrees
Acq. time 1.015 sec
Width 18867.9 Hz
1128 repetitions
OBSERVE C13, 75.452598 MHz
DECOURS H1, 300.0712025 MHz
Power 17 dB
CONTINUOUSLY ON
WALTZ-16 modulated
DATA PROCESSING
Line broadening 1.0 Hz
FT size 131072
Total time 10867 hr, 54 min



3-(4-Acetoxy-1-ethoxymethyl-1H-imidazol-2-yl)-2,2-dimethyl-propionic acid methyl ester **108**

To a solution of **112** (4.60 g, 15.9 mmol, 1 eq.) in THF (150 mL) at -78 °C under a positive pressure of Ar, ^tBuLi in pentane (17.4 mmol, 11.2 mL, 1.55M, 1.1 eq.) was added drop-wise. The solution was left 1 h at -78 °C before methyl chloroformate (2.5 mL, 32.4 mmol, 1.9 eq.) was added neat. The reaction was warmed to room temperature and left stirring for 2 h. The organic solvent was removed under reduced pressure and the crude was purified by flash column chromatography (3 Hexanes: 7 AcOEt) to yield 1.44 g of an impure product. The crude product was then submitted to methanolysis by refluxing overnight in methanol (50 mL) with concentrated H₂SO₄ (0.3 mL). The mixture was then quenched with saturated NaHCO₃ and ethyl acetate (100 mL) was added. The organic layer was washed with of saturated NaHCO₃ (2 × 50 mL), brine (50 mL) and dried over MgSO₄. Once again the crude product (0.97 g) was used and dissolved in dry THF (40 mL) cooled to 0 °C. NaH (0.320 g, 8 mmol, 60% dispersion in mineral oil) was added portion-wise over 30 min and left at room temperature for 30 min. EOM-Cl was then added neat (0.45 mL, 4.8 mmol, 1.2 eq.) and left at room temperature overnight. The reaction was quenched with H₂O and ethyl acetate was added (50 mL). The organic phase was washed with saturated NaHCO₃ (2 × 25 mL), brine (25 mL) and dried over MgSO₄. The organic solvents were removed under reduced pressure and the crude product purified by flash column chromatography (7 AcOEt: 3 Hexanes) to yield the desired compound as a white solid (0.72 g, yield: 15% overall). ¹H (300 MHz, CDCl₃) δ 7.62 (s, 1H, *J*= 2.7 Hz), 5.30 (s, 2H), 3.86 (s, 3H), 3.66 (s, 3H), 3.43 (q, *J*= 6.9 Hz, 2H), 1.32 (s, 6H), 1.17 (t, *J*= 6.9 Hz, 3H); MS (ESI +): exact mass calculated for C₁₄H₂₃N₂O₅ [M + H]⁺ 299.16. Found 299.18.



3-(1H-Imidazol-2-yl)-2,2-dimethyl-propionic acid methyl ester **111**:

To a solution of 2,2-dimethyl-4-oxo-butyric acid methyl ester 6.90 g (47.9 mmol, 1 eq.) in methanol (40 mL), ammonium carbonate (4.6 g, 47.9 mmol, 1 eq.) was added and the solution was stirred for 30 min at room temperature. A solution of aqueous glyoxal (40 wt % in H₂O, 6.95 g, 47.9 mmol, 1 eq.) in methanol (10 mL) was added. The reaction was left stirring at room temperature overnight. The methanol was then removed under reduced pressure and the remaining solution was dissolved in warm ethyl acetate (200 mL). The organic phase was washed with brine (3 × 20 mL) and dried over MgSO₄. Upon evaporation of the solvent an off white solid precipitated which was filtered to yield the desired product (5.60 g 64% yield). ¹H (300 MHz, CDCl₃) δ 6.92 (s, 2H), 3.66 (s, 3H), 2.96 (s, 2H), 1.20 (s, 6H); ¹³C (75.5 MHz, CDCl₃) δ 179.0, 145.4, 121.7 (bs), 52.2, 43.1, 38.4, 25.4;

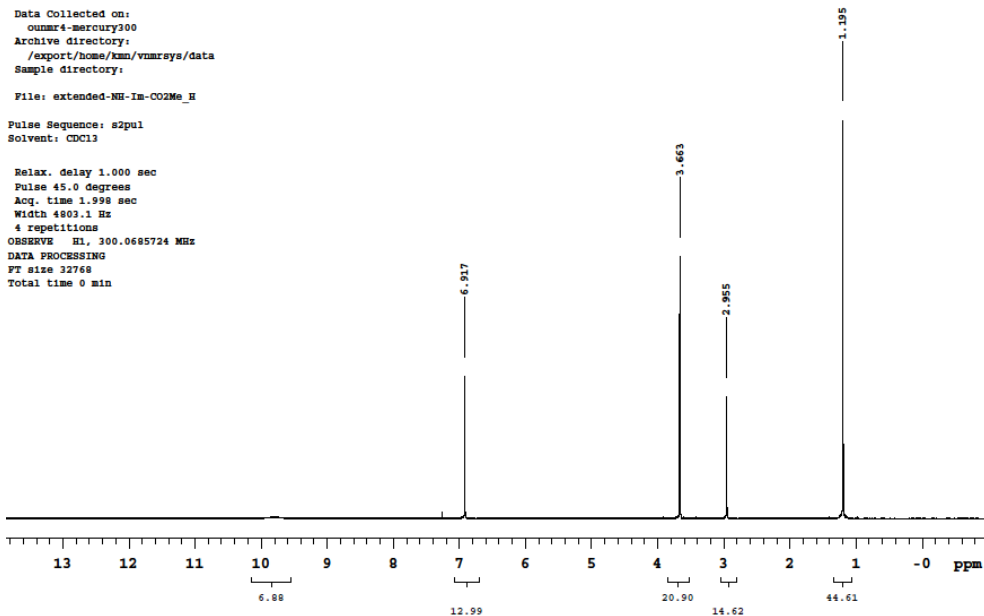
STANDARD 1H OBSERVE

Data Collected on:
ounmr4-mercury300
Archive directory:
/export/home/kmn/vnmrsys/data
Sample directory:

File: extended-NH-Im-CO2Me_H

Pulse Sequence: s2pul
Solvent: CDCl3

Relax. delay 1.000 sec
Pulse 45.0 degrees
Acq. time 1.998 sec
Width 4803.1 Hz
4 repetitions
OBSERVE H1, 300.0685724 MHz
DATA PROCESSING
FT size 32768
Total time 0 min



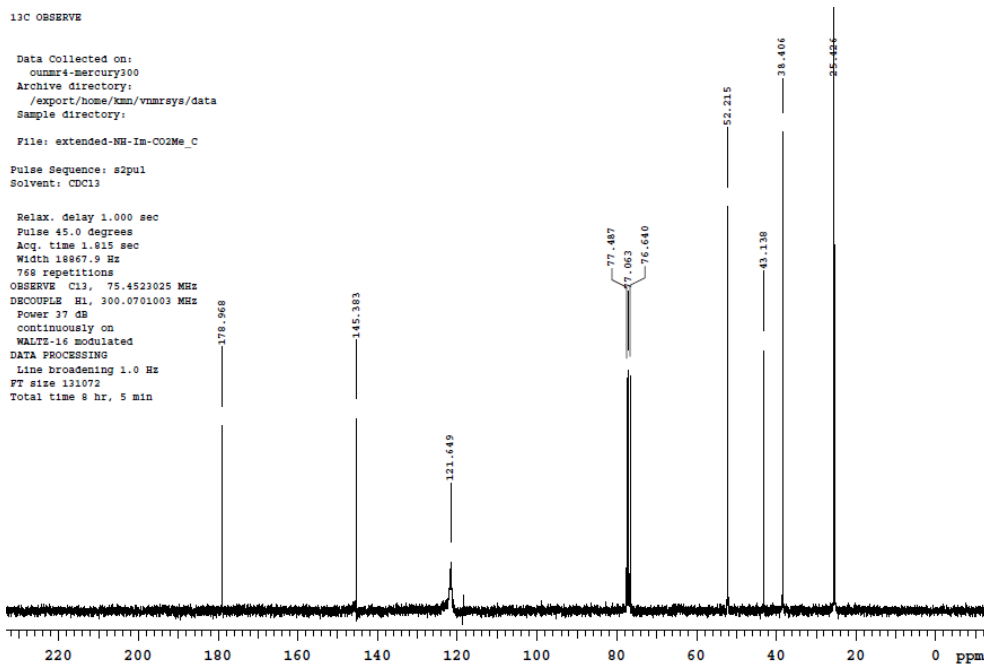
13C OBSERVE

Data Collected on:
ounmr4-mercury300
Archive directory:
/export/home/kmn/vnmrsys/data
Sample directory:

File: extended-NH-Im-CO2Me_C

Pulse Sequence: s2pul
Solvent: CDCl3

Relax. delay 1.000 sec
Pulse 45.0 degrees
Acq. time 1.815 sec
Width 18867.9 Hz
768 repetitions
OBSERVE C13, 75.4523025 MHz
DECOUPLE H1, 300.0701003 MHz
Power 37 dB
continuously on
WALTZ-16 modulated
DATA PROCESSING
Line broadening 1.0 Hz
FT size 131072
Total time 8 hr, 5 min



3-(1-Dimethylsulfamoyl-1H-imidazol-2-yl)-2,2-dimethyl-propionic acid methyl ester **112**:

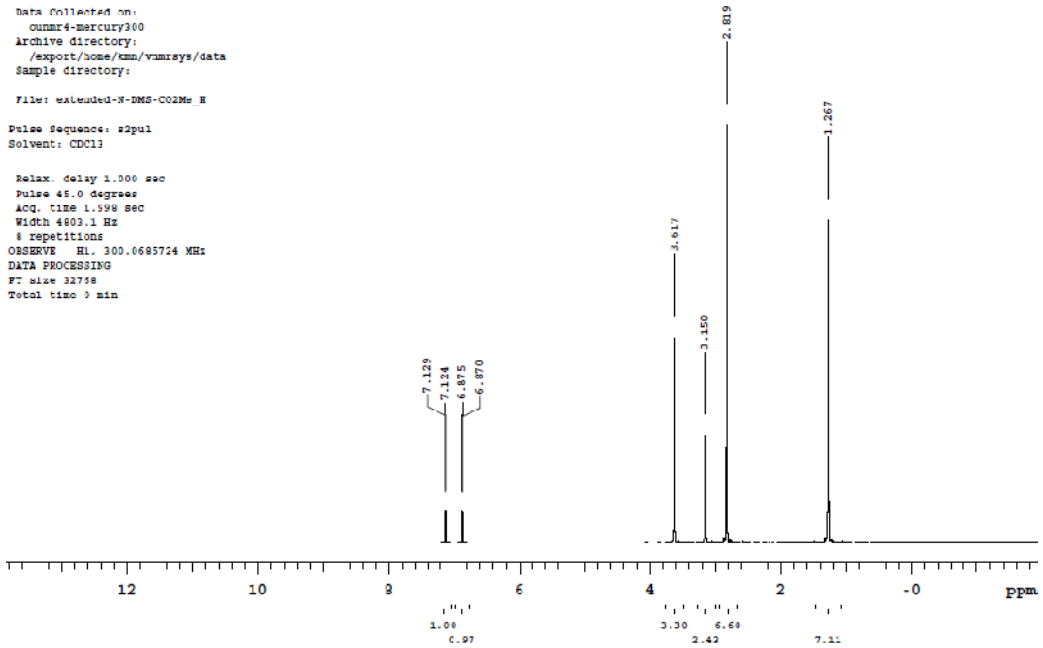
To a stirred solution of imidazole **111** (4.60 g, 25.2 mmol, 1 eq.) in dry THF (130 mL) cooled to 0 °C, NaH (1.60 g, 40 mmol, 1.6 eq., 60% dispersion in mineral oil) was added portion-wise over 30 min and left at room temperature for 30 min. 1-*N,N*-dimethylsulfamoyl chloride was then added neat (3.3 mL, 30.7 mmol, 1.2 eq.) and left at room temperature overnight. The reaction was quenched with H₂O and ethyl acetate was added (200 mL). The organic phase was then washed with of saturated NaHCO₃ (2 × 50 mL), brine (50 mL) and dried over MgSO₄. The organic solvents were removed under reduced pressure and the resulting crude product purified by flash column chromatography (6 AcOEt: 4 Hexanes) to yield of the desired compound as a white solid (6.80 g, 93% yield). ¹H (300 MHz, CDCl₃) δ 7.12 (d, *J*= 1.5 Hz, 1H), 6.87 (d, *J*= 1.5 Hz, 1H), 3.62 (s, 3H), 2.82 (s, 6H), 1.27 (s, 6H); ¹³C (75.5 MHz, CDCl₃) δ 177.7, 146.4, 127.5, 119.1, 51.9, 42.1, 38.2, 37.9, 25.6.

STANDARD 1H OBSERVE

Data Collected on:
 oumr4-mercury300
 Archive directory:
 /export/home/km/vnmrsvs/data
 Sample directory:

File: extended-N-DMS-CO2Me_E
 Pulse Sequence: s2pul
 Solvent: CDCl3

Relax. delay 1.000 sec
 Pulse 45.0 degrees
 Acq. time 1.998 sec
 Width 4803.1 Hz
 8 repetitions
 OBSERVE H1, 300.0695724 MHz
 DATA PROCESSING
 FT size 32798
 Total time 9 min

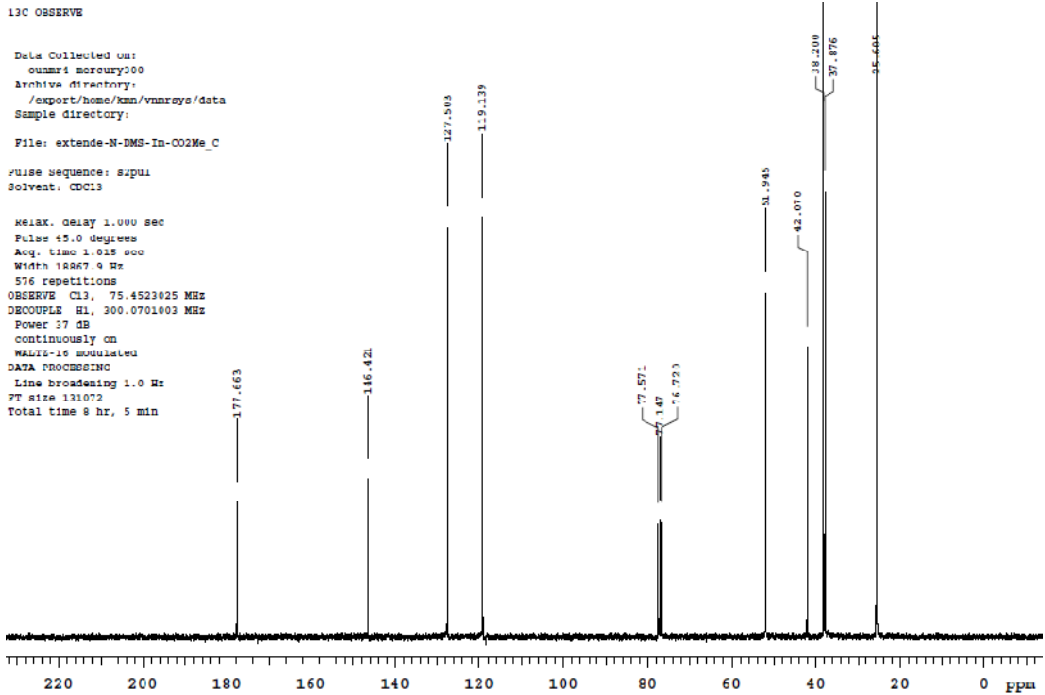


13C OBSERVE

Data Collected on:
 oumr4-mercury300
 Archive directory:
 /export/home/km/vnmrsvs/data
 Sample directory:

File: extended-N-DMS-In-CO2Me_C
 Pulse Sequence: s2pul
 Solvent: CDCl3

Relax. delay 1.090 sec
 Pulse 45.0 degrees
 Acq. time 1.015 sec
 Width 12867.0 Hz
 576 repetitions
 OBSERVE C13, 75.4523025 MHz
 DECOUPLE H1, 300.0701003 MHz
 Power 17 dB
 continuously on
 WALTZ-16 modulated
 DATA PROCESSING
 Line broadening 1.0 Hz
 FT size 131072
 Total time 8 hr, 5 min



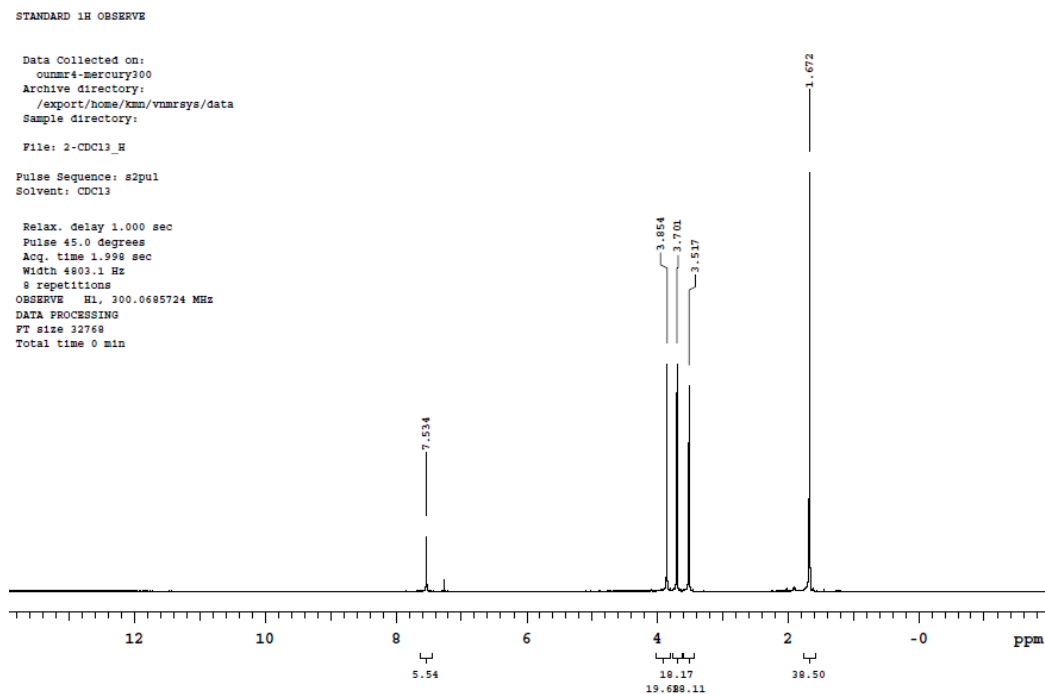
2-(2-Methoxycarbonyl-2-methyl-propyl)-3H-imidazole-4-carboxylic acid ethyl ester **117**:

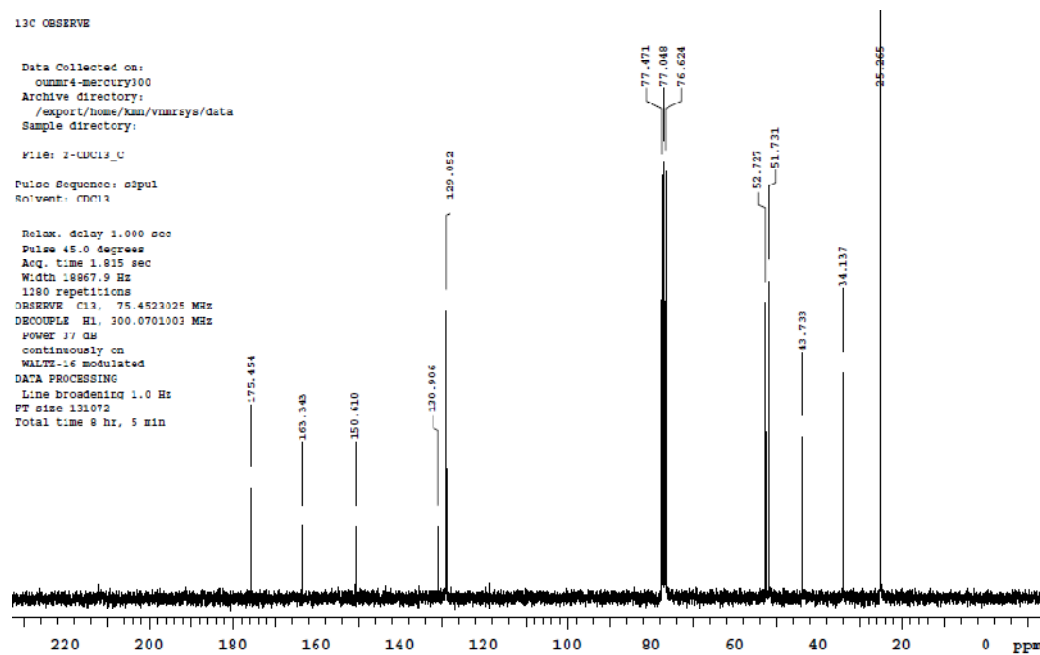
A solution of dimethyldioxirane in acetone (0.1 M, 60 mL) was added to **115** (0.600 g, 4.22 mmol, 1 eq.), after 30 min the solvent was removed under reduced pressure and the crude product redissolved in MeOH (25 mL). 2,2-dimethyl-4-oxo-butyric acid methyl ester **85** (0.608 mg, 4.23 mmol, 1 eq.) and ammonium carbonate (0.405 mg, 4.23 mmol, 1 eq.) were added. The solution was stirred overnight at room temperature. The methanol was then removed under reduced pressure and the resulting crude product purified by flash column chromatography (8 AcOEt: 2 Hexanes) to yield of the desired compound as a white solid (0.60 g, 56% yield). Major isomer: ^1H (300 MHz, CDCl_3) δ 7.63 (d, $J= 1.5$ Hz, 1H), 7.01 (d, $J= 1.5$ Hz, 1H), 4.36 (q, $J= 7.5$ Hz, 2H), 3.73 (s, 3H), 3.03 (s, 2H), 1.37 (t, $J= 6.9$ Hz, 3H), 1.23 (s, 6H); MS (ESI +): exact mass calculated for $\text{C}_{12}\text{H}_{18}\text{N}_2\text{O}_4\text{Na}$ $[\text{M} + \text{Na}]^+$ 277.12. Found 27.10.

2-(2-Methoxycarbonyl-2-methyl-propyl)-1-methoxymethyl-1H-imidazole-4-carboxylic acid ethyl ester **122**

To a solution of **99** (1.70 g, 7.51 mmol) in dry THF (75 mL) cooled to 0 °C, NaH (0.45 g, 11.4 mmol, 1.5 eq., 60% dispersion in mineral oil) was added portion-wise over 30 min and left at room temperature for 30 min and cooled to 0 °C. Iodomethane was added neat (0.58 mL, 9.0 mmol, 1.2 eq.) and the solution was warmed to room temperature overnight. The reaction was quenched with H_2O and ethyl acetate was added (50 mL). The organic phase was then washed with saturated NaHCO_3 (2×25 mL), brine (25 mL) and dried over MgSO_4 . The organic solvents were removed under vacuum and the resulting crude product purified by

flash column chromatography (6 AcOEt: 4 Hexanes) to yield **122** as a white solid (1.48 g 82% yield). Melting point: 82-84 °C; IR (KBr) 3129, 3084, 2993, 2956, 1737, 1704, 1556, 1440, 1346, 1251, 1226, 1012; ¹H (300 MHz, CDCl₃) δ 7.55 (s, 1H), 3.87 (s, 3H), 3.71 (s, 3H), 3.53 (s, 3H), 1.69(s, 6H); ¹³C (75.5 MHz, CDCl₃) δ 175.5, 163.3, 150.6, 130.9, 121.1, 52.7, 51.7, 43.7, 34.1, 25.3; HRMS (ESI +): exact mass calculated for C₁₁H₁₆N₂O₄Na [M + Na]⁺ 263.1002. Found 263.0943.

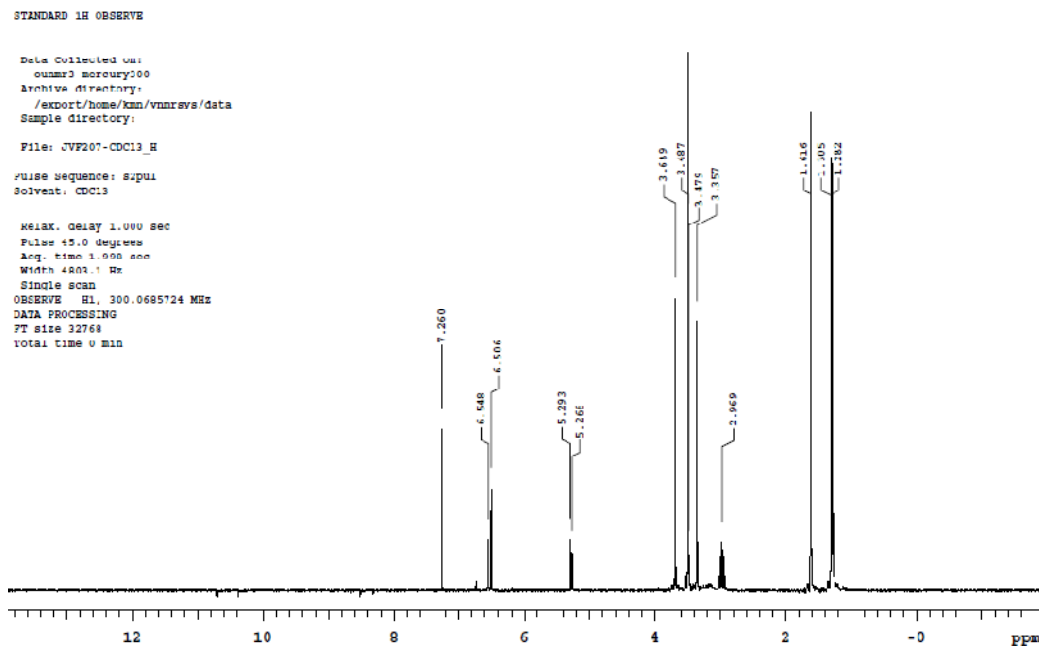


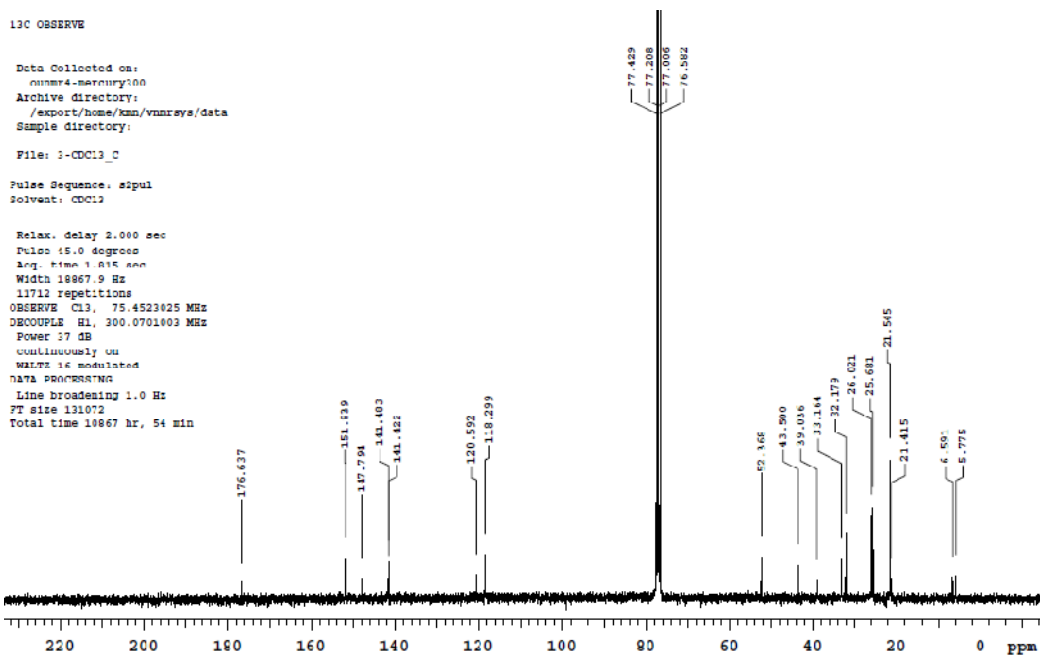


2-{4-[Bis-(2-isopropyl-1-methyl-1H-imidazol-4-yl)-methyl]-1H-imidazol-2-yl}-2-methyl-propionic acid methyl ester **128**

To a solution of **121** (1.09 g, 4.35 mmol) in CH₂Cl₂ (20 mL) at room temperature under a positive pressure of Ar, EtMgBr in diethyl ether (4.8 mmol, 1.5 mL, 3.05 M, 1.1 eq.) was added drop-wise. The solution was left 1 h at room temperature before **122** (0.500 g, 2.18 mmol, 0.5 eq.) was added in methylene chloride (2 mL). The reaction was left stirring for 40 h and then quenched with saturated NaHCO₃. The organic phase was washed with of saturated NaHCO₃ (2 × 50 mL), brine (50 mL) and dried over MgSO₄. The organic solvent was removed under vacuum and to the crude product, redissolved in dichloroethane (20 mL), triethylsilane (0.69 mL, 5.36 mmol, 2 eq.) and trifluoroacetic acid (0.48 mL, 6.54 mmol, 3 eq.) were added. The reaction was refluxed for 20 h. The solvent was removed under reduced pressure and redissolved in EtOAc (50 mL). The organic phase was then washed with saturated NaHCO₃ (2 × 50 mL), brine (50 mL) and

dried over MgSO_4 . The crude product was purified by alumina chromatography activity grade (II) in three phases: 1) (acetone 3: CH_2Cl_2 7) 2) CH_2Cl_2 and 3) (MeOH 1: 9 CH_2Cl_2) to yield 0.33 g of an orange oil (yield 53%). ^1H (300 MHz, CDCl_3) δ 6.55 (s, 1H), 6.51 (s, 1H), 5.27 (s, 1H), 3.69 (s, 3H) 3.49 (s, 6H), 3.36 (s, 3H), 2.97 (sep, $J= 6.9$ Hz, 3H), 1.62 (s, 6H), 1.30 (d, $J= 7.2$ Hz, 12H); ^{13}C (75.5 MHz, CDCl_3) δ 176.6, 151.8, 147.8, 141.5, 141.4, 120.6, 118.3, 52.4, 43.5, 39.0, 33.2, 26.0, 25.7, 21.5.



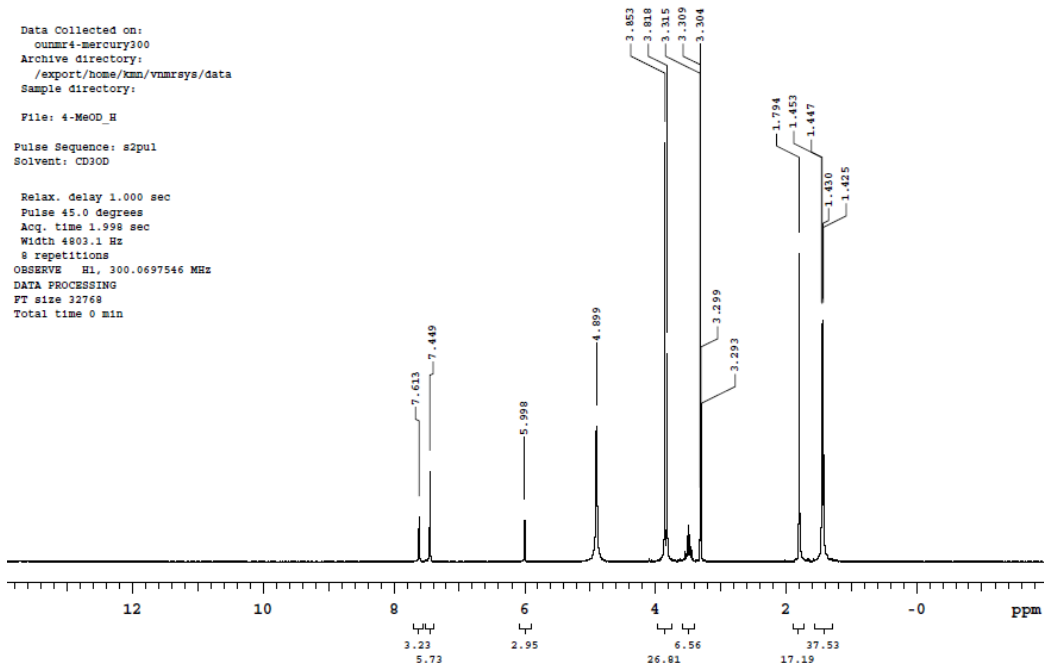


2-{4-[Bis-(2-isopropyl-1-methyl-1H-imidazol-4-yl)-methyl]-1H-imidazol-2-yl}-2-methyl-propionic acid **105**

Ester **128** was dissolved in 6N HCl (20 mL) and the solution refluxed for 2 h. The solvent was removed under reduced pressure to yield quantitatively the desired product **105**. Melting point: 82-84 °C; IR (KBr) 3052, 2800, 1741, 1704, 1654, 1519, 1222, 1181; ¹H (300 MHz, CD₃OD) δ 7.61 (s, 1H), 7.45 (s, 2H) 6.00 (s, 1H), 3.85 (s, 6H), 3.82 (s, 3H), 3.49 (sep, *J*= 6.6 Hz, 3H), 1.79 (s, 6H), 1.44 (dd, *J*₁= 6.9 Hz, *J*₂= 1.5 Hz, 12H); ¹³C (75.5 MHz, CD₃OD) δ 172.8, 153.6, 149.7, 128.2, 127.8, 125.0, 122.9, 43.7, 35.8, 33.8, 29.8, 25.4, 23.1, 18.3; HRMS (ESI +): exact mass calculated for C₂₃H₃₅N₆O₂ [M + H]⁺ 427.2816. Found 427.2783.

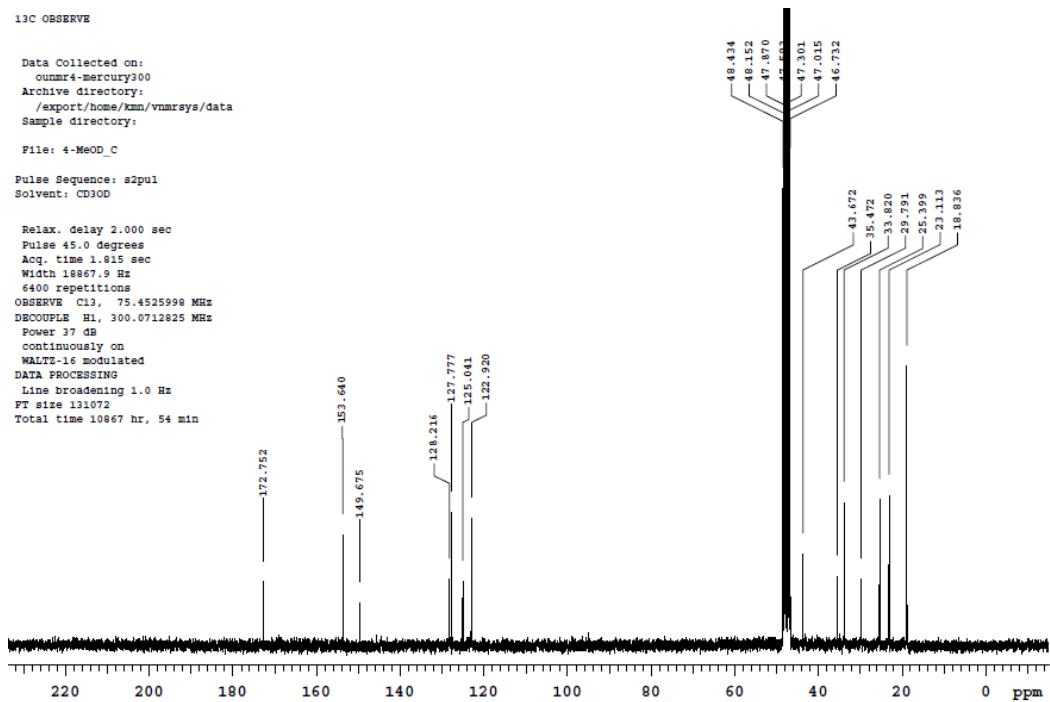
STANDARD 1H OBSERVE

Data Collected on:
 oumm4-mercury300
 Archive directory:
 /export/home/km/vnmrsys/data
 Sample directory:
 File: 4-MeOD_H
 Pulse Sequence: s2pul
 Solvent: CD3OD
 Relax. delay 1.000 sec
 Pulse 45.0 degrees
 Acq. time 1.998 sec
 Width 4803.1 Hz
 8 repetitions
 OBSERVE H1, 300.0697546 MHz
 DATA PROCESSING
 FT size 32768
 Total time 0 min



13C OBSERVE

Data Collected on:
 oumm4-mercury300
 Archive directory:
 /export/home/km/vnmrsys/data
 Sample directory:
 File: 4-MeOD_C
 Pulse Sequence: s2pul
 Solvent: CD3OD
 Relax. delay 2.000 sec
 Pulse 45.0 degrees
 Acq. time 1.815 sec
 Width 18867.9 Hz
 6400 repetitions
 OBSERVE C13, 75.4525998 MHz
 DECOUPLE H1, 300.0712825 MHz
 Power 37 dB
 continuously on
 WALTZ-16 modulated
 DATA PROCESSING
 Line broadening 1.0 Hz
 FT size 131072
 Total time 10867 hr, 54 min



Synthesis of **129**

To a solution of **105** (49.6 mg, 0.10 mmol, 1 eq.) in MeOH (4 mL), tetrakis (acetonitrile) copper hexafluorophosphate (34.5 mg, 0.01 mmol, 1 eq.) and potassium carbonate (28.4 mg, 0.21 mmol, 2.3 eq.) were added. The solution was exposed to air and turned green. After removing methanol under reduced pressure and redissolving the compound in methylene chloride, the filtered solution was left overnight in the freezer to yield green crystals suitable for X-ray crystallography; after vacuum drying the crystals a powder formed yielding the product (25 mg, 26% yield).

We acknowledge and thank Dr. D. Powell for his expertise in determining the crystal structure of **129**.

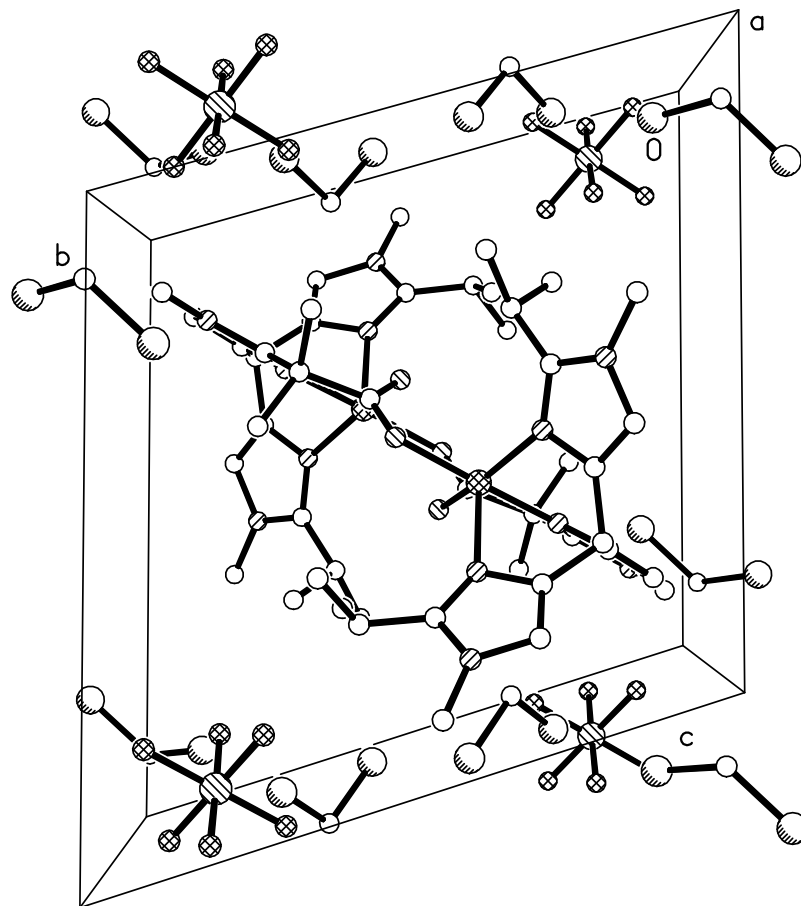


Table 4.3: Crystal data and structure refinement for **107**

Empirical formula	$C_{53} H_{80} Cl_{14} Cu_2 F_{12} N_{12} O_4 P_2$
Formula weight	1862.61
Crystal system	Triclinic
Space group	$P\bar{1}$
Unit cell dimensions	$a = 12.312(2) \text{ \AA}$, $\alpha = 72.775(6)^\circ$ $b = 12.845(2) \text{ \AA}$, $\beta = 85.473(6)^\circ$ $c = 12.909(2) \text{ \AA}$, $\gamma = 80.076(6)^\circ$
Volume	$1919.9(5) \text{ \AA}^3$
Z, Z'	1, 1/2
Density (calculated)	1.611 Mg/m^3
Wavelength	0.71073 \AA
Temperature	$100(2) \text{ K}$
F(000)	948
Absorption coefficient	1.162 mm^{-1}
Absorption correction	Semi-empirical from equivalents
Max. and min. transmission	0.747 and 0.638
Theta range for data collection	1.65 to 28.30°
Reflections collected	26936
Independent reflections	9526 [R(int)= 0.0338]
Data / restraints / parameters	9526 / 47 / 543
$wR(F^2 \text{ all data})$	$wR2 = 0.0913$
$R(F \text{ obsd data})$	$R1 = 0.0366$
Goodness-of-fit on F^2	1.008
Observed data [$I > 2\sigma(I)$]	7984
Largest and mean shift / s.u.	0.002 and 0.000
Largest diff. peak and hole	0.601 and -0.378 e/\AA^3
$wR2 = \{ \sum [w(F_o^2 - F_c^2)^2] / \sum [w(F_o^2)^2] \}^{1/2}$, $R1 = \sum F_o - F_c / \sum F_o $	

Addition attempt of **44** to **100**:

To a solution of **44** (0.872 g, 2.00 mmol, 1 eq.) in CH₂Cl₂ (40 mL) at room temperature under a positive pressure of Ar, BuMgCl in diethyl ether (2.2 mmol, 1.4 mL, 1.6 M, 1.1 eq.) was added drop-wise. The solution was left 1 h at room temperature before **100** (0.271 g, 1.00 mmol, 0.5 eq.) was added in methylene chloride (2 mL). The reaction was left stirring for 40 h and then quenched with saturated NaHCO₃. The organic phase was washed with saturated NaHCO₃ (2 × 50 mL), of brine (50 mL) and dried over MgSO₄. The organic solvent was removed under vacuum and the ¹H NMR spectrum of the crude mixture showed only starting materials.

Complexation experiments of **106**:

The extended side-chain tripod **106** (50 mg, 0.15 mmol, 1 eq.) was dissolved in MeOH (3 mL) and 1 equivalent of metal salt was added. After stirring for 15 min the NaHCO₃ (15 mg, 0.20 mmol, 1.2eq) was added and a precipitate formed. Attempts to redissolve it in organic solvents failed. Metal salts used: Fe(OTf)₂(CH₃CN)₂¹⁷¹, Ni(acac)₂·2H₂O and CoCl₂·6H₂O.

References

- (1) Costas, M.; Mehn, M. P.; Jensen, M. P.; L. Que, J. *Chem. Rev.* **2004**, *104*, 939-986.
- (2) Que, L. J. *Nat. Struct. Mol. Biol.* **2000**, *7*, 182-184.
- (3) Straganz, G. D.; Nidetzky, B. *ChemBioChem* **2006**, *7*, 1536-1548.
- (4) Dunwell, J. M.; Khuri, S.; Gane, P. J. *Microbiol. Mol. Biol. Rev.* **2000**, *64*, 153-179.
- (5) Dunwell, J. M.; Purvis, A.; Khuri, S. *Phytochemistry* **2004**, *65*, 7-17.
- (6) Dunwell, J. M.; Culham, A.; Carter, C. E.; Sosa-Aguirre, C. R.; Goodenough, P. W. *Trends Biochem. Sci.* **2001**, *126*, 740-746.
- (7) Lane, B. G.; Dunwell, J. M.; Ray, J. A.; Schmitt, M. R.; Cuming, A. C. *J. Biol. Chem.* **1993**, *268*, 12239-12242.
- (8) Gane, P. J.; Dunwell, J. M.; Warwicker, J. J. *Mol. Evol.* **1998**, *46*, 488-493.
- (9) Woo, E.-J.; Dunwell, J. M.; Goodenough, P. W.; Marvier, A. C.; Pickersgill, R. W. *Nat. Struct. Mol. Biol.* **2000**, *7*, 1036-1040.
- (10) Requena, L.; Borneman, S. *Biochem. J.* **1999**, *343*, 185-190.
- (11) Anand, R.; Dorrestein, P. C.; Kinsland, C.; Begley, T. P.; Ealick, S. E. *Biochemistry* **2002**, *41*, 7659-7669.
- (12) Tanner, A.; Bowater, L.; Fairhurst, S. A.; Bornemann, S. *J. Biol. Chem.* **2001**, *276*, 43627-43634.
- (13) Siegbahn, P. E. *Inorg. Chem.* **2004**, *43*, 5944-5953.
- (14) Balogh-Hergovich, E.; Speier, G. *J. Org. Chem.* **2001**, *66*, 7974-7978.
- (15) Barney, B. M.; Schaab, M. R.; LoBrutto, R.; Francisco, W. A. *Protein Expression Purif.* **2004**, *35*, 131-141.
- (16) Bowater, L.; Fairhurst, S. A.; Just, V. J.; Bornemann, S. *FEBS Lett.* **2004**, *557*, 45-48.
- (17) Gopal, B.; Madan, L. L.; Betz, S. F.; Kossiakoff, A. A. *Biochemistry* **2005**, *44*, 193-201.
- (18) Schaab, M. R.; Barney, B. M.; Francisco, W. A. *Biochemistry* **2006**, *45*, 1009-1016.

- (19) Merkens, H.; Kappl, R.; Jakob, R. P.; Schmid, F. X.; Fetzner, S. *Biochemistry* **2008**, *47*, 12185-12196.
- (20) Oka, T.; Simpson, F. J. *Biochem. Biophys. Res. Commun.* **1971**, *43*, 1-5.
- (21) Kooter, I. M.; Steiner, R. A.; Dijkstra, B. W.; Noort, P. I. v.; Egmond, M. R.; Huber, M. *Eur. J. Biochem.* **2002**, *269*, 2971-2979.
- (22) Hund, H.-K.; Lingens, J. B. F.; Kappl, J. H. R.; Fetzner, S. *Eur. J. Biochem.* **1999**, *263*, 871-878.
- (23) Fusetti, F.; Steiner, K. A.; Noort, P. I. v.; Pijning, T.; Rozeboom, H. J.; Kalk, K. H.; Egmond, M. R.; Dijkstra, B. W. *Structure* **2002**, *10*, 259-268.
- (24) Steiner, R. A.; Meyer-Klaucke, W.; Dijkstra, B. W. *Biochemistry* **2002**, *41*, 7963-7968.
- (25) Fiorucci, S.; Golebiowski, J.; Cabrol-Bass, D.; Antonczak, S. *ChemPhysChem* **2004**, *5*, 1726-1733.
- (26) Fiorucci, S.; Golebiowski, J.; Cabrol-Bass, D.; Antonczak, S. *Proteins: Struct., Funct., Bioinf.* **2006**, *64*, 845-850.
- (27) Steiner, R. A.; Kalk, K. H.; Dijkstra, B. W. *Proc. Natl. Acad. Sci. USA* **2002**, *99*, 16625-16630.
- (28) Antonczak, S.; Fiorucci, S.; Golebiowski, J.; Cabrol-Bass, D. *Phys. Chem. Chem. Phys.* **2009**, *11*, 1491-1501.
- (29) Utaka, M.; Takeda, A. *J. Chem. Soc., Chem. Commun.* **1985**, 1824-1826.
- (30) Lippai, I.; Speier, G.; Huttner, G.; Zsolnai, L. *Chem. Commun.* **1997**, 741-742.
- (31) Lippai, I.; Speier, G. *J. Mol. Catal. A: Chem.* **1998**, *130*, 139-148.
- (32) Balogh-Hergovich, E.; Speier, G.; Argay, G. *J. Chem. Soc., Chem. Commun.* **1991**, 551-552.
- (33) Balogh-Hergovich, E.; Kaizer, J.; Speier, G.; Fülöp, V.; Parkanyi, L. *Inorg. Chem.* **1999**, *38*, 3787.
- (34) Balogh-Hergovich, E.; Kaizer, J.; Speier, G.; Huttner, G.; Jacobi, A. *Inorg. Chem.* **2000**, *39*, 4224-4229.
- (35) Kaizer, J.; Pap, J.; Speier, G.; Réglie, M.; Giorgi, M. *Transition Met. Chem. (Dordrecht, Neth.)* **2004**, *29*, 630-633.
- (36) Malkhasian, A. Y. S.; Finch, M. E.; Nikolovski, B.; Menon, A.; Kucera, B. E.; Chavez, F. A. *Inorg. Chem.* **2007**, *46*, 2950-2952.

- (37) Balogh-Hergovich, E.; Kaizer, J.; Speier, G. *J. Mol. Catal. A: Chem.* **2003**, *206*, 83-87.
- (38) Barhacs, L.; Kaizer, J.; Pap, J.; Speier, G. *Inorg. Chim. Acta* **2001**, *320*, 83-91.
- (39) Wray, J. W.; Abeles, R. H. *J. Biol. Chem.* **1995**, *270*, 3147-3153.
- (40) Myers, R. W.; Wray, J. W.; Fish, S.; Abeles, R. H. *J. Biol. Chem.* **1993**, *268*, 24785-24791.
- (41) Dai, Y.; Wensink, P. C.; Abeles, R. H. *J. Biol. Chem.* **1999**, *274*, 1193-1195.
- (42) Wray, J. W.; Abeles, R. H. *J. Biol. Chem.* **1993**, *268*, 21466-21469.
- (43) Dai, Y.; Wensink, P. C.; Abeles, R. H. *The Journal of Biological Chemistry* **1999**, *274*, 1193-1195.
- (44) Popchapsky, T. C.; Popchapsky, S. C.; Ju, T.; Hoefler, C.; Liang, J. *J. Biomol. NMR* **2006**, *34*, 117-127.
- (45) Mo, H.; Dai, Y.; Pochapsky, S. S.; Pochapsky, T. C. *J. Biomol. NMR* **1999**, *14*, 287-288.
- (46) Pochapsky, S. S.; Sunshine, J. C.; Pochapsky, T. C. *J. Am. Chem. Soc.* **2008**, *130*, 2156-2157.
- (47) Pochapsky, T. C.; Pochapsky, S. S.; Ju, T.; Mo, H.; Al-Mjeni, F.; Maroney, M. J. *Nat. Struct. Mol. Biol.* **2002**, *9*, 966-972.
- (48) Al-Mjeni, F.; Ju, T.; Pochapsky, T. C.; Maroney, M. J. *Biochemistry* **2002**, *41*, 6761-6779.
- (49) Ju, T.; Goldsmith, R. B.; Chai, S. C.; Maroney, M. J.; Pochapsky, S. S.; Pochapsky, T. C. *J. Mol. Biol.* **2006**, *393*, 823-834.
- (50) Xu, Q.; Schwarzenbacher, R.; Krishna, S. S.; McMullan, D.; Agarwalla, S.; Quijano, k.; Abdubek, P.; Ambing, E.; Axelrod, H.; Biorac, T.; Canaves, J. M.; Chiu, H.-J.; Elsliger, M.-A.; Grittini, C.; Grzechnik, S. K.; DiBonato, M.; Hale, J.; Hampton, E.; Han, G. W.; Haugen, J.; Hornsby, M.; Jaroszewski, L.; Moy, K.; Paulsen, E. N. J.; Reyes, R.; Rife, C.; Spraggon, G.; Stevens, R. C.; Bedem, H. v. d.; Velasquez, J.; White, A.; Wolf, G.; Hodgson, K. O.; Wooley, J.; Deacon, A. M.; Godzik, A.; Lesley, S. A.; Wilson, I. A. *Proteins: Struct., Funct., Bioinf.* **2006**, *64*, 808-813.
- (51) Chai, S. C.; Ju, T.; Goldsmith, R. B.; Maroney, M. J.; Pochapsky, T. C. *Biochemistry* **2008**, *47*, 2428-2438.
- (52) Dai, Y.; Pochapsky, T. C.; Abeles, R. H. *Biochemistry* **2001**, *40*, 6379-6387.

- (53) Szajna, E.; Dobrowolski, P.; Fuller, A.; Arif, A. M.; Berreau, L. M. *Inorg. Chem.* **2004**, *43*, 3988-3997.
- (54) Berreau, L. M. *Comments Inorg. Chem.* **2007**, *28*, 123-171.
- (55) Szajna, E.; Arif, A. M.; Berreau, L. M. *J. Am. Chem. Soc.* **2005**, *127*, 17186-17187.
- (56) Szajna-Fuller, E.; Rudzka, K.; Arif, A. M.; Berreau, L. M. *Inorg. Chem.* **2007**, *46*, 5499-5507.
- (57) Sigal, E. *Am. J. Physiol.* **1991**, *260*, L13-L28.
- (58) Yamamoto, S. *Biochim. Biophys. Acta, Mol. Cell Biol. Lipids* **1992**, *1128*, 117-131.
- (59) Samuelsson, B.; Dahlen, S. E.; Lindgren, J. A.; Rouzer, C. A.; Serhan, C. N. *Science* **1987**, *237*, 1171-1176.
- (60) Rioux, N.; Castonguay, A. *Carcinogenesis* **1998**, *19*, 1393-1400.
- (61) Noordermeer, M. A.; Veldink, G. A.; Vliegthart, J. F. G. *ChemBioChem* **2001**, *2*, 494.
- (62) Siedow, J. N. *Annu. Rev. Plant Physiol. Plant Mol. Biol.* **1991**, *42*, 145-188.
- (63) Clapp, C. H.; Senchak, S. E.; Stover, T. J.; Potter, T. C.; Findeis, P. M.; Novak, M. J. *J. Am. Chem. Soc.* **2001**, *123*, 747-748.
- (64) Hamberg, M.; Hamberg, G. *Biochem. Biophys. Res. Commun.* **1980**, *95*, 1090-1097.
- (65) Schilstra, M. J.; Veldink, G. A.; Vliegthart, J. F. G. *Biochemistry* **1994**, *33*, 3974-3979.
- (66) Zhang, Y.; Gebhard, M. S.; Solomon, E. I. *J. Am. Chem. Soc.* **1991**, *113*, 5162-5175.
- (67) Slappendel, S.; Veldink, G. A.; Vliegthart, J. F. G.; Aasa, R.; Malmström, B. G. *Biochim. Biophys. Acta, Gen. Subj.* **1981**, *667*, 77-86.
- (68) Glickman, M. H.; Klinman, J. P. *Biochemistry* **1995**, *34*, 14077-14092.
- (69) Glickman, M. H.; Wiseman, J. S.; Klinman, J. P. *J. Am. Chem. Soc.* **1994**, *116*, 793-794.
- (70) Hwang, C.-C.; Grissom, C. B. *J. Am. Chem. Soc.* **1994**, *116*, 795-796.
- (71) Jonsson, T.; Glickman, M. H.; Sun, S.; Klinman, J. P. *J. Am. Chem. Soc.* **1996**, *118*, 10319-10320.

- (72) Lewis, E. R.; Johansen, E.; Holman, T. R. *J. Am. Chem. Soc.* **1999**, *121*, 1395-1396.
- (73) Minor, W.; Steczko, J.; Bolin, J. T.; Otwinowski, Z.; Axelrod, B. *Biochemistry* **1993**, *32*, 6320-6323.
- (74) Boyington, J. C.; Gaffney, B. J.; Amzel, L. M. *Science* **1993**, *260*, 1482-1486.
- (75) Minor, W.; Steczko, J.; Stec, B.; Otwinowski, Z.; Bolin, J. T.; Walter, R.; Axelrod, B. *Biochemistry* **1996**, *35*, 10687-10701.
- (76) Skrzypczak-Jankun, E.; Amzel, L. M.; Kroa, B. A.; M. O. Funk, J. *Proteins: Struct., Funct., Gen.* **1997**, *29*, 15-31.
- (77) Gillmor, S. A.; Villaseñor, A.; Fletterick, R.; Sigal, E.; Browner, M. F. *Nat. Struct. Mol. Biol.* **1997**, *4*, 1003-1009.
- (78) Lehnert, N.; Solomon, E. I. *J. Biol. Inorg. Chem.* **2003**, *8*, 294-305.
- (79) Pavlosky, M. A.; Zhang, Y.; Westre, T. E.; Gan, Q.-F.; Pavel, E. G.; Campochiaro, C.; Hedman, B.; Hodgson, K. O.; Solomon, E. I. *J. Am. Chem. Soc.* **1995**, *117*, 4316-4327.
- (80) Scarrow, R. C.; Trimitsis, M. G.; Buck, C. P.; Grove, G. N.; Cowling, R. A.; Nelson, M. J. *Biochemistry* **1994**, *33*, 15023-15035.
- (81) Nelson, M. J.; Seitz, S. P. In *Active Oxygen in Biochemistry*; Valentine, J. S., Foote, C., Greenberg, A., F., L. J., Eds.; Blackie Academic & Professional: London: 1995; Vol. 3, p 276-312.
- (82) Borowski, T.; Broclawik, E. *J. Phys. Chem. B* **2003**, *107*, 4639-4646.
- (83) Nelson, M. J.; Seitz, S. P.; Cowling, R. A. *Biochemistry* **1990**, *29*, 6897-6903.
- (84) Tomchick, D. R.; Phan, P.; Cymborowski, M.; Minor, W.; Holman, T. R. *Biochemistry* **2001**, *40*, 7509-7517.
- (85) Nelson, M. J. *Biochemistry* **1988**, *27*, 4273-4278.
- (86) Holman, T. R.; Zhou, J.; Solomon, E. I. *J. Am. Chem. Soc.* **1998**, *120*, 12564-12572.
- (87) Neidig, M. L.; Weckler, A. T.; Schenk, G.; Holman, T. R.; Solomon, E. I. *J. Am. Chem. Soc.* **2007**, *129*, 7531-7537.
- (88) Kohen, A.; Klinman, J. P. *Acc. Chem. Res.* **1998**, *31*, 397-404.
- (89) Knapp, M. J.; Rickert, K.; Klinman, J. P. *J. Am. Chem. Soc.* **2002**, *124*, 3865-3874.

- (90) Klinman, J. P. *Pure Appl. Chem.* **2003**, *75*, 601-608.
- (91) Tejero, I.; Carcia-Viloca, M.; González-Lafont, À.; Lluch, J. M.; York, D. M. *J. Phys Chem. B* **2006**, *110*, 24708-24719.
- (92) Hammes-Schiffer, S. *Acc. Chem. Res.* **2006**, *39*, 93-100.
- (93) Olsson, M. H. M.; Parson, W. W.; Warshel, A. *Chem. Rev.* **2006**, *106*, 1737-1756.
- (94) Fukuzumi, S. *Helv. Chim. Acta* **2006**, *89*, 2425-2440.
- (95) Knapp, M. J.; Seebeck, F. P.; Klinman, J. P. *J. Am. Chem. Soc.* **2001**, *123*, 2931-2932.
- (96) Knapp, M. J.; Klinman, J. P. *Biochemistry* **2003**, *42*, 11466-11475.
- (97) Skrzypczak-Jankun, E.; Bross, R. A.; Carroll, R. T.; Dunham, W. R.; Funk, M. O. *J. Am. Chem. Soc.* **2001**, *123*, 10814-10820.
- (98) Tachibana, M.; Sasaki, K.; Ueda, A.; Sakai, M.; Sakakibara, Y.; Ohno, A.; Okamoto, T. *Chem. Lett.* **1991**, 993-996.
- (99) Ogo, S.; Wada, S.; Watanabe, Y.; Iwase, M.; Wada, A.; Harata, M.; Jitsukawa, K.; Masuda, H.; Einaga, H. *Angew. Chem., Int. Ed.* **1998**, *37*, 2102-2104.
- (100) Ogo, S.; Yamahara, R.; Roach, M.; Suenobu, T.; Aki, M.; Ogura, T.; Kitagawa, T.; Masuda, H.; Fukuzumi, S.; Watanabe, Y. *Inorg. Chem.* **2002**, *41*, 5513-5520.
- (101) Jonas, R. T.; Stack, T. D. P. *J. Am. Chem. Soc.* **1997**, *119*, 8566-8567.
- (102) Goldsmith, C. R.; Jonas, R. T.; Stack, T. D. P. *Journal of the American Chemical Society* **2002**, *124*, 83-96.
- (103) Lockwood, M. A.; Blubaugh, T. J.; Collier, A. M.; Lovell, S.; Mayer, J. A. *Angew. Chem., Int. Ed.* **1999**, *38*, 225-227.
- (104) Roth, J. P.; Yoder, J. C.; Won, T.-J.; Mayer, J. M. *Science* **2001**, *294*, 2524-2526.
- (105) Gardner, K. A.; Mayer, J. M. *Science* **1995**, *269*, 1849-1851.
- (106) Mayer, J. M. *Acc. Chem. Res.* **1998**, *31*, 441-450.
- (107) Bakac, A. *J. Am. Chem. Soc.* **2000**, *122*, 1092-1097.
- (108) Su, C.; Oliw, E. H. *J. Biol. Chem.* **1998**, *273*, 13072-13079.
- (109) Hamberg, M.; Su, C.; Oliw, E. *J. Biol. Chem.* **1998**, *273*, 13080-13088.

- (110) Su, C.; Sahlin, M.; Oliw, E. H. *J. Biol. Chem.* **2000**, *275*, 18830-18835.
- (111) Goldsmith, C. R.; Cole, A. P.; Stack, T. D. P. *J. Am. Chem. Soc.* **2005**, *127*, 9904-9912.
- (112) Goldsmith, C. R.; Stack, T. D. P. *Inorg. Chem.* **2006**, *45*, 6048-6055.
- (113) Roth, J. P.; Mayer, J. M. *Inorg. Chem.* **1999**, *38*, 2760-2761.
- (114) Roth, J. P.; Lovell, S.; Mayer, J. M. *J. Am. Chem. Soc.* **2000**, *122*, 5486-5498.
- (115) Yoder, J. C.; Roth, J. P.; Gussenhoven, E. M.; Larsen, A. S.; Mayer, J. M. *J. Am. Chem. Soc.* **2003**, *125*, 2629-2640.
- (116) Rodriguez, M.-C.; Morgenstern-Badarau, I.; Cesario, M.; Guilhem, J.; Keita, B.; Nadjo, L. *Inorg. Chem.* **1996**, *35*, 7804-7810.
- (117) Policar, C.; Durot, S.; Lambert, F.; Cesario, M.; Ramiandrasoa, F.; Morgenstern-Badarau, I. *Eur. J. Inorg. Chem.* **2001**, 1807-1818.
- (118) Peters, L.; Hübner, E.; Burzlaff, N. *J. Organomet. Chem.* **2005**, *690*, 2009-2016.
- (119) Marques, H. M.; Munro, O. Q.; Munro, T.; Wet, M. d.; Vashi, P. R. *Inorg. Chem.* **1999**, *38*, 2312-2319.
- (120) Johnson, C. R.; Henderson, W. W.; Sheperd, R. E. *Inorg. Chem.* **1984**, *23*, 2754-2763.
- (121) Tang, C. C.; Davalian, D.; Huang, P.; Breslow, R. *J. Am. Chem. Soc.* **1978**, *100*, 3918-3922.
- (122) Collman, J. P.; Zhong, M.; Wang, Z. *Org. Lett.* **1999**, *1*, 949-951.
- (123) Breslow, R.; Hunt, J. T.; Smiley, R.; Tarnowski, T. *J. Am. Chem. Soc.* **1983**, *105*, 5337-5342.
- (124) Katritzky, A. R.; Slawinski, J. J.; Brunner, F.; Gorun, S. *J. Chem. Soc. Perkin Trans. 1* **1989**, 1139.
- (125) Bensusan, H. B.; Naidu, M. S. R. *Biochemistry* **1967**, *6*, 12.
- (126) Kirk, K. L. *J. Heterocyclic Chem.* **1985**, *22*, 57-59.
- (127) Stensiö, K.-E.; Wahlberg, K.; Wahren, R. *Acta Chem. Scand.* **1973**, *27*, 2179-2183.
- (128) Iddon, B.; Kahn, N.; Lim, B. L. *J. Chem. Soc. Perkin Trans. 1* **1987**, 1437-1443.
- (129) Butz, R. H.-J.; Lindell, S. D. *J. Org. Chem.* **2002**, *67*, 2699-2701.

- (130) Turner, R. M.; Lindell, S. D.; Ley, S. V. *J. Org. Chem.* **1991**, *56*, 5739-5740.
- (131) Kim, J.-W.; Abdelaal, S. M.; Bauer, L.; Heimer, N. E. *J. Heterocyclic Chem.* **1995**, *32*, 611-620.
- (132) Ngochindo, R. I. *J. Chem. Soc. Perkin Trans. 1* **1990**, 1645-1648.
- (133) Carpenter, A. J.; Chadwick, D. J. *Tetrahedron* **1986**, *42*, 2351-2358.
- (134) Macco, A. A.; Godefroi, E. F.; Drouen, J. J. M. *J. Org. Chem.* **1975**, *40*, 252-255.
- (135) Coutts, I. G. C.; Jieng, S.; Khandelwahl, G. D.; Wood, M. L. *J. Heterocyclic Chem.* **1994**, *31*, 857-860.
- (136) Itoh, T.; Hasegawa, H.; Nagata, K.; Okada, M.; Ohsawa, A. *Tetrahedron Lett.* **1992**, *33*, 5399-5402.
- (137) Itoh, T.; Miyazaki, M.; Nagata, K.; Ohsawa, A. *Tetrahedron* **2000**, *56*, 4383-4395.
- (138) Wenzel, A. G.; Jacobsen, E. N. *J. Am. Chem. Soc.* **2002**, *124*, 12964-12965.
- (139) Demjanov, N. J.; Lushnikov, M. J. *Russ. Phys. Chem.* **1903**, *35*, 26.
- (140) Smith, P. A. S.; Baer, D. R. *Org. React.* **1960**, *11*, 157.
- (141) Volkman, J.; Nicholas, K. M. *Org. Lett.* **2004**, *6*, 4301-4302.
- (142) Akiyama, M.; Hara, Y.; Tanabe, M. *J. Chem. Soc. Perkin Trans. 2* **1978**, 288-292.
- (143) Braussaud, N.; R  ther, T.; Cavell, K. J.; Skelton, B. W.; White, A. H. *Synthesis* **2001**, *4*, 626-632.
- (144) Lucas, P.; Mehdi, N. E.; Ho, H. A.; B  langer, D.; Breau, L. *Synthesis* **2000**, *9*, 1253.
- (145) Subramanyam, C.; Mallamo, J. P.; Jr., J. A. D.; Earley, W. G.; Kumar, V.; Aimone, L. D.; Ault, B.; Miller, M. S.; Luttinger, D. A.; DeHaven-Hudkins, D. L. *J. Med. Chem.* **1995**, *38*, 21-27.
- (146) Luca, L. D.; Giacomelli, G.; Masala, S.; Porcheddu, A. *J. Org. Chem.* **2003**, *68*, 4999-5001.
- (147) Epp, J. B.; Widlanski, T. S. *J. Org. Chem.* **1999**, *64*, 293-295.
- (148) Yamaoka, H.; Moriya, N.; Ikunaka, M. *Org. Process Res. Dev.* **2004**, *8*, 931-938.
- (149) Miller, R. A.; Hoerrner, S. *Org. Lett.* **2003**, *5*, 285-287.

- (150) Katritzky, A. R.; Rewcastle, G. W.; Fan, W.-Q. *J. Org. Chem.* **1988**, *53*, 5685-5689.
- (151) Manoharan, T. S.; Brown, R. S. *J. Org. Chem.* **1988**, *53*.
- (152) Luca, L. D.; Giacomelli, G.; Porcheddu, A. *Org. Lett.* **2001**, *3*, 3041-3043.
- (153) Dodey, P.; Leclerc, G. *J. Heterocyclic Chem.* **1994**, *31*, 1121-1123.
- (154) Moore, J. D.; Finney, N. S. *Org. Lett.* **2002**, *4*, 3001-3003.
- (155) Kuhakarn, C.; Kittigowittana, K.; Pohmakotr, M.; Reutrakul, V. *Tetrahedron* **2005**, *61*, 8995-9000.
- (156) Meyer, S. D.; Schreiber, S. L. *J. Org. Chem.* **1994**, *59*, 7549-7552.
- (157) Domingo, L. R.; Saez, J. A.; Pérez, P. *Chem. Phys. Lett.* **2007**, *438*, 341-345.
- (158) Mefthuddin, M.; C., V. L.; Kamal, F. A. In *European Patent Office; SABIC*, Ed.; A. Awwad: 2002; Vol. EP 1 088 811 B1, p 1-11.
- (159) Batten, M. P.; Canty, A. J.; Cavell, K. J.; Rütther, T.; Skelton, B. W.; White, A. H. *Inorg. Chim. Acta* **2006**, *359*, 1710-1724.
- (160) Reggelin, M.; Doerr, S. *Synlett* **2004**, *6*, 1117-1117.
- (161) Roe, A. *J. Chem. Soc.* **1963**, 2195-2200.
- (162) Becke, A. D. *Phys. Rev. A* **1988**, *38*, 3098-3100.
- (163) Becke, A. D. *J. Chem. Phys.* **1993**, *98*, 1372-1377.
- (164) Frisch, M. J.; Trucks, G. W.; Schlegel, H. B.; Scuseria, G. E.; Robb, M. A.; Cheeseman, J. R.; Montgomery, J. A.; Jr., T. V.; Kudin, K. N.; Burant, J. C.; Millam, J. M.; Iyengar, S. S.; Tomasi, J.; Barone, V.; Mennucci, B.; Cossi, M.; Scalmani, G.; Rega, N.; Petersson, G. A.; Nakatsuji, H.; Hada, M.; Ehara, M.; Toyota, K.; Fukuda, R.; Hasegawa, J.; Ishida, M.; Nakajima, T.; Honda, Y.; Kitao, O.; Nakai, H.; Klene, M.; Li, X.; Knox, J. E.; Hratchian, H. P.; Cross, J. B.; Adamo, C.; Jaramillo, J.; Gomperts, R.; Stratmann, R. E.; Yazyev, O.; Austin, A. J.; Cammi, R.; Pomelli, C.; Ochterski, J. W.; Ayala, P. Y.; Morokuma, K.; Voth, G. A.; Salvador, P.; Dannenberg, J. J.; Zakrzewski, V. G.; Dapprich, S.; A. D. Daniels, M. C. S.; Farkas, O.; Malick, D. K.; Rabuck, A. D.; Raghavachari, K.; Foresman, J. B.; Ortiz, J. V.; Cui, Q.; Baboul, A. G.; Clifford, S.; Cioslowski, J.; Stefanov, B. B.; Liu, G.; Liashenko, A.; Piskorz, P.; Komaromi, I.; Martin, R. L.; Fox, D. J.; Keith, T.; Al-Laham, M. A.; Peng, C. Y.; Nanayakkara, A.; Challacombe, M.; Gill, P. M. W.; Johnson, B.; Chen, W.; Wong, M. W.; Gonzalez, C.; Pople, J. A. In *Revision B.04*; Gaussian, Inc.: Pittsburgh PA, 2003.

- (165) In *Spartan'04 for Macintosh*
Wavefunction, Inc.: Irvine, CA.
- (166) Reddy, P. A.; Hsiang, B. C. H.; Latifi, T. N.; Hill, M. W.; Woodward, K. E.; Rothman, S. M.; Ferrendelli, J. A.; Covey, D. F. *J. Med. Chem.* **1996**, *39*, 1898-1906.
- (167) Arduengo, A. J. I.; Gentry, F. P. J.; Taverkere, P. K.; Simmons, H. E. I. In *USPTO Patent*; Patents, U. S., Ed.; E. I. du Pont de Nemours and Company: USA, 2001; Vol. 6,177,575, p 1-13.
- (168) Gridnev, A. A.; Mihaltseva, I. M. *Synth. Commun.* **1994**, *24*, 1547-1555.
- (169) Ihmels, H.; Maggini, M.; Prato, M.; Scorrano, G. *Tetrahedron Lett.* **1991**, *32*, 6215-6318.
- (170) Ernest, I. *Collection Czechoslov. Chem. Commun.* **1954**, *19*, 1179-1190.
- (171) Hagen, K. S. *Inorg. Chem.* **2000**, *39*, 5867-5869.
- (172) Steel, P. J. *Coord. Chem. Rev.* **1990**, *106*, 227-265.
- (173) Wu, L. P.; Yamagiwa, Y.; Ino, I.; Sugimoto, K.; Kuroda-Sowa, T.; Kamikawa, T.; Munakata, M. *Polyhedron* **1999**, *18*, 2047-2053.
- (174) Higgs, T. C.; Helliwell, M.; McInnes, E. J. L.; Mabbs, F. E.; Harding, C. J.; Garner, C. D. *J. Chem. Soc., Dalton Trans.* **1997**, *6*, 927-933.
- (175) Kujime, M.; Fujii, H. *Tetrahedron Lett.* **2005**, *46*, 2809-2812.
- (176) He, Y.; Chen, Y.; Du, H.; Schmid, L. A.; Lovely, C. J. *Tetrahedron Lett.* **2004**, *45*, 5529-5532.